Supported Liquid Catalysts for Removal of High Temperature Fuel Cell Contaminants

Final Report

Start Date: October 1, 1998
End Date: September 30, 1999

Alan W. Weimer (PI), Peter Czerpak, and Patrick Hilbert
Department of Chemical Engineering
University of Colorado
Boulder, CO 80309-0424

Report Issued: January, 2000

Final Report: DE-FG26-98FT40122

Abstract

A novel catalytic synthesis gas oxidation process using molten carbonate salts supported on compatible fluidized iron oxide particles ("supported-liquid-phase-catalyst" (SLPC) fluidized bed process) was investigated. This process combines the advantages of large scale fluidized bed processing with molten salt bath oxidation. Molten salt catalysts can be supported within porous fluidized particles in order to improve mass transfer rates between the liquid catalysts and the reactant gases. Synthesis gas can be oxidized at reduced temperatures resulting in low NO_x formation while trace sulfides and halides are captured in-situ. Hence, catalytic oxidation of synthesis gas can be carried out simultaneously with hot gas cleanup. Such SLPC fluidized bed processes are affected by inter-particle liquid capillary forces that may lead to agglomeration and de-fluidization of the bed. An understanding of the origin and strength of these forces is needed so that they can be overcome in practice.

Process design is based on thermodynamic free energy minimization calculations that indicate the suitability of eutectic Na_2CO_3/K_2CO_3 mixtures for capturing trace impurities in-situ (< 1 ppm SO_x released) while minimizing the formation of NO_x (< 10 ppm). Iron oxide has been identified as a preferred support material since it is non-reactive with sodium, is inexpensive, has high density (i.e. inertia), and can be obtained in various particle sizes and porosities. Force balance modeling has been used to design a surrogate ambient temperature system that is hydrodynamically similar to the real system, thus allowing complementary investigation of the governing fluidization hydrodynamics.

The primary objective of this research was to understand the origin of and to quantify the liquid capillary interparticle forces affecting the molten carbonate SLPC fluidized bed process. *Substantial theoretical and experimental exploratory results indicate process feasibility.* The potential environmental gain from success is enormous, impacting all areas of the world where coal is burned to supply steam or direct industrial heat. Project success may lead to an integrated combustion system providing for simultaneous catalytic oxidation and hot gas cleanup of raw synthesis gas from an upstream coal gasifier.

Table of Contents

List of Graphical Materials

I. Executive Summary

An investigation was carried out for the use of supported molten salt catalysts to (1) selectively capture trace contaminants in synthesis gas being fed to fuel cells (without oxidation) and (2) to simultaneously combust/cleanup hot synthesis gas being fed to a fluidized bed combustor. The first application is directed towards hot gas cleanup without oxidation while the second is directed towards hot gas cleanup with simultaneous oxidation, both applications using supported molten salt. In both instances, thermodynamic free energy minimization studies were carried out in order to evaluate the effectiveness of the molten salt. Studies focused on both the possible reaction with certain fluidized solid support materials and the ability to effectively capture trace contaminants in the synthesis gas stream. Experimental studies were also carried out to evaluate the ability to support molten salt on fluidized particles. Theoretical force balance studies complemented the experimental work and provided an understanding of the inter-particle forces that need to be overcome in practice.

Thermodynamic calculations indicated that certain molten salt catalyst support materials such as Fe_2O_3, ZrO_2, and CaO were non-reactive and, hence, compatible with molten carbonate salts. However, the studies also indicated that it was difficult, if not impossible, to capture trace contaminants without oxidizing the synthesis gas. Details regarding the thermodynamic studies are reported in Appendix A.

Experimental studies focused on "proof-of-concept" experiments with regard to the feasibility of fluidizing support particles in the presence of a liquid molten salt. It was found that porous particles that could contain molten salt within the particles could be fluidized with the molten salt content approaching 10 wt%. It was also found that larger particles could support more salt than finer particles. Details regarding the experimental studies are reported in Appendix B.

Theoretical force balance studies focused on an understanding of the liquid capillary inter-particle forces controlling the process hydrodynamics. An expression was derived that accounted for such forces in a supported liquid phase catalyst (SLPC) process. Inertial forces and surface tension forces were found to be important. It is essential that inertial forces overcome surface tension forces in order to maintain fluidization in the bed. Hence, the theoretical development explained why larger more dense particles that were porous were best at supporting liquids in fluidized systems. A surrogate ambient temperature system was designed based upon these results. Some preliminary results with the surrogate system are presented.

In general, it was found from the thermodynamic free energy minimization studies that trace contaminants in synthesis gas could not be captured independent of oxidation using supported molten salts. Hence, the original intention of using a molten salt SLPC system for removal of high temperature fuel cell contaminants did not appear feasible since the synthesis gas would ultimately oxidize. In view of this, the project focused on the possibility of using molten carbonate SLPC processes for simultaneous low temperature oxidation processing and hot gas cleanup.

The body of this report is concerned with presenting the summarized results for the feasible case of using a supported molten carbonate eutectic salt mixture (Na_2CO_3/K_2CO_3) as a selective oxidizer for synthesis gas oxidation and simultaneous hot gas cleanup. A product gas containing less than 1 ppm SO_x and < 10 ppm NO_x can be obtained for such a process. The appendices can be referred to for details and are self-contained with their own references. Although the results presented here are very encouraging and support further research in the area, they are preliminary. A Provisional Patent Application has been filed for this novel process.

II. Introduction

A novel method allowing the selective oxidation of synthesis gas at reduced temperatures with almost no NO_x, SO_x, or halide emissions is to use a molten salt oxidation catalyst supported by particles in a fluidized bed (Figure 1). This large-scale method for reduced temperature selective oxidation, with simultaneous *in-situ* capture of trace contaminants (S, Cl species, etc.), is one in which catalytic molten salt (e.g. Na_2CO_3/K_2CO_3 eutectic mixtures) oxidation is carried out within the pores of compatible fluidized support particles. Such a process combines the advantages of fluidized bed combustion and molten salt bath oxidation. It takes advantage of the large fluidized bed particle surface area and increased residence time (over a conventional molten salt bath) to provide for increased mass transfer rates per unit volume of the reactor between active salt surfaces and combustible species. The potential environmental gain from success is enormous, impacting all areas of the world where synthesis gas is produced from coal and burned to supply electricity. Project success may lead to an integrated combustion system providing for simultaneous catalytic oxidation and hot gas cleanup of raw synthesis gas from an upstream coal gasifier.

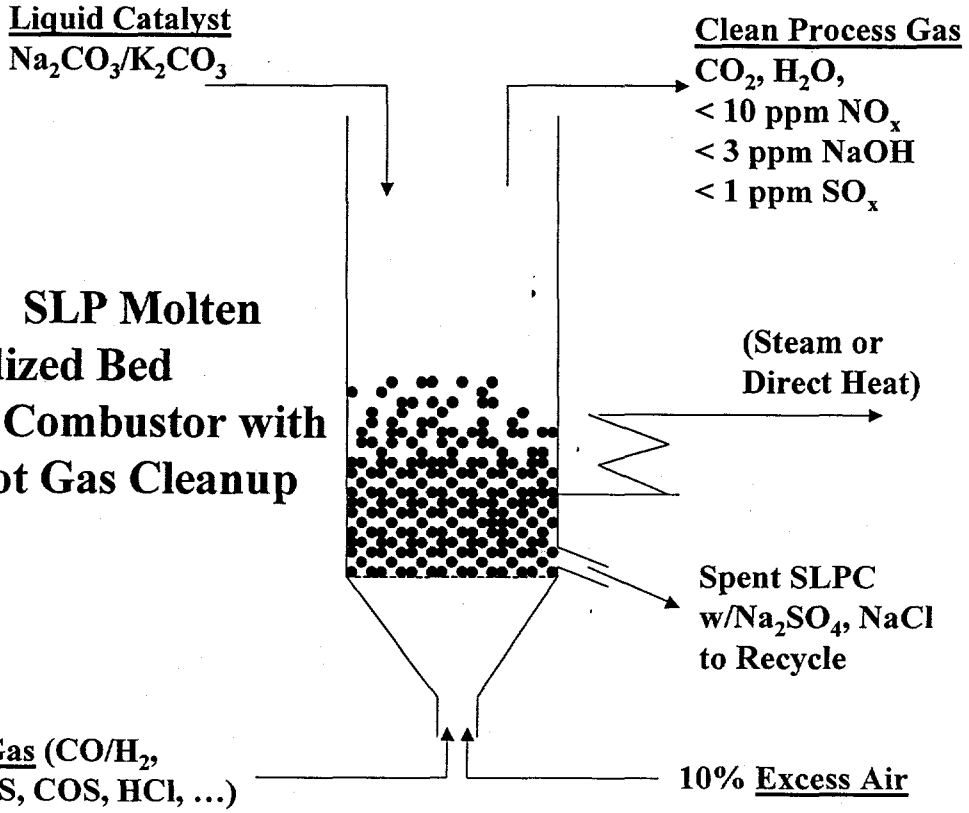

Figure 1. SLP Molten Salt Fluidized Bed Catalytic Combustor with In-situ Hot Gas Cleanup

A. Problem Statement

The primary concern with this process is the fluidizability of particles in the presence of a supported molten salt both without and with reaction occurring. Hence, a focus of this research is an understanding of the liquid capillary forces affecting the fluidization of such support particles.

B. Objectives

The research involves *substantial exploratory theoretical* (thermodynamic free energy minimization calculations for selecting suitable particle support materials and molten salts; particle force balance calculations for understanding governing inertial and liquid capillary forces) *and experimental* ("proof of concept" experiments demonstrating the fluidization of particles supporting molten salts) *results that indicate process feasibility.* A surrogate system has also been designed that allows fluidization hydrodynamics to be investigated at ambient temperature. The surrogate system is hydrodynamically similar to the real system. *The objective of the research is a basic understanding of the liquid capillary forces controlling fluidization of the supported molten carbonate fluidized bed process.*

III. Background Science

A. Supported Liquid Phase Molten Salt Catalysis

Molten salts have been used to catalyze various oxidation reactions[1-5]. Most non-charged materials are soluble in molten salts. This solubility is probably related to the crystal structure of salts in the molten state. Data from X-rays taken at temperatures above their melting point indicate that molten salts still retain a quasi-lattice structure. The solubility of the reactants (solute) in the molten salt is based on the theory that the solute assumes an electronic charge in the semi-crystalline melt. This charge gives the solute an electrostatic orientation similar to the ionic component of the molten salt. The process of polarizing or orienting the normally neutral species results in a reduction of the energy required to initiate and sustain chemical reactions. In addition, there are substantial decreases in the unburned hydrocarbon products[6] relative to conventional oxidation. Molten carbonates, such as Na_2CO_3 and K_2CO_3, have been particularly active in simultaneously capturing trace sulfides and halides that react with the salt and are retained in the melt as inorganic salts rather than released to the atmosphere as volatile gases[7-11].

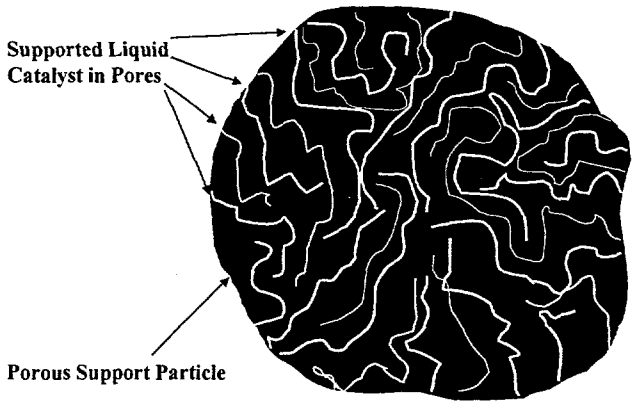

Figure 2. Supported Liquid Phase Catalyst (SLPC)

One of the possibilities to heterogenize a homogeneously catalyzed (liquid) reaction system is the use of SLPCs[12-16]. SLP catalysis is the coating of a porous support particle's pores with a catalytically active liquid to catalyze gas phase reactions (Figure 2). These hybrid contacts have the advantage, compared to a homogeneously catalyzed reaction in a liquid/gas reaction system (e.g. bubble column reactor or, for this work, a molten salt bath), to make possible a much larger gas/liquid exchange area per unit volume of the reactor, as well as a reduction of the educt's path length in the catalyst solution.

There have only been three studies reported for SLPC molten salt systems (all in fixed bed systems): (1) the hydrodechlorination of CCl_4 with H_2 over several silica-supported $PdCl_2$-containing molten salt catalysts[17], (2) the dissociation of methanol to synthesis gas over supported molten Cu-Cl-KCl or CuCl-$ZnCl_2$-KCl on SiO_2, Al_2O_3, and $ZnSiO_3$ supports[18] and (3) the catalytic oxidation of diesel exhaust particulates over various supported binary eutectic salt mixtures[19].

B. Fluidized Bed Considerations

Compared to fixed beds, fluidized bed reactors are most suitable for the performance of a SLP-catalyzed reaction because of their inherent isothermal behavior, high volumetric throughputs, and very large surface area for reaction provided by the fluidized particles[20]. The suitability for SLP catalyzed reactions has been demonstrated using a hydroformylation reaction catalyzed by an Rh complex dissolved in di-Me glycol phthalate on a fluidized alumina support[21-27]. Although fluidization of support particles with liquid loadings has been demonstrated, a critical need is to understand the effect of liquid loading, liquid properties, support particle properties and fluidized bed hydrodynamics on the tendency of the fluidized bed to defluidize, the result of particle agglomeration. [28-30]. It is particularly crucial to understand these effects for the particular system of interest, supported molten carbonate salts on compatible particles at reaction conditions.

The presence of a molten salt liquid phase dispersed within a solid phase support powder induces undesirable agglomerative effects resulting from liquid capillary forces between the particles. *Extensive exploratory work presented below indicates that suitable support particles can be fluidized in the presence of a substantial loading of molten salt. The support particles must be non-reactive with the molten salt, must have internal porosity to contain the SLPC internally, and must have substantial inertia (size, density, and velocity) to overcome agglomerative surface forces.*

IV. Experimental Results and Discussion

There is no previous work (other than the preliminary results to be presented here) in which molten salt has been investigated for use as an SLPC for fluidized particles. Our preliminary studies have focused on (1) selecting suitable support materials for the molten carbonates, (2) thermodynamic calculations to assess the capture of trace contaminants for these systems, (3) high temperature "proof-of-concept" fluidization studies to assess the viability of fluidization in the presence of a SLP molten salt, (4) particle force balance modeling to develop an understanding of the preliminary experimental results, and (5) design of a hydrodynamically similar surrogate system to allow ambient temperature studies.

A. Viable Support Material Selection

A support material must be selected that is low cost and compatible with Na_2CO_3/K_2CO_3 and raw coal gasifier product gases at typical gasifier outlet temperatures, i.e. 815°C (1088 K). Since fluidized bed coal combustion processes typically use fluidizable SiO_2 (500 to 1000 μm average particle size) particles and since spray dried Al_2O_3 is readily available and used extensively for fluidized bed catalytic processes (such as fluidized catalytic cracking, FCC), a first inclination would be to extend the use of these materials to the SLP carbonate catalyst systems. However, for coal

Table 1. Free Energy Minimization Products (Reactivity of Na_2CO_3 with SLPC Support Materials)

T = 1100 K

(1 mole Na_2CO_3 + 9 moles Support → Products)

Support	Gaseous Products	Other Products
SiO_2	1 mole (~ 100% CO_2) $Na_2CO_3 + 9SiO_2 \rightarrow CO_2 + (19/3)SiO_2 + (1/3)Na_6Si_8O_{19}$	19/3 mole SiO_2; 1/3 mole $Na_6Si_8O_{19}$
Al_2O_3	1 mole (~ 100% CO_2) $Na_2CO_3 + 9\ Al_2O_3 \rightarrow CO_2 + 2\ Na^*Al_9O_{14}$	2 moles $Na^*Al_9O_{14}$
SiC	None $Na_2CO_3 + 9\ SiC \rightarrow 8\ SiC + 2\ C + (Na_2O)(SiO_2)$	8 moles β-SiC; 2 moles C; 1 mole $(Na_2O)(SiO_2)$
ZrO_2	None (No Reaction Products @ 1100 K)	1 mole Na_2CO_3; 9 moles ZrO_2
Fe_2O_3	None (No Reaction Products @ 1100 K)	1 mole Na_2CO_3; 9 moles Fe_2O_3
CaO	None (No Reaction Products @ 1100 K)	1 mole Na_2CO_3; 9 moles CaO

combustion systems, sodium (Na) salts are "sticky" and have been reported to create problems in fluidized bed boilers (SiO_2 based fluidization) fed with high Na content coal[31,32]. In order to address this concern, preliminary free energy minimization calculations using the F*A*C*T (Facility for the Analysis of Chemical Thermodynamics) software[33] were carried out in order to screen potential support materials by evaluating equilibrium products for various Na_2CO_3/support material systems at T = 1100 K and P = 1 atm. Some of the results are summarized in Table 1. Clearly, SiO_2, Al_2O_3, and SiC are reactive with Na_2CO_3 and, hence, are not suitable catalyst supports for the system of interest. Sodium carbonate (Na_2CO_3) reacts with SiO_2 to produce sodium silicate ($Na_6Si_8O_{19}$) and reacts with Al_2O_3 to produce β-alumina ($Na^*Al_9O_{14}$) as the thermodynamically stable products for these systems, respectively. Silicon carbide (SiC) was looked at as a possible high temperature stable species, however, preliminary thermodynamic calculations indicate the formation of sodium metasilicate [$(Na_2O)(SiO_2)$] as the stable product. This investigation indicates that Fe_2O_3, CaO, and ZrO_2 are stable non-reactive materials in the presence of Na_2CO_3 at T = 1100 K. The Fe_2O_3 particles are readily available and low cost. Fe_2O_3 also has a high density (5.28 g/cc) and can be obtained in relatively large particle sizes with various internal porosities. Hence, Fe_2O_3 is a desirable fluidized bed support material for the SLP molten salt process.

B. Trace Contaminant Capture

Thermodynamic calculations have been extended to evaluate equilibrium product species for systems of raw coal gasifier (synthesis gas) product gases/10% excess air, both without and with (Table 2) Na_2CO_3/support materials being present at temperatures of 1100 and 1200K. It is clear in

evaluating the equilibrium products of combustion for a typical gasifier using Illinois No. 6 coal (air feed)/10% excess air[34] that SO_x forms at large concentrations (> 3000 ppm) for all temperatures and that the formation of NO_x increases with increased temperature. Hence, a most desirable situation is one in which the complete combustion can be carried out at reduced temperatures (catalytic) where the resulting NO_x concentration is low (<10 ppm for T < 1100 K) and where SO_x formation is virtually eliminated. Such a process appears viable from the preliminary free energy minimization results summarized in Table 2. In this case, for combustion at temperatures less than approximately 1100 K and with Na_2CO_3/support present at 1 mole Na_2CO_3 per 100 moles of gasifier product (+ 10% excess air), the resulting SO_x concentration is < 1 ppm and NO_x concentration is < 10 ppm (see Table 2). As noted in earlier referenced studies with molten carbonates, typical molten salt bath combustion operating temperatures are well below 1100 K, thus supporting low NO_x concentrations. It is important to note (Table 2) that volatile NaOH concentration will be low (≈ 3 ppm at T = 1100K).

Table 2. Calculated Combustion Products Using SLP Na_2CO_3 Catalyst

(100 moles feed gas + 1 mole Na_2CO_3 + 9 moles support)

Mole Fraction of Product Gas	
N_2:	0.7510
CO_2:	0.1675
H_2O:	0.0751
Ar:	0.0043

Moles of SLPC/Support
9 moles CaO, Fe_2O_3, or ZrO_2
0.57 mole Na_2SO_4
0.43 mole Na_2CO_3

ppm of Product Gas	T = 1100K	1200K
O_2:	2114	2114
CO:	< 1	< 1
H_2:	< 1	< 1
SO_x:	< 1	< 1
NO_x:	9	21
NaOH:	3	33

C. Fluidization of Supported Molten Salt

"Proof-of-concept" experiments demonstrated that porous support particles can be fluidized in the presence of substantial molten salt loadings (between 5 and 10 wt%). These positive experimental results, along with a fundamental understanding of the governing force balances (i.e. liquid capillary vs. inertial, etc.) to be discussed below, provide motivation for surrogate system studies.

A high temperature fluidized bed reactor for the loading of particles with molten salts under fluidized conditions was designed, constructed, and instrumented for "proof-of-concept" fluidization studies[35,36]. The approach taken was to start out at low temperatures using a low melting temperature salt ($LiNO_3$, mp = 251°C [524 K]) supported on SiO_2 and Al_2O_3. Fluidization studies were carried out initially for non-porous silica particles (350, 550, 850, 1100 μm; see Figure 3) and then for porous alumina (450 μm, SA = 318 m^2/g, Figure 4) and silica (110 to 227 μm, Figure 5) support particles at temperature up to 500°C. Experiments were carried out to investigate the parameters needed to fluidize support particles in the presence of a substantial liquid loading of molten salt. A 7.5 cm diameter Inconel™ fluidized bed with a perforated plate distributor was constructed and placed within a vertical tube furnace for heating. Three hundred fifty grams (350 g) of support particles were fluidized with air. The bed was equipped with various differential pressure transmitters to study the fluidization of support particles. Minimum fluidization velocity was determined at ambient and operating temperature for every particle system. The addition of salt to the bed was carried out for superficial gas velocities, u_o, that ranged up to 3 times minimum, i.e. $u_o/u_{mf} = 3$. The salt was added

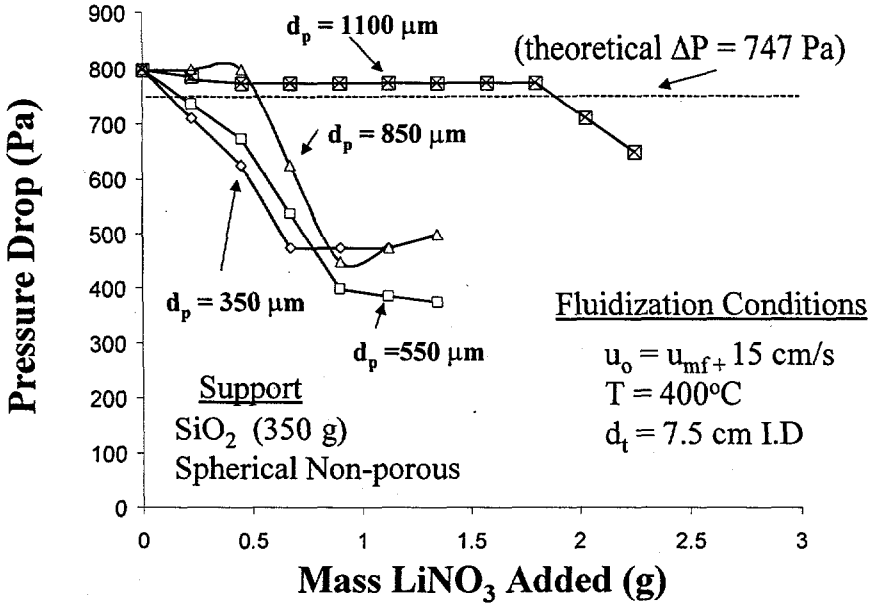

Figure 3. Effect of $LiNO_3$ Addition on Fluidization for Non-porous Silica Particles (T = 400°C)

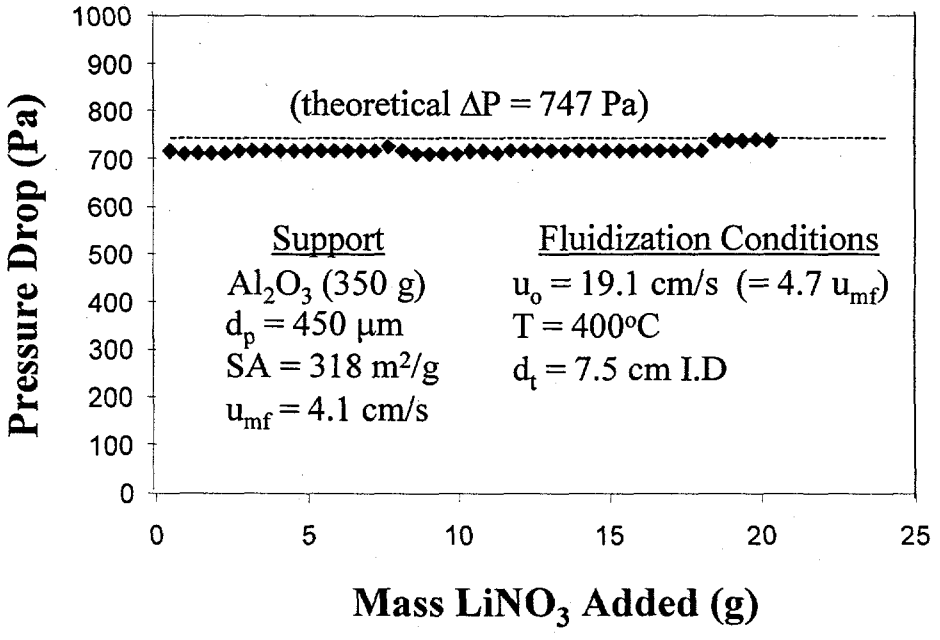

Figure 4. Effect of $LiNO_3$ Addition on Fluidization for Porous Alumina Particles (T = 400°C)

as a concentrated aqueous salt solution that was injected into the fluidized bed from above. The water flashed off with an initial decrease in bed temperature that quickly recovered within seconds. Material balances were carried out on the salt after each run. Inductively coupled plasma (ICP) analytical methods were used to verify the salt loading. For example, when using $LiNO_3$ as the additive salt, Li concentration was measured by ICP in the spent support particles after the runs so as to verify its addition to the bed.

De-fluidization occurred almost immediately upon addition of salt to non-porous silica (glass beads) particles (Figure 3). The particles agglomerate and drop out of fluidization, resulting in a decreased bed pressure drop. It was found, however, that larger particles could maintain fluidization for increased salt loadings. Nonetheless, only 1.75 g $LiNO_3$ could be added per 350 g of support, even for 1100 μm diameter particles.

Substantial $LiNO_3$ (> 20 g $LiNO_3$/350 g support) could be loaded within the porous fluidized alumina support particles (450 μm, 318 m^2/g, Figure 4). The fluidization in the bed was maintained for over a week during this experiment. The experiment was shut down prior to any de-fluidization. These results clearly indicate that porous support particles are needed so the liquid phase can fill part

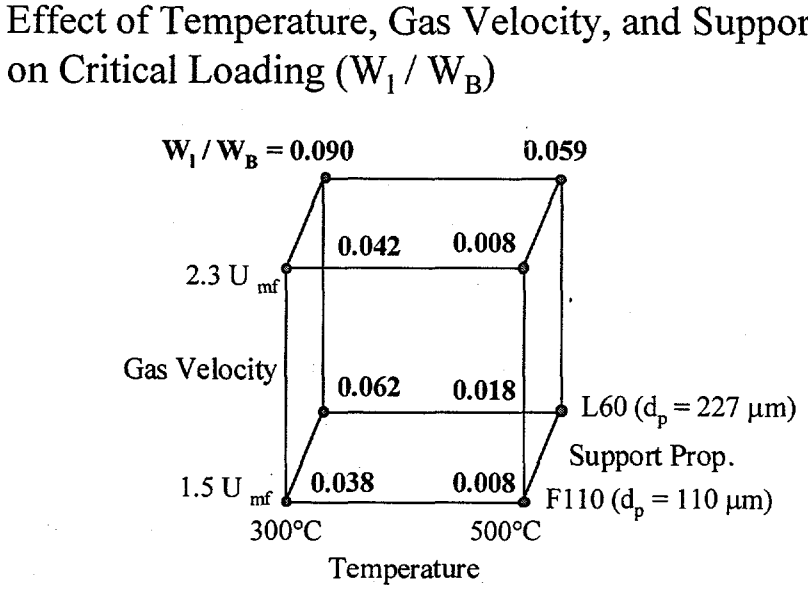

Figure 5. Designed Experiment Results for Molten $LiNO_3$ Loading

of the internal pore volume while allowing the external agglomerative liquid capillary surface forces to be minimized.

A designed experiment (see Figure 5) was carried out to determine the effect of temperature (300°C, 500°C), superficial gas velocity (u_o/u_{mf} = 1.5, 2.3), and support particle diameter (110, 227 μm SiO_2) on the amount of molten $LiNO_3$ that could be loaded on the porous particles prior to de-fluidization. Salt loading values of up to 0.090 kg molten salt loading per kg bed support material

(i.e. W_l/W_B) were sustained under fluidized conditions. Larger particles enable a correspondingly larger critical salt loading. This is because they have fewer surface contacts to form liquid bridges (smaller agglomerates formed) and higher separate particle kinetic energy when fluidized that enable the agglomerates to collide with more energy to break them apart. Increased gas velocity also correlates to having a higher particle kinetic energy. Elevated temperatures reduce the critical salt loading. The gas viscosity increases (smaller N_{Re}), which interacts with the decreasing liquid coating's surface tension and viscosity. It is believed that these competing phenomena cause the capillary forces due to liquid bridging to be smaller. Again, these results confirmed that porous support particles can be fluidized in the presence of a substantial liquid loading (almost 10% by mass).

D. Force Balance Analysis

A modified force balance is considered in order to better understand the experimental results. It accounts explicitly for liquid capillary cohesive forces between porous particles supporting liquids. The Ergun equation was developed as a correlation for determination of pressure drop in a non-flowing bed of particles[37]:

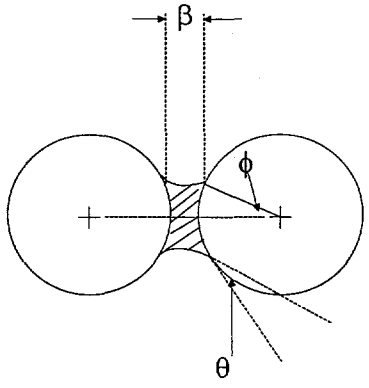

Figure 6. Pendular Liquid Bridge Between Two Spherical Particles

$$\Delta P(g_c)/l = 150\,((1-\varepsilon_{mf})^2/(\phi_s^2\varepsilon_{mf}^3))\,\mu_g\,u_{mf}/(d_p^2) + 1.75\,((1-\varepsilon_{mf})/(\phi_s\,\varepsilon_{mf}^3))\,u_{mf}^2\,\rho_g/d_p \quad (1)$$

At the point of minimum fluidization, according to Wen and Yu[38]:

$$\Delta P(g_c)/l = (1-\varepsilon_{mf})\,g\,(\rho_p - \rho_g) \quad (2)$$

Wen and Yu[38] equated these two equations and developed a relationship for calculating the minimum fluidization velocity, u_{mf}. However, for many systems operating at elevated temperatures, u_{mf} of the particles departs from the traditional value due to a "stickiness" that develops between the particles[39-41]. At this temperature, often referred to as the sintering temperature, interparticle forces[42,43] become significant. Liss et al.[44] added a cohesive force term accounting for a surface stress to equation (2):

$$\Delta P(g_c)/l = (1-\varepsilon_{mf})\,g\,(\rho_p - \rho_g) + 6\,S\,(1-\varepsilon_{mf})/d_p \quad (3)$$

They carried out experiments to develop the cohesive number's, $N_{Co} = 6S/((\rho_p - \rho_g)d_p g)$, dimensionless temperature functionality at minimum fluidization conditions.

In the case where a liquid phase is intentionally introduced into the bed of particles, a different expression for the cohesive force is needed. Research has shown that capillary forces[45], when present, are typically an order of magnitude higher than van der Waals forces[46-48], unless a separate liquid phase is introduced[49,50] in which case they are much higher[51]. When this happens, only the interparticle forces due to the surface tension of the liquid need to be considered.

The cohesive force that results during a pendular state of liquid loading seen in Figure (6) for a fully wetting liquid (i.e. contact angle of zero) is a function of the liquid surface tension, particle

diameter, and ϕ (the angle defining the size of the liquid bridge) seen in figure 6. Clift[52] expresses this relationship for a smooth spherical surface as:

$$F_c = \pi d_p \sigma [1/(1 + \tan(\phi)] \quad (4)$$

Equation (4) does not account explicitly for liquid loading, q, i.e. liquid contained within the pores of porous fluidized support particles (a measure of the pore volume filled with liquid). By introducing the lumped parameter, $\psi = \psi$(q, surface properties), equation (4) can be rewritten as:

$$F_c = \pi d_p \sigma \psi \quad (5)$$

Equation (5) is the cohesive force with units of force. It more explicitly accounts for SLPC surface properties via ψ.

If we divide F_c by the volume of the sphere and $1/(1 - \varepsilon_{mf})$ we can derive an expression for the cohesive force per unit volume:

$$F_c/V = 6\sigma\psi(1 - \varepsilon_{mf})/d_p^2 \quad (6)$$

Similar to the process used by Liss et al[44], we now rewrite equation (3) as:

$$\Delta P(g_c)/l = (1 - \varepsilon_{mf})\, g\, (\rho_p - \rho_g) + 6\sigma\psi(1 - \varepsilon_{mf})g_c/d_p^2 \quad (7)$$

Equating equations (1) and (7) and rearranging we obtain:

$$150\, ((1 - \varepsilon_{mf})\, /(\phi_s^2\, \varepsilon_{mf}^3))\, N_{Re} + (1.75\, /(\phi_s \varepsilon_{mf}^3))\, N_{Re}^2 = N_{Ga} + 6\, (N_{Re} / N_{Ca})\, \psi \quad (8)$$

where:

$$N_{Ga} = (\rho_g\, (\rho_p - \rho_g) d_p^3\, g)/\mu_g^2 \quad (9)$$

$$N_{Re} = \rho_g u_{mf} d_p/\mu_g \quad (10)$$

$$N_{Ca} = u_{mf}\, \mu_g/(\sigma g_c) \quad (11)$$

E. Surrogate System

From the force balance relationship derived above, N_{Re}, N_{Ga}, and the ratio of N_{Re}/N_{Ca} should be identical for the real and surrogate systems to be hydrodynamically similar. In addition, low vapor pressure liquids should be used so as to minimize volatile loss of liquid during the studies. Silicone oils are a desirable liquid for surrogate investigations[53-55].

The targeted real process for investigation is one using 1 mm Fe_2O_3 support particles loaded with molten Na_2CO_3 at 950°C (1223 K) being fluidized with a typical fuel gas/10% excess air mixture (see Table 3). The calculated base surrogate system is one using 400 μm silica support particles loaded with silicone oil at ambient temperature and fluidized with a 50/50 gas mixture of argon/nitrogen. The ambient temperature studies will evaluate the effect of varying particle porosity, ε_p, and liquid loading, q on ψ. A comparison of the real and base surrogate systems is given in Table

3. The surrogate system will allow ambient temperature experimentation for determining the functionality of ψ in the real Fe_2O_3 supported molten Na_2CO_3 process.

It is important to note that this approach can be applied to an understanding of liquid capillary forces for SLPC systems in general. For example, N_{Re}, N_{Ga}, and N_{Re}/N_{Ca} can be adjusted and fixed for different systems (systems other than the supported molten salt system).

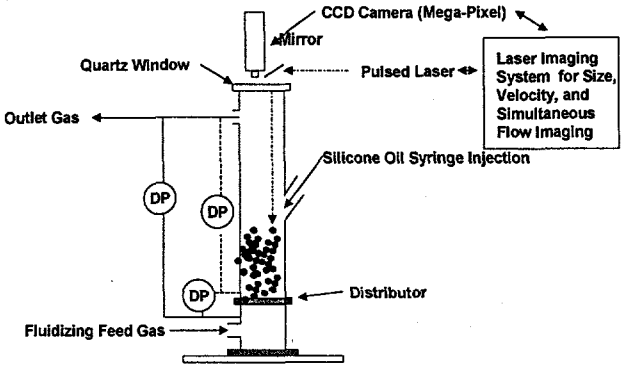

Figure 7. Fluidized Bed Apparatus for Liquid-Capillary Force Balance Studies Using Surrogate Silicone Oil/Silica System

Table 3. Similarity Between Real System and Ambient Temperature Surrogate System

	Real System	Surrogate System
Particle Diameter, d_p (m)	Fe_2O_3 ; 1×10^{-3}	SiO_2 ; 4×10^{-4}
Particle Density, ρ_p (kg/m^3)	" ; 5280	" ; 2650
Gas Density, ρ_g (kg/m^3)	Fuel Gas/Air; 0.26	Ar/N_2 ; 1.3
Gas Viscosity, μ_g (kg/m-s)	" ; 4.77×10^{-5}	" ; 1.91×10^{-5}
Liquid Surface Tension, σ (N/m)	Molten Na_2CO_3; 0.206	Silicone Oil; 1.65×10^{-2}
Min. Fluidization Vel., u_{mf} (m/s)	1	0.2
Temperature, T (K)	1223	298
Reynolds Number, N_{Re}	5.45	5.42
Galileo Number, N_{Ga}	5918	5905
Capillary Number, N_{Ca}	2.315×10^{-4}	2.301×10^{-4}
Ratio, N_{Re}/N_{Ca}	23530	23560

Surface tension effects at ambient temperature for other supported liquid systems can be studied by investigating bed behavior using different glycerin/water mixtures.

The primary objectives of this aspect of the research are (1) to understand the origin of the liquid capillary interparticle forces affecting a SLP molten salt fluidized bed process and (2) to quantify these forces so that they can be overcome in practice.

The liquid capillary forces originate from the supported liquid loaded in the pores of the support particles. ψ can be quantified at minimum fluidization conditions from the governing force balance equation derived previously:

$$150\,((1-\varepsilon_{mf})/(\phi_s^2\,\varepsilon_{mf}^3))\,N_{Re} + (1.75/(\phi_s\,\varepsilon_{mf}^3))\,N_{Re}^2 = N_{Ga} + 6\,(N_{Re}/N_{Ca})\,\psi \qquad (8)$$

With ψ determined, the liquid capillary forces can be quantified from our proposed liquid capillary force term for SLPC:

$$F_c = \pi\, d_p\, \sigma\, \psi \qquad (5)$$

A 6.5 cm (2-1/2 inch) I.D. fluidized bed apparatus (made of quartz and Plexiglas™) (Figure 7) was constructed for the experimental program. Typical fluidization parameters such as expanded bed height, L_f, and the minimum fluidization velocity, u_{mf}, are measured by conventional differential pressure (DP) methods employing transmitters[56]. Three DP measurements are available: (1) across the distributor, (2) across the fluidized particles, and (3) across the distributor and fluidized particles.

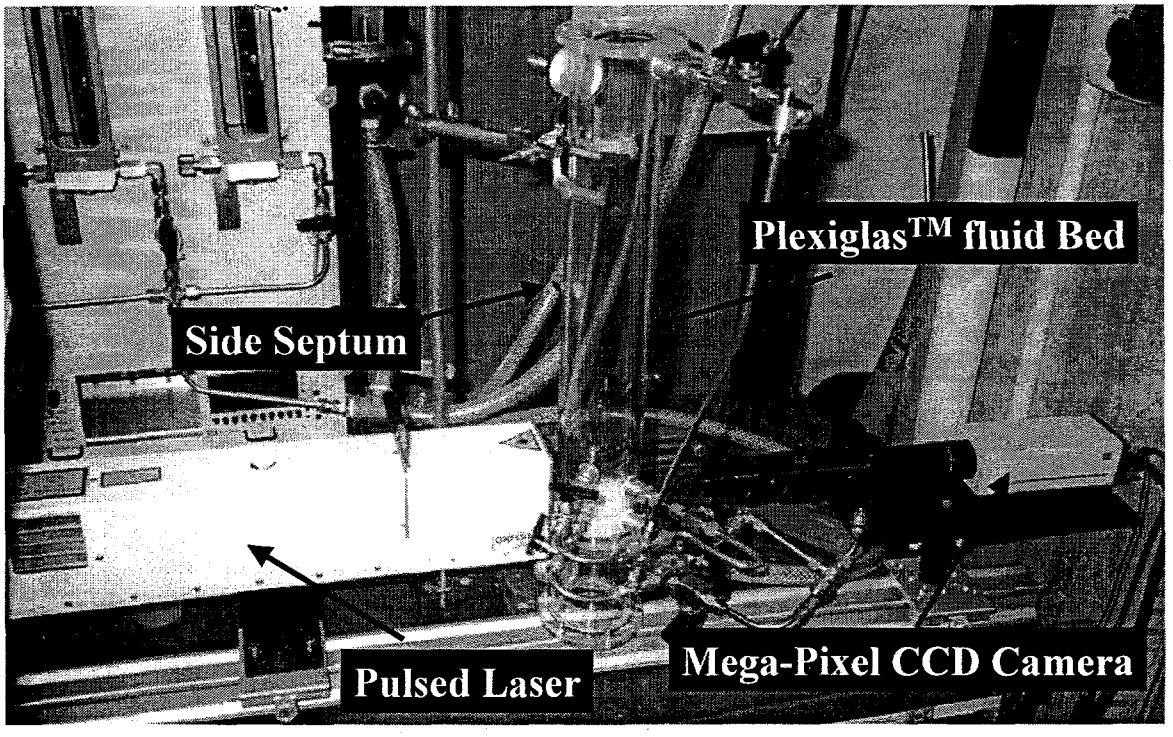

Figure 8. Laser Imaging System Interfaced to Current Laboratory Fluidized Bed (Back Lighting)

The bed is equipped with a side septum, allowing the accurate injection of silicone oil directly into the fluidized bed via a syringe. Gas flow will be controlled using mass flow controllers.

The bed is also equipped with a recently purchased state-of-the-art Oxford Lasers Company Visisizer™ MP complete pulsed laser imaging system (Model HSI1000 pulsed laser; Mega Pixels CCD, Software with Pentium III Computer; Oxford Lasers, Inc.; Acton, MA) for high-resolution imaging. It allows direct measurement of particle size and particle velocity within the upper surface of the bed (when set up for front lighting as shown in Figure 7). It can also be set up horizontally

along the side of the bed with back lit images (fluid bed wall) and allow the visualization of the side of the upper surface of the bed (Figure 8). Particle agglomerate formation can be monitored continuously with this system and important inertial parameters such as particle size (Figures 9 and 10) and velocity can be tracked in real time as a function of liquid loading. Individual particles are tracked via sequential digital snapshots.

The initial approach will be to systematically vary the liquid loading, q, so as to determine its effect on the functionality of ψ. For example, porous 400 μm silica particles (with measured pore volume) will be fluidized with a 50/50 N_2/Ar gas mixture at ambient temperature. The minimum fluidization velocity, u_{mf}, will be determined using standard pressure drop methods. This measurement of u_{mf} will be carried out for different loadings (i.e. q) of silicone oil (e.g. Dow Corning 200® polydimethylsiloxane silicone oil) added by injection. Liquid loading experiments can be carried out for 400μm silica particles of different surface areas and porosities in order to develop an expression for ψ. For a given set of experiments, ψ is determined by evaluating the force balance equation (equation (8)) at the point of minimum fluidization.

Since the values of ρ_p increase with increasing q values according to the equation:

Figure 9. Using the Pulsed Laser for Real Time Imaging of Fluidization Process (top view)

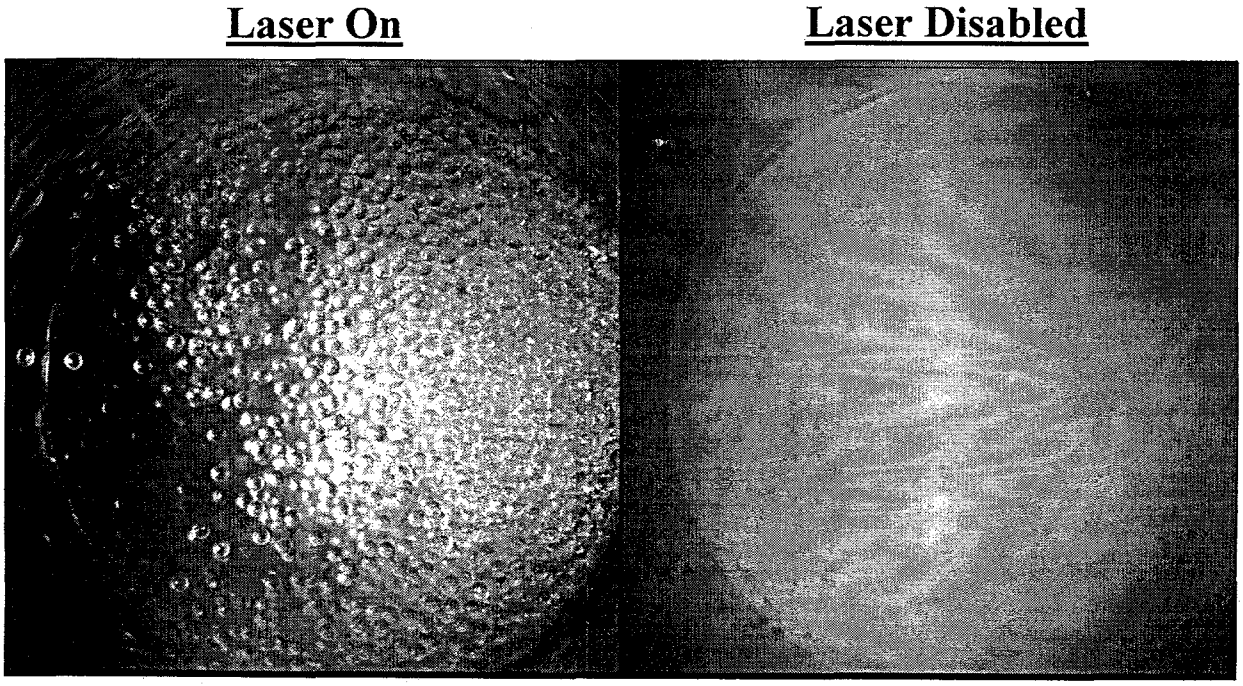

$$\rho_p = \rho_p(@\ q=0) + \varepsilon_p q \rho_l \qquad (12)$$

(assuming no coating of the particle with silicone oil changing the volume – can be verified with the laser system imaging) where ρ_l is the density of the impregnating liquid, u_{mf} values would increase proportionally to q in the absence of interparticle forces. However, Jutka et al.[25] have shown that the

Figure 10. Visisizer™ Output for Measured Particle Size Distribution (from laser real time software) Compared to Sieve

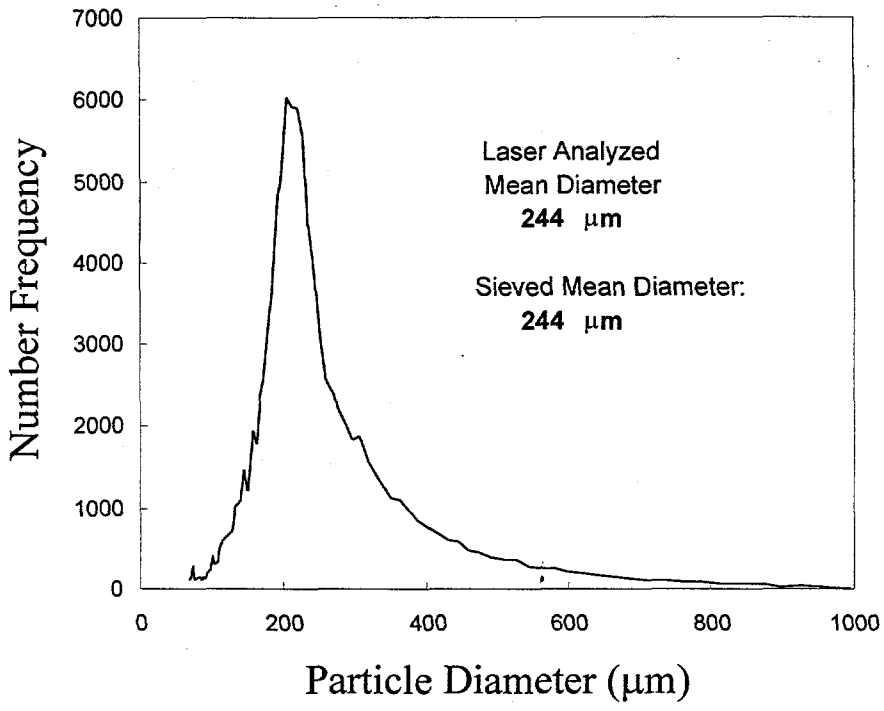

experimentally determined u_{mf} values are higher than the predicted ones and that this difference increases with increased loading, q. As discussed throughout this report, the basis for these forces is the liquid bridges formed between contacting support particles, causing an interaction of the particles due to the Laplace pressure.

We can account for liquid capillary forces in calculating the minimum fluidization velocity, u_{mf}, by re-arranging equation (8):

$$u_{mf} = (\mu_g/(\rho_g d_p)) \{[C_1^2 + C_2(N_{Ga} + N_{SLPC})]^{1/2} - C_1\} \quad (13)$$

where:

$$C_1 = 42.86 (1 - \varepsilon_{mf})/\phi_s \quad (14)$$

$$C_2 = \phi_s \varepsilon_{mf}^3/1.75 \quad (15)$$

$$N_{SLPC} = 6\sigma g_c \rho_g d_p \psi/\mu_g^2 \quad (16)$$

From our theoretical development, the proposed dimensionless number, N_{SLPC}, in equation (13) accounts for the additional energy alluded to by Jutka et al [25] that is required to fluidize the support

particles in the presence of a liquid loading, q. Without this term, equation (13) is identical to that developed by Wen and Yu[38] where they proposed that typical values for C_1 and C_2 for fluidized bed systems are $C_1 = 33.7$ and $C_2 = 0.0408$.

It is critical for successful operation of the SLPC reactor process to understand the origin and effect of liquid capillary forces so that they can be measured and overcome in the process. Future work should be directed towards this understanding.

V. Summary and Conclusions

Thermodynamic calculations show that Fe_2O_3 particles are non-reactive in the presence of sodium salts and that supported Na_2CO_3 allows the capture of trace contaminants found in raw synthesis gas. Experimental and force balance modeling studies indicate that molten salts can be supported on fluidized porous support particles and that inertial forces need to dominate (large dense particles are most desirable). The future research includes experimental studies for a surrogate system to investigate the liquid capillary forces for molten Na_2CO_3 supported on 1 mm diameter fluidized Fe_2O_3 particles in a synthesis gas combustion environment. The novel molten carbonate SLPC process has potentially broad application for the simultaneous catalytic oxidation of synthesis gas with in-situ capture of trace contaminants (S, Cl, etc.) (i.e. hot gas cleanup).

VI. Nomenclature

C_1: = 42.86 $(1 - \varepsilon_{mf})/\phi_s$, used in equation (13)
C_2: = $\phi_s \cdot \varepsilon_{mf}^3/1.75$, used in equation (13)
d_p: = diameter of a sphere having the same volume as that of a particle (m)
d_t: = tube diameter (m)
F_c: = cohesive force (N)
g: = gravitational acceleration (=9.81 m/s^2)
g_c: = conversion factor (= 1 $kg \cdot m/N \cdot s^2$)
L_f: = expanded bed height (m)
l: = distance up fluidized bed (m)
N_{Ca}: = dimensionless Capillary Number ($=u_{mf} \cdot \mu_g/(\sigma \cdot g_c)$
N_{Co}: = dimensionless Cohesion Number ($=6 \cdot S/((\rho_p - \rho_g) \cdot d_p \cdot g)$)
N_{Ga}: = dimensionless Galileo Number ($=(\rho_g \cdot (\rho_p - \rho_g) \cdot d_p^3 \cdot g)/\mu_g^2$)
N_{Re}: = dimensionless Reynolds Number at minimum fluidization ($=\rho_g \cdot u_{mf} \cdot d_p/\mu_g$)
N_{SLPC}: = derived dimensionless SLPC Number ($=6 \cdot \sigma \cdot g_c \cdot \rho_g \cdot d_p \cdot \psi/\mu_g^2$)
q: = loading factor, fraction of pore volume filled with liquid
S: = surface stress ($kg/m \cdot s^2$)
SA: = surface area per mass of a support particle (m^2/g)
T: = temperature (K)
u_o: = superficial gas velocity (m/s)
u_{mf}: = minimum fluidization velocity (m/s)
V: = volume (m^3)
W_B: = total mass of fluidized bed support material (kg)
W_l: = total mass of liquid loaded on fluidized bed support material (kg)

Greek Letter

ψ: = proposed dimensionless liquid capillary force term for SLPC
ε_{mf}: = fluidized bed voidage at minimum fluidization
ε_p: = particle porosity (voidage within a support particle)
ϕ: = angle defining the size of the liquid bridge for contacting wetted spheres
ϕ_s: = sphericity of a particle
μ_g: = gas viscosity ($kg/m \cdot s$)
ρ_g: = gas density (kg/m^3)
ρ_l: = liquid density (kg/m^3)
ρ_p: = particle density (kg/m^3)
σ: = surface tension (N/m)
ΔP: = pressure drop across fluidized bed (N/m^2)

VII: References

[1] Edwards, B.H., J.N. Paullin, and K. Coghlan-Jordan, "Emerging Technologies for the Control of Hazardous Wastes," J. Hazard Mat., 12, 201 (1985).

[2] Freeman, H.M., "Innovative Thermal Processes for the Destruction of Hazardous Wastes," AIChE Symp. Ser., 81 (243), 139 (1985).

[3] Freeman, H.M., D.A. Olexsey, D.A. Oberacker, and R.E. Mournighan, "Thermal Destruction of Hazardous Waste – A State of the Art Review," J. Hazard. Mat., 14, 103 (1987).

[4] Oppelt, E.T., "Hazardous Waste Destruction," Environ. Sci. Technol., 20 (4), 312 (1986).

[5] Upadhye, R., "Molten Salt Takes the Bang Out of High Explosives," http://www.llnl.gov/str/Upadhye.html (2000).

[6] Greenberg, J., "Method of Catalytically Inducing Oxidation of Carbonaceous Materials by the Use of Molten Salts," U.S. Patent 3647358 (1972).

[7] Edwards, B., J. Paullin, and K. Coghlan-Jordan, "Emerging Technologies for the Destruction of Hazardous Wastes – Molten Salt Combustion," Pollution Technology Rev., 99, 146 (1983).

[8] Johanson, J., S. Yosim, L. Kellogg, and S. Sudar, "Elimination of Hazardous Wastes by the Molten Salt Oxidation Process," Proc. Annu. Res. Symp., 8th. PN83-210450, 2344 (1983).

[9] Stelman, D., A. Stewart, S. Yosim, and R. Gay, "Treatment of Mixed Wastes by the Molten Salt Oxidation Process," Therm. Treat. Radioact. Hazard. Chem. Mixed. Med. Waste. Proc. Incineration. Conf. 11th, 795 (1992).

[10] Upadhye, R., C. Pruneda, and B. Watkins, "Molten Salt Destruction of Energetic Material Wastes as an Alternative to Open Burning, Environ. Sci. Res., 51, 267 (1996).

[11] Yosim, S. and K. Barclay, "Destruction of Hazardous Wastes by Molten Salt Combustion," Proc. Natl. Conf. Hazard. Waste Manage., 146 (1978).

[12] Meyer, C., U. Richers, and D. Hesse, "Distribution of Liquids in Porous Systems and its Relationship to the Stability of Supported Liquid Phase Catalysts, Hung. J. Ind. Chem., 22 (3), 191 (1994).

[13] Rony, P., "Diffusional Kinetics within Supported Liquid Phase Catalysts, J. Catalysis, 14, 142 (1969).

[14] Hoffmeister, M. and D. Hesse, "The Influence of the Pore Structure on the Operational Behavior of Supported Liquid Phase Catalysts," Chem. Eng. Sci., 45 (8), 2575 (1990).

[15] Gottsleben, F., M. Hoffmeister, and D. Hesse, "Liquid Distribution in Porous Support Materials and Model Calculations on the Exchange Behavior of Supported Liquid Phase Catalysts," DECHEMA Monogram 122 (Katalyse), 269 (1991).

[16] Kolodziej, A.S. and J. Rogut, "A Study of the Internal Diffusion of Gases in Porous Catalysts in the Presence of a Liquid Phase," Chem. Eng. Process., 31 (4), 255 (1992).

[17] Wu, X., Y.A. Letuchy, and D.P. Eyman, "Catalytic Hydrodechlorination of CCl_4 over Silica-Supported $PdCl_2$-containing Molten Salt Catalysts: The Promotional Effects of $CoCl_2$ and $CuCl_2$, J. Catalysis, 161 (1), 164-177 (1996).

[18] Schmitz, A.D. D.P. Eyman, and K.B. Gloer, "Highly-active Methanol Dissociation Catalysts Derived from Supported Molten Salts," Energy Fuel, 8 (3), 729-740 (1994).

[19] Jelles, S.J., B.A.A.L. van Setten, M. Makkee, and J.A. Moulijn, "Supported Liquid PhaseCatalysts: A New Approach for Catalytic Oxidation in Diesel Exhaust Particulate Emission Control," Catalysis and Automotive Pollution Control IV, 116, 667-674 (1998).

[20] Ohlrogge, M., "Untersuchungen zum Wirbelschichteinsatz bei der Hydroformylierung von Propen mit Fluessigfilm-Traegerkatalysatoren," Ph.D. Dissertation, University of Hannover, Germany (1988).

[21] Brusewitz, R. and D. Hesse, "Use of Supported Liquid Phase Catalysts in Fluidized Bed Reactors," DECHEMA Monogram 122 (Katalyse), 283 (1991).

[22] Brusewitz, R. and D. Hesse, "Problems in Use of Supported Liquid-Phase Catalysts in Fluidized Bed Reactors," Chem. Eng. Technol., 15, 35-389 (1992).

[23] Hesse, D. and M.S. Redondon de Beloqui, "Effect of Pore Structure on the Operational Behavior of Supported Liquid Phase Catalysts," DECHEMA Monogram 118 (Katalyse), 305 (1989).

[24] Janus, H. and D. Hesse, "Use of Chromatography for Studying the Percolation Probability of Impregnated Support Systems," DECHEMA Monogram 118 (Katalyse), 287 (1989).

[25] Jutka, C., R. Bruesewitz, and D. Hesse, "Investigations on the use of Supported-Liquid-Phase Catalysts in Fluidized Bed Reactors," AIChE Symp. Ser., 88 (289), 122 (1992).

[26] Richers, U. and D. Hesse, "Stability of Supported Liquid Phase Catalysts," Chem. -Ing. – Tech., 64 (7), 630 (1992).

[27] Yin, Y., M. Te, F.-Y. Jiao, G.-G. Su, and R.-X. Gao, "Study of Supported Liquid Phase Catalysts for Hydroformylation of Olefins Contained in FCC Dry Gas," Proc. Int. Conf. Pet. Refin. Petrochem. Process., 2, 614, Int. Acad. Publ., Beijing (1991)

[28] Tardos, G., D. Mazone, and R. Pfeffer, "Destabilization of Fluidized Beds due to Agglomeration. Part 1. Theoretical Model," Canadian J. Chem. Eng., 63, 377 (1985).

[29] Lian, G.P., C. Thornton, and M.J. Adams, "Discrete Particle Simulation of Agglomerate Impact Coalescence," Chem. Eng. Sci., 53 (19), 3381-3391 (1998).

[30] Tardos, G. and R. Pfeffer, "Chemical Reaction Induced Agglomeration and Defluidization of Fluidized Beds,""Powd. Technol., 85, 29-35 (1995).

[31] Jeffers, S., "Control Problem Waste Feeds in Fluid Beds," Chemical Engineering Progress, May, 59-63 (1999).

[32] Vuthalauru, H.B., T.M. Linjewile, D.-K. Zhang, and A.R. Manzoori, "Investigations into the Control of Agglomeration and Defluidization During Fluidized Bed Combustion of Low-rank Coals, Fuel, 78, 419-425 (1999).

[33] Thompson, W.T., A.D. Pelton, and C.S. Bale, "Facility for the Analysis of Chemical Thermodynamics [FACT]," Thermfact ltd., Mount-Royal, Quebec, Canada (1985).

[34] Mangold, E.C., and M.A. Muradaz, Coal Liquefaction and Gasification Technologies, Ann Arbor Science Publishers, Ann Arbor (1982).

[35] Hilbert, P.M., P.J. Czerpak, and A.W. Weimer, "Supported Liquid Phase Molten Salt Catalytic Fluidized Bed Reactor for Combined Hot Gas Cleanup/Low Temperature Combustion," paper presented at the 1999 Annual AIChE Meeting, Dallas, November (1999).

[36] Weimer, A.W., P.J. Czerpak, and P.M. Hilbert, "Supported Molten Salt Fluidized Bed Process," U.S. Provisional Patent Application, April (1999).

[37] Ergun, S., "Fluid Flow Through Packed Columns," Chem. Eng. Progr., 48, 89 (1952).

[38] Wen, C. and Y. Yu, "A Generalized Method for Predicting the Minimum Fluidization Velocity, AIChE Journal, 12, 610 (1966).

[39] Mikami, T., H. Kamiya, and M. Horioi, "The Mechanism of Defluidization of Iron Particles in a Fluidized Bed," Powder Technol., 89, 231 (1996).

[40] Seville, J., H. Silomon-Pflug, and P. Knight, "Modeling of Sintering in High Temperature Gas Fluidization," Powder Technol., 97, 160 (1998).

[41] Formisani, B., R. Giromonte, and L. Mancuso, "Analysis of the Fluidization Process of Particle Beds at High Temperature," Chem. Eng. Sci., 53 (5), 951-961 (1998).

[42] Xie, H.Y., "the Role of Interparticle Forces in the Fluidization of Fine Powders," Powder Technol., 94 (2), 1099-1108 (1997).

[43] Ma, X.X. and K. Kato, "Effect of Interparticle Adhesion Forces on Elutriation of Fine Powders from a Fluidized Bed of a Binary Particle Mixture," Powder Technol., 95 (2), 93-101 (1998).

[44] Liss, B., T.R. Blake, A.M. Squires, and R. Bryson, "Incipient Defluidization of Sinterable Solids," in Fluidization (4th International Conference held in Kashikojima, Japan), D. Kunii and R. Toei, Editors, United Engineering Trustees, New York, 249-256 (1984).

[45] Schubert, H., "Capillary Forces – Modeling and Application in Particulate Technology, "Powder Technol., 37, 107 (1984).

[46] Rietema, K., "Theoretical Derivation of Interparticle forces," in The Dynamics of Fine Powders, 65-93, Elsevier Science Publishers (New York), 1991.

[47] Hamaker, H., "The London Van der Waals Attraction Between Spherical Particles," Physica, 4, 1058 (1937).

[48] Lennard-Jones, J., "The Equation of State of Gases and Critical Phenomena," Physica, 4, 941 (1937).

[49] Seville, J.P.K. and R. Clift, "The Effect of Thin Liquid Layers on Fluidization Characteristics," Powder Technol., 37, 117-129 (1984).

[50] Yamazaki, R., N.-S. Han, Z.-F. Sun, and G. Jimbo, "Effect of Chemisorbed Water on Bed Voidage of High Temperature Fluidized Bed," Powder Technol., 84, 15-22 (1995).

[51] Massimilla, L. and G. Donsi, "Cohesive Forces Between Particles of Fluid-Bed Catalysts," Powder Technol., 15, 253-260 (1970).

[52] Clift, R., Particle-Particle Interactions in Gas-Particle Systems," in Powtech '85 Particle Technology, Inst. Chem. Engrs. Symp. Ser. No. 91, 27-44 (1985).

[53] Wright, P.C. and J.A. Raper, "Examination of Dispersed Liquid-Phase Three-Phase Fluidized Beds: Part 1. Non-porous, Uniform Particle Systems, Powder Technol., 97, 208-226 (1998).

[54] Wright, P.C. and J.A. Raper, "Role of Liquid Bridge Forces in Cohesive Fluidization," Trans. IChemE, 76 (A), 753-760 (1998).

[55] Rhodes, M. J. and L.J. McLaughlin, "Predicting the Influence of Added Liquid on Gas Fluidized Bed Behavior," paper presented at the 1999 Annual AIChE Meeting, Dallas (November, 1999).

[56] Geldart, D. (editor), Gas Fluidization Technology, John Wiley & Sons (1986).

Appendix A: Thermodynamic Modeling

A.1) FACT Introduction

This section focuses on the results of thermodynamic equilibrium Gibbs Free Energy Minimization Calculations completed using the Facility for the Analysis of Chemical Thermodynamics (FACT) Equilib program module (Bale, Pelton et al. 1996). A variety of combustible gas streams were combined with an array of salts and support particles. The systems developed were tested under low/high temperature conditions and oxidizing/reducing conditions. The results of the FACT simulations were analyzed to determine which systems proved the most effective in capturing sulfur and mercury along with lowering NO_x production.

For an overview detailing Gibbs Free Energy Minimization Calculations for ideal systems using the Newton-Raphson Solution of the Gibbs Free energy equations, see Smoot's Pulverized–Coal Combustion and Gasification (Smoot and Pratt 1979). The analysis is mathematically cumbersome, but is quite elegant in its ability to predict equilibrium compositions systems based on a fixed output temperature and pressure. The Equilib program module was run in both the ideal gas and ideal solution mode for all of the simulations.

A.2) FACT Input Models

Two different models were developed to determine the molar ratios of gaseous feed constituents in combination with an array of salts and supports. The first model used CH_4 as the combustible reactant mixed with 10% excess air. The pre-mixed fuel/air was then used to fluidize a bed of fine ceramic particles with a designated salt loading. The model takes into account the effect of temperature, pressure, viscosity and varying voidage at minimum fluidization to obtain accurate molar ratios for input into the FACT Equilib program. This model showed that the ε_{mf} was a weak function of temperature and particle size with values typically being around 0.5. Only a limited number of actual simulations were completed with this model; therefore, the details of the results are not included here. The results exhibited the same trends in terms of sulfur capture and relative reactivity of the support with the chosen salt seen using the second model..

The second model for which a majority of the equilibrium calculations were performed used the off-gas from different coal gasifiers as the combustible reactant. In this model, it was assumed: (1) that the bed voidage at minimum fluidization was 0.5 based on the results from the first model, (2) the salt loading was 10 wt %, and (3) the support had no internal pore volume. These assumptions greatly simplified the necessary calculations to determine the molar ratios of the reactants to be inputted into FACT. Figure A.1 describes how the models were developed.

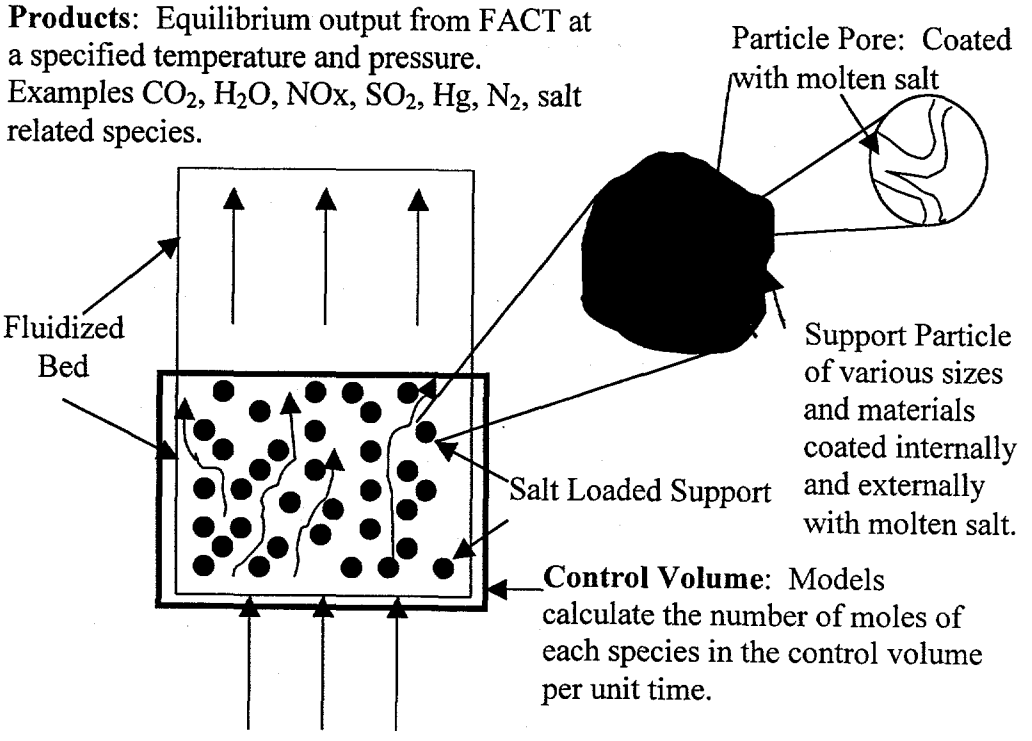

Figure A.1 FACT entering Molar Ratios Models Diagram.

The four main purposes of these calculations centered on demonstrating that:

(1) The sulfur present in the off-gas from a typical gasification process is captured in the liquid/solid phase when combusted in the presence of various molten salt/support systems.

(2) The ability to run the combustion reaction at lower temperatures and maintain high combustion efficiencies due to the known oxidative catalytic effect of molten carbonates and nitrates. The result of lower temperature operation being the desirable reduction in the production of NO_x compounds.

(3) Non-reactive salt/support systems exist.

(4) The removal of trace amounts of mercury present in the off-gas from a coal gasifier is possible.

A.3) Potential Supports

The first desirable quality in a support is its chemical stability in the presence of various molten salts at elevated temperatures. Once this is established, cost is mostly likely the next most important characteristic. From the cost standpoint, silica and alumina are the most attractive, in light of their widespread availability in myriad particle size ranges and pore distributions. Unfortunately, as will be demonstrated, these two supports are not stable in the presence of the majority of molten salts investigated. A list of supports investigated is contained in Table A.1.

A.4) Potential Salts

In the case of the molten salts, the initial selection criteria were based on the salt's melting point and thermal stability. The carbonates were best suited for a temperature range just over 800°C (1472°F) due their melting point and their known oxidative catalytic effect. The nitrates were selected due to their catalytic potential at lower temperatures and lower melting points for low temperature capture in molten carbonate fuel cell systems. Na_2WO_4 was chosen due to its melting point being lower than 800°C and the potential for forming Na_2SO_4. Na_2SO_4 was chosen, as a baseline, assuming that it would not capture additional sulfur from the gas phase. Table A.2 contains the salt species chosen for experimentation along with some of their important properties.

The first step involved determining which salts/supports did not react with each other. It was assumed that, if the salt and support reacted with each other, the system would have been even more difficult to fluidize. From Tables A.1 and A.2, a matrix was created to determine which salt/support systems are stable over a specified temperature range. Table A.3 lists the molar ratios of salt per support based on one mole of support assuming a 10% weight loading of salt.

Equilib simulations were run from 1100-1500 K while varying the temperature by 50 K increments for the all salts with the exception of the nitrates which all dissociates by 1100 K. The nitrate simulations were run from 500-1100 K. FACT Equilib output was inspected to determine if a reaction occurred between the

salt and support for each system. Table A.4 lists the **potential supports in yellow** as 'a' and 'e'. Table A.4 clearly shows that both silica and alumina are reactive with all of the carbonates from 1100-1500 K. They form various glassy compounds.

Table A.1 List of Potential Supports and Important Properties.

Support	Molecular Weight	Density ($gm/cm^{3)}$
SiO_2	60.08	2.6
Al_2O_3	101.96	3.97
ZrO_2	123.22	6.67
NiO	74.69	5.89
Fe_2O_3	159.69	5.28
WC	195.86	15.63
TiO_2	79.88	3.84
CaO	56.07	3.34
$(Ca)_3(PO_4)_2$	310.07	3.14

Table A.2 Selected Salt Species and Important Properties.

Salt	Molecular Weight	Melting Point (C)	Density (gm/cm^3)
Na_2CO_3	105.89	858	1.9547 @ 900°C
K_2CO_3	138.2	899	1.8747 @ 950°C
Li_2CO_3	73.89	618	1.806 @ 800°C
Na_2WO_4	293.82	698	3.79 @ 780°C
Na_2SO_4	142.04	884	2.04 @ 950°C
Cs_2CO_3	325.82	527	Not Available
B_2O_3	69.62	450	1.52 @ 1030°C
$LiNO_3$	68.95	252	1.7022 @ 400°C
$NaNO_3$	84.99	307	1.836 @ 400°C
KNO_3	101.1	334	1.7537 @ 500°C
$AgNO_3$	169.87	212	3.76754 @ 400°C

A.5) Gasifier Outputs Mixed with 10% Excess Air

The next step in this section was to determine a baseline to compare the results for systems containing salt. To accomplish this, outputs from six typical gasifiers were chosen and mixed with 10% excess air and allowed to equilibrate over the desired temperature range without any salt present. Table A.5 lists the off-gas from various types of coal gasifiers. The gasifiers typically use different rank coal and varying steam/oxygen or steam/air feeds during the gasification process. Table A.6 lists the mole fractions of gasifier species mixed with 10% excess air, which were then entered into the FACT Equilib program. The output from the FACT Equilib program represents the equilibrium products from a high temperature combustor used to combust various gasifier product gases with 10% excess air.

Table A.3 Molar Ratios between Salts/Support Based on 1 mole of Support and 10 wt% Loading.

Matrix (i,j)	SiO_2	Al_2O_3	ZrO_2	NiO	Fe_2O_3	WC	TiO_2	CaO	$(Ca)_3(PO4)_2$
Na_2CO_3	0.06	0.11	0.13	0.08	0.17	0.21	0.08	0.06	0.33
K_2CO_3	0.05	0.08	0.10	0.06	0.13	0.16	0.06	0.05	0.25
Li_2CO_3	0.09	0.15	0.19	0.11	0.24	0.29	0.12	0.08	0.47
Na_2WO_4	0.02	0.04	0.05	0.03	0.06	0.07	0.03	0.02	0.12
Na_2SO_4	0.05	0.08	0.10	0.06	0.12	0.15	0.06	0.04	0.24
Cs_2CO_3	0.02	0.03	0.04	0.03	0.05	0.07	0.03	0.02	0.11
B_2O_3	0.01	0.16	0.20	0.12	0.25	0.31	0.13	0.09	0.50
LiNO3	0.10	0.16	0.20	0.12	0.26	0.32	0.13	0.09	0.50
NaNO3	0.08	0.13	0.16	0.10	0.21	0.26	0.10	0.07	0.41
KNO3	0.07	0.11	0.14	0.08	0.18	0.22	0.09	0.06	0.34
AgNO3	0.04	0.07	0.08	0.05	0.10	0.13	0.05	0.04	0.20

Table A.4 Reactivity of Various Salt/Support Systems.

Salt, Support	SiO_2	Al_2O_3	ZrO_2	NiO	Fe_2O_3	WC	TiO_2	CaO	$(Ca)_3(PO_4)_2$
Na_2CO_3			a	a	a	*b*		a	*b*
K_2CO_3			a	a	a	*b*		a	a
Li_2CO_3				a		*b*		a	a
Na_2WO_4	a	a	a	a	a	*b*	a	a	a
Cs_2CO_3	a	a		a	a		a	a	a
$LiNO_3$				e	e			e	e
$NaNO_3$			e	e	*b*			e	*b*
KNO_3			a	a	a		*b*	a	a
$AgNO_3$									

'a' The salt and support are non-reactive over the entire temperature range tested.
'b' The salt and support are only non-reactive over a part of the temperature range tested.
'c' The salt and support are reactive over the entire temperature range tested.
'd' The salt is unstable over the entire range tested.
'e' The salt and support do not react over the entire temperature range, but the salt does dissociate at the higher temperatures of the range tested.

Table A.5 Gasifier Outputs for 100 moles of Product.

	Lurgi (Teggers 1979)	**Winkler(Teggers 1979)**	**Kopper-Totzek (Teggers 1979)**	**Texaco (Mangold, Muradaz et al. 1982)**	**IGCC**	**Shell-Koppers (Mangold, Muradaz et al. 1982)**
Air/O_2 Feed	O_2	O_2	O_2	Air	Air	O_2
Type of Coal	UNK	Brown	UNK	low-bituminous	UNK	W. German Bituminous
CO	11.55	45.00	57.00	19.46	22.90	65.60
CH_4	10.65	1.50	0.10	0.10	1.00	0.40
H_2	43.15	38.45	28.70	11.61	9.50	31.30
COS	0.15	0.05	0.03	0.05	0.00	0.00
H_2S	0.30	0.15	0.20	0.52	0.10	0.40
NH_3	0.00	0.00	0.00	0.11	0.00	0.00
CO_2	32.88	13.99	12.49	7.68	4.40	1.50
C_2H_6	0.90	0.00	0.00	0.00	0.00	0.00
N_2	0.25	0.70	1.20	59.76	60.00	0.60
O_2	0.00	0.00	0.00	0.00	0.00	0.00
Ar	0.15	0.10	0.20	0.68	2.07	0.20
Hg*	1.06E-6	4.12E-6	5.22E-6	1.78E-6	2.10E-6	6.00E-6
HCl*	0.02	0.06	0.08	0.03	0.03	0.09
Total Moles	100	100	100	100	100	100

* Hg and HCl were not included in referenced gasifier outputs.

Table A.6 Species Mole Fraction with 10% Excess Air and Gasifier Output for Various Gasifiers.

	Lurgi	**Winkler**	**Koppers-Totzek**	**Texaco**	**IGCC**	**Shell-Koppers**
CO	3.24E-2	1.34E-1	1.75E-1	1.06E-1	1.17E-1	1.83E-1
CH_4	2.99E-2	4.48E-3	3.07E-4	5.47E-4	5.12E-3	1.12E-3
H_2	1.212E-1	1.15E-1	8.81E-2	6.35E-2	4.86E-2	8.74E-2
COS	4.213E-4	1.49E-4	9.21E-5	2.74E-4	0.00	0.00
H_2S	8.427E-4	4.48E-4	6.14E-4	2.84E-3	5.12E-4	1.12E-3
NH_3	0.00	0.00	0.00	6.02E-4	0.00	0.00
CO_2	9.236E-2	4.18E-2	3.83E-2	4.20E-2	2.25E-2	4.19E-3
C_2H_6	2.53E-3	0.00	0.00	0.00	0.00	0.00
N_2	5.69E-1	2.09E-3	5.51E-1	6.85E-1	6.93E-1	5.71E-1
O_2	1.51E-1	0.00	1.46E-1	9.51E-2	1.02E-1	1.51E-1
Ar	4.213E-4	2.99E-4	6.14E-4	3.72E-3	1.06E-2	3.07E-4
Hg*	2.97E-9	1.23E-8	1.60E-8	9.74E-9	1.07E-8	1.68E-8
HCl*	4.45E-5	1.85E-4	2.40E-4	1.46E-4	1.61E-4	2.52E-4
Total Moles	1	1	1	1	1	1

Significant gaseous species were selected from the Equilib equilibrium outputs and entered into a spreadsheet. The type of gasifier did not have a significant

affect on the systems' equilibrium mole fractions for various gaseous species. In light of this fact, the Koppers-Totzek gasifier output was chosen to represent all of gasifiers outputs. Figure A.1 contains the equilibrium speciation for the Koppers-Totzek gasifier. The carbon monoxide and hydrogen mole fractions are significantly lower due to the oxidation process. The hydrogen mole fraction was less than 1E-10, which is the reason it is not included in Figure A.2. There are high concentrations of CO_2 and H_2O, which is expected after oxidizing the hydrogen and carbon monoxide. The primary species of concern: NO_x, SO_x, and Hg are all present. As expected, NO_x production increases with temperature from about 20 ppm-v at 1100 K up to 300 ppm-v at 1500 K. The SO_2 concentration is a weak function of temperature with only a slight concentration increase as the temperature goes up. Its typical concentration in the Koppers-Totzek system is around 800 ppm. Figure A.3 shows SO_2 mole fractions for all of the gasifiers. The differences in the amount of SO_2 are proportional to the amount of sulfur present in the original gas stream. The Texaco Gasifier equilibrium concentration of SO_2 is the highest, but it also has the highest concentration of H_2S and COS in its FACT input listed in Table A.5. If the SO_2 mole fractions for the respective gasifiers are normalized by the amount of sulfur entering the system, the result seen in Figure A.4 shows that all normalized concentrations are all essentially one.

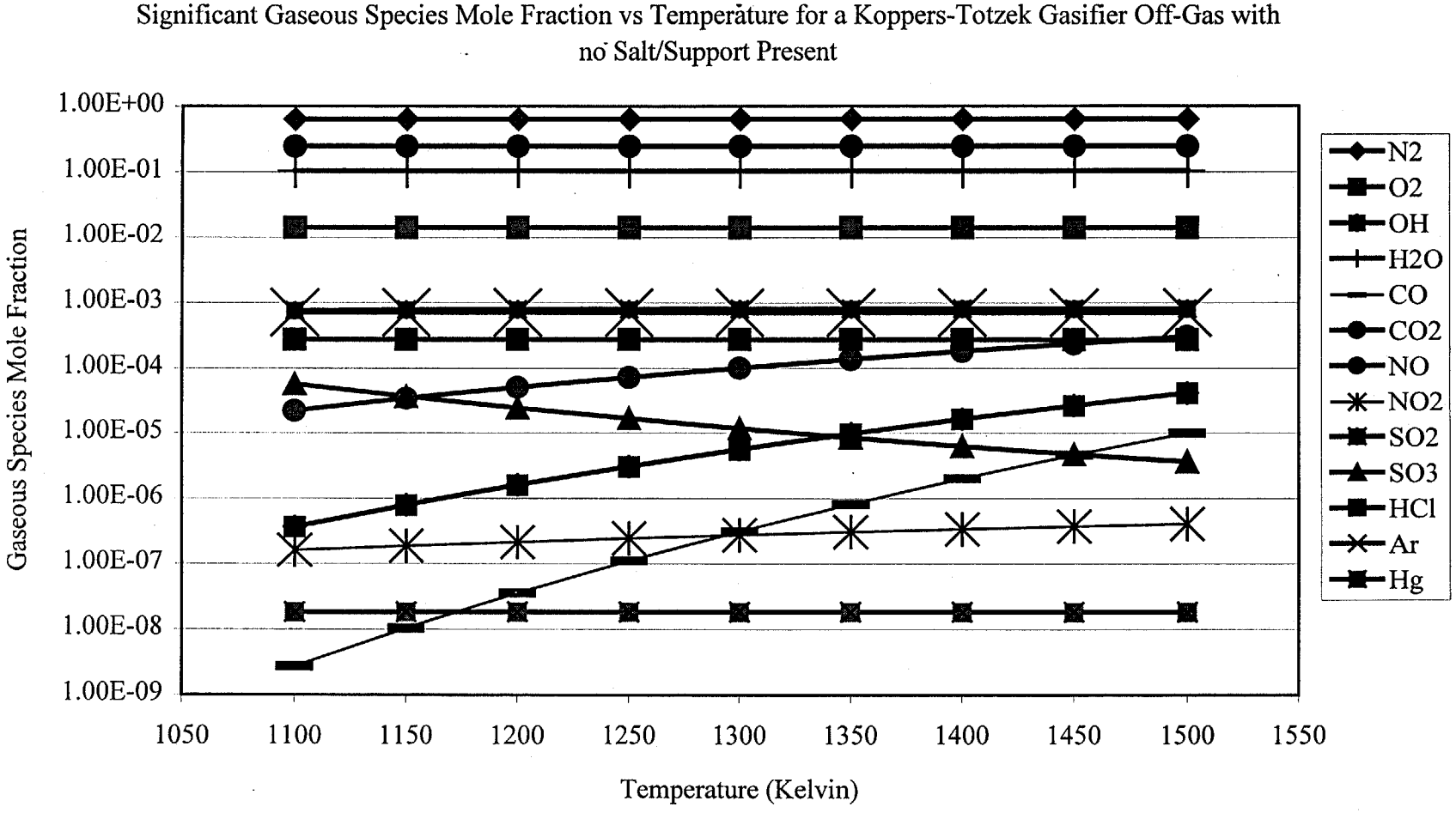

Figure A.2 Significant Gaseous Species for a Koppers-Totzek Off-Gas with no Salt/Support mixed with 10% Excess Air.

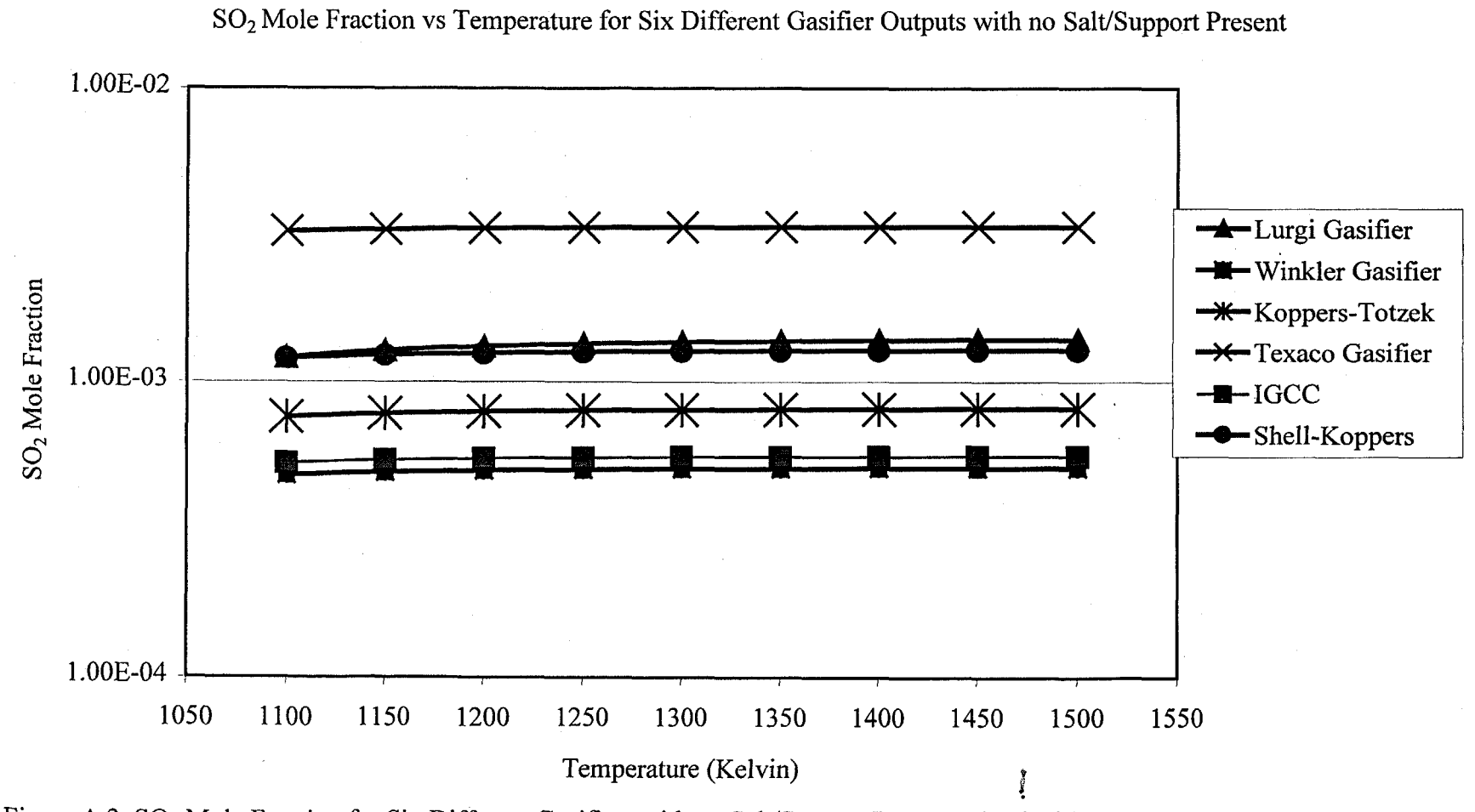

Figure A.3 SO_2 Mole Fraction for Six Different Gasifiers with no Salt/Support Present mixed with 10% Excess Air.

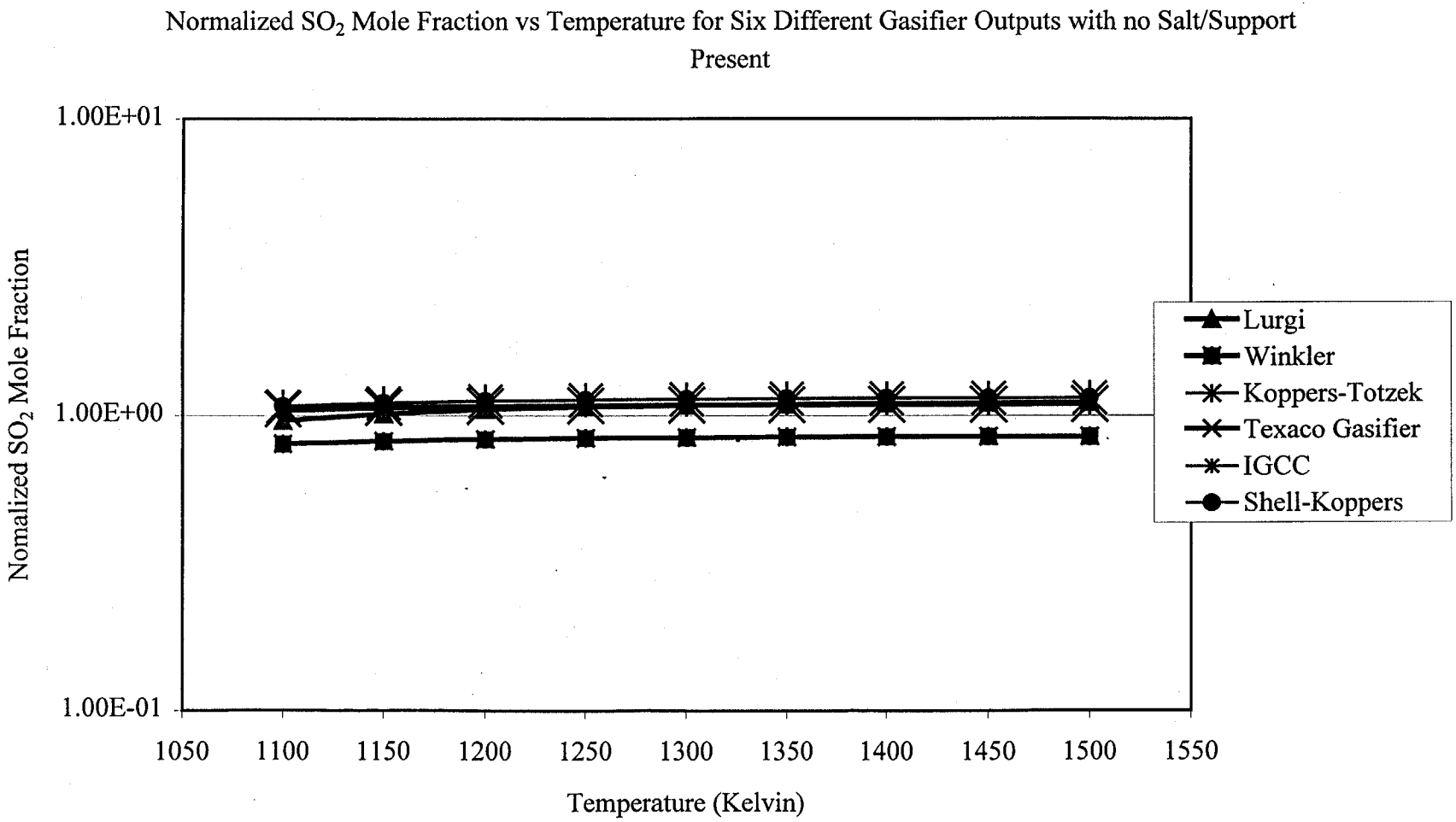

Figure A.4 Normalized SO_2 Mole Fraction for Six Different Gasifiers with no Salt/Support Present mixed with 10% Excess Air.

A.6) Salt/Support/Gasifier Equilibrium Simulations

There were four primary regions investigated as dictated by in Figure A.5. High temperature simulations were completed using the carbonates along with Na_2WO_4, Na_2SO_4, and B_2O_3 in conjunction with the supports found in Table A.1. Each simulation was assigned a three number designator in the form of (i.j.k). 'i', 'j', and 'k' represent the number of the salt, support, and gasifier off-gas used respectively. For example, experiment (1.3.3) signifies a system with Na_2CO_3, ZrO_2, and the Koppers-Totzek Off-Gas. Oxidizing condition simulations were completed to test the applicability of these systems as a hot gas clean up strategy where the combustion and clean up processes physically occur within the same fluidized bed reactor. The reducing condition simulations were analyzed to ascertain the feasibility of SLPC with molten salts as a hot gas clean up strategy for molten carbonate fuel cells.

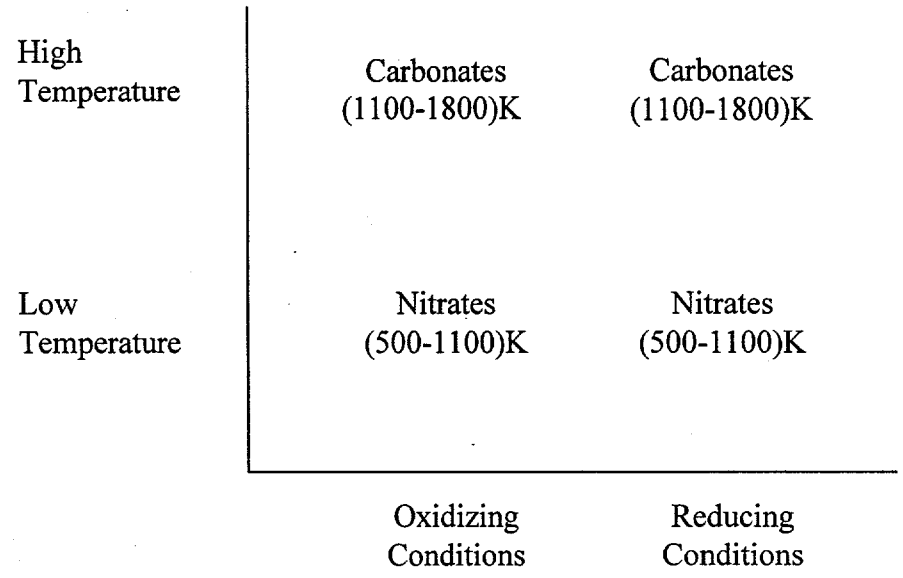

Figure A.5 Experimental Design Matrix for FACT Simulations.

A.6a) High Temperature/Oxidizing Conditions Simulations

The initial purpose for exploring the equilibrium speciation with FACT was to investigate systems at high temperature under oxidizing conditions to demonstrate in-situ capture of sulfur in the form of a molten sulfate and reduced NO_x formation compared to current fossil fuel power generation processes. Looking back to Table A.4, there are a large number of possible salt, support, and gasifier combinations that warrant examination. Even after eliminating the systems where the salt and the support react, there are still too many simulations to run. Having seen that the gasifier input does not dramatically affect the equilibrium speciation, simulations were only run for one type of gasifier in each region investigated.

The first step for the high temperature region under oxidizing conditions involved picking a gasifier, in this case the Koppers-Totzek (k=3) was chosen. Next, simulations were run from 1100-1800 K for each salt with a corresponding non-reactive support. The FACT molar ratio inputs are listed in Table A.7. As long as the support is non-reactive with the salt and gaseous constituents in the system, its presence should not affect the equilibrium speciation. In most cases ZrO_2 satisfied this criterion except for the cases where lithium or cesium was present in the system. In these cases, NiO was substituted as the non-reactive support. Figure A.6 shows the SO_2 mole fraction for the high temperature salts. The nitrates were not included in this section due their lack of thermal stability in the temperature region investigated.

After inspecting Figure A.6, a number of observations can be made. First, the supported salts, Na_2WO_4 and B_2O_3, do not capture any sulfur. No liquid or solid sulfur species form during Na_2WO_4's and B_2O_3's respective simulations and their individual SO_2 concentrations are very similar to that of Na_2SO_4. The Na_2SO_4's SO_2 concentration does start to increase relative to Na_2WO_4's and B_2O_3's at 1600 K due to the gradual thermal decomposition of Na_2SO_4.

The second finding, which is more exciting than the first, is that all of the carbonates do in fact capture sulfur in the solid/liquid phase as a sulfate, thus, reducing the amount of SO_2 in the gas phase. It appears that Cs_2CO_3 is the most effective for capturing sulfur, until a mistake in the FACT thermodynamic database was discovered. The thermodynamic database has Cs_2CO_3 (s) as the stable species above 800 K. Below 800 K Cs_2CO_3 (liquid) is the stable species. With this in mind, Cs_2CO_3 would undergo a phase transition at 800 K, but in the direction of decreasing entropy as temperature increases. With results for Cs_2CO_3 suspect, K_2CO_3 is the best candidate from the perspective of SO_2 reduction. The carbonates as a group consistently do a better job capturing sulfur at the lower portion of the temperature range.

Another concern with using the molten salts at elevated temperatures is the amount of salt related gaseous species that form. Figures A.7-A.10 all plot the significant salt related gaseous species for the individual molten carbonate systems. From the four graphs, it appears that Na_2CO_3, K_2CO_3, and Li_2CO_3 have approximately the same gaseous species concentrations as a function of temperature. At temperatures greater than 1400 K the formation of the gaseous salt hydroxide becomes significant reaching concentrations of 10000 ppm. From these figures it is obvious that running the process at the lowest temperature that is kinetically feasible

will facilitate reducing the dissociation of the molten salt and reduce the amount of sulfur leaving the system in the form of a gaseous sulfate.

Table A.7 FACT entering Molar Ratios for High Temperature Salts, a Koppers-Totzek Off-Gas, and a Non-Reactive Support under Oxidizing Conditions.

	(1.3.3)	(2.3.3)	(3.4.3)	(4.3.3)
Support	1.000E+00	1.000E+00	1.000E+00	1.000E+00
Salt	1.293E-01	9.907E-02	1.123E-01	4.660E-02
CO	6.129E-05	5.825E-05	5.955E-05	5.351E-05
CH_4	1.075E-07	1.022E-07	1.045E-07	9.388E-08
H_2	3.086E-05	2.933E-05	2.999E-05	2.694E-05
COS	3.226E-08	3.066E-08	3.134E-08	2.817E-08
H_2S	2.150E-07	2.044E-07	2.090E-07	1.878E-07
NH_3	0.000E+00	0.000E+00	0.000E+00	0.000E+00
CO_2	1.343E-05	1.276E-05	1.305E-05	1.173E-05
N_2	1.930E-04	1.835E-04	1.876E-04	1.686E-04
O_2	5.097E-05	4.845E-05	4.953E-05	4.451E-05
Ar	2.150E-07	2.044E-07	2.090E-07	1.878E-07
Hg	5.608E-12	5.330E-12	5.449E-12	4.897E-12
HCl	8.412E-08	7.995E-08	8.174E-08	7.345E-08

	(5.3.3)	(6.4.3)	(7.3.3)
Support	1.000E+00	1.000E+00	1.000E+00
Salt	9.639E-02	2.547E-02	1.967E-01
CO	5.800E-05	5.177E-05	6.901E-05
CH_4	1.017E-07	9.083E-08	1.211E-07
H_2	2.920E-05	2.607E-05	3.475E-05
COS	3.052E-08	2.725E-08	3.632E-08
H_2S	2.035E-07	1.817E-07	2.421E-07
NH_3	0.000E+00	0.000E+00	0.000E+00
CO_2	1.271E-05	1.134E-05	1.512E-05
N_2	1.827E-04	1.631E-04	2.174E-04
O_2	4.823E-05	4.306E-05	5.739E-05
Ar	2.035E-07	1.817E-07	2.421E-07
Hg	5.307E-12	4.737E-12	6.314E-12
HCl	7.960E-08	7.106E-08	9.472E-08

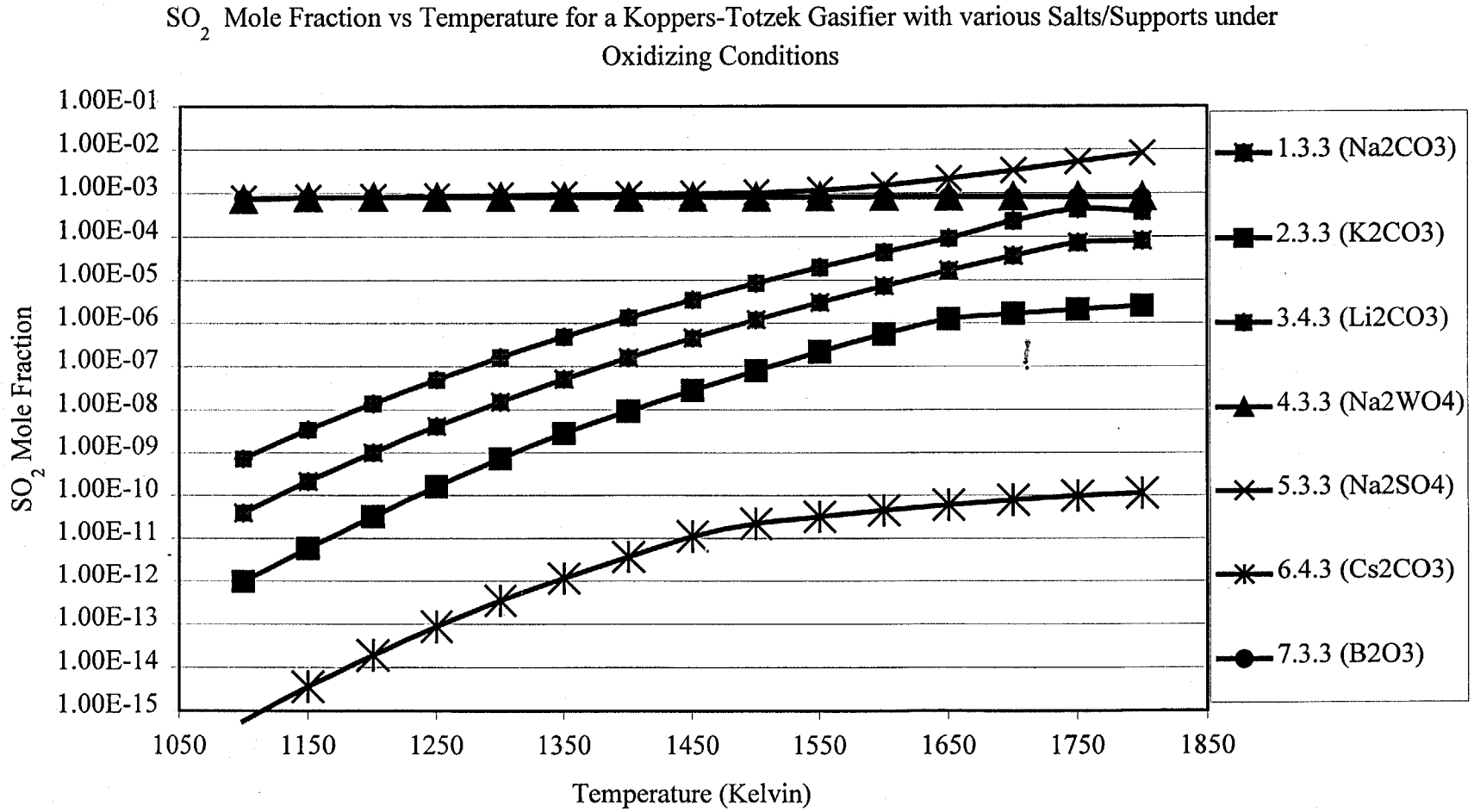

Figure A.6 SO_2 Mole Fraction for a Koppers-Totzek Off-Gas and High Temperature Salts with a Non-Reactive Support under Oxidizing Conditions.

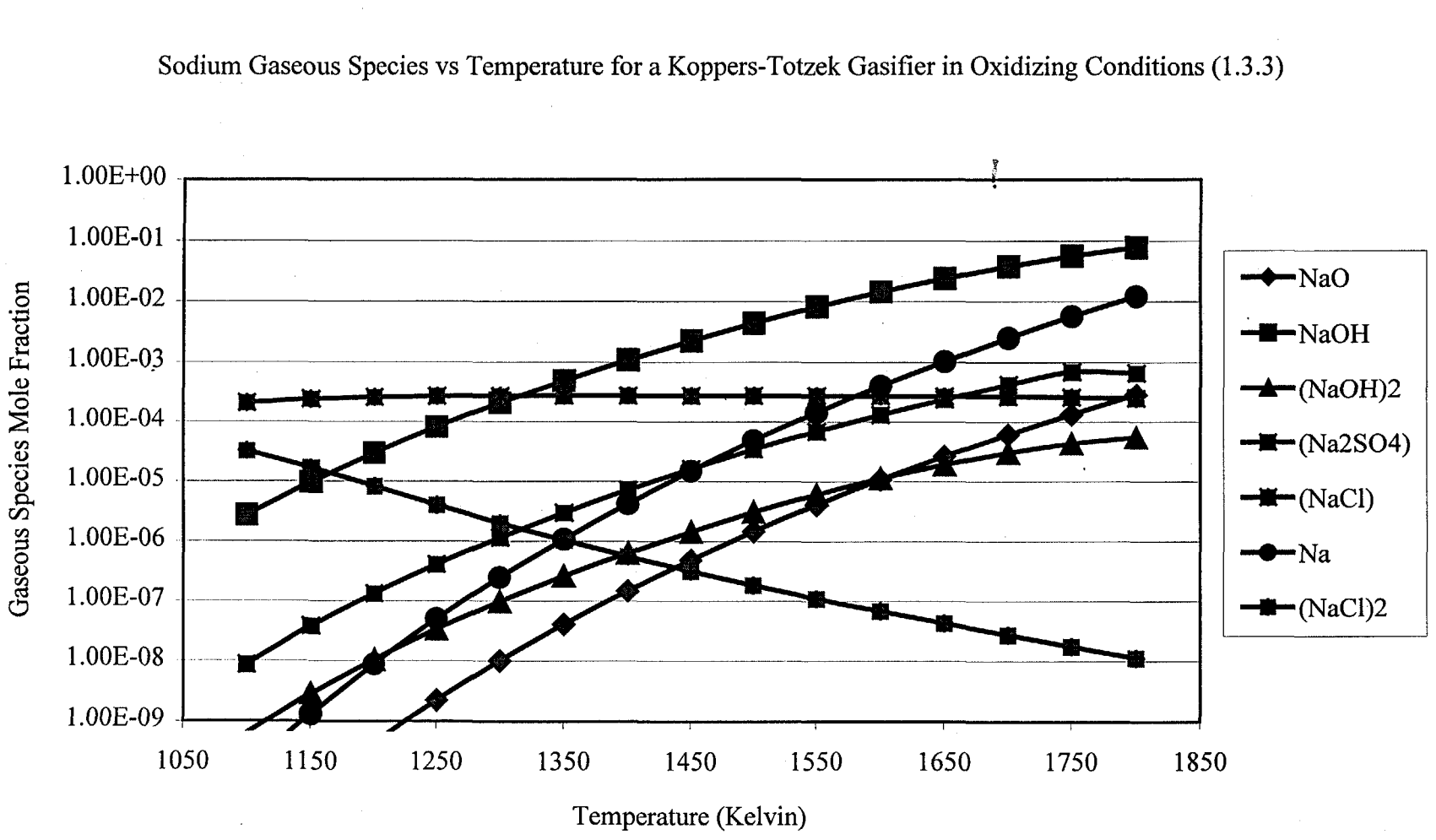

Figure A.7 Sodium Gaseous Species Mole Fraction for Na_2CO_3 and a Koppers-Totzek Off-Gas with ZrO_2 under Oxidizing Conditions (1.3.3).

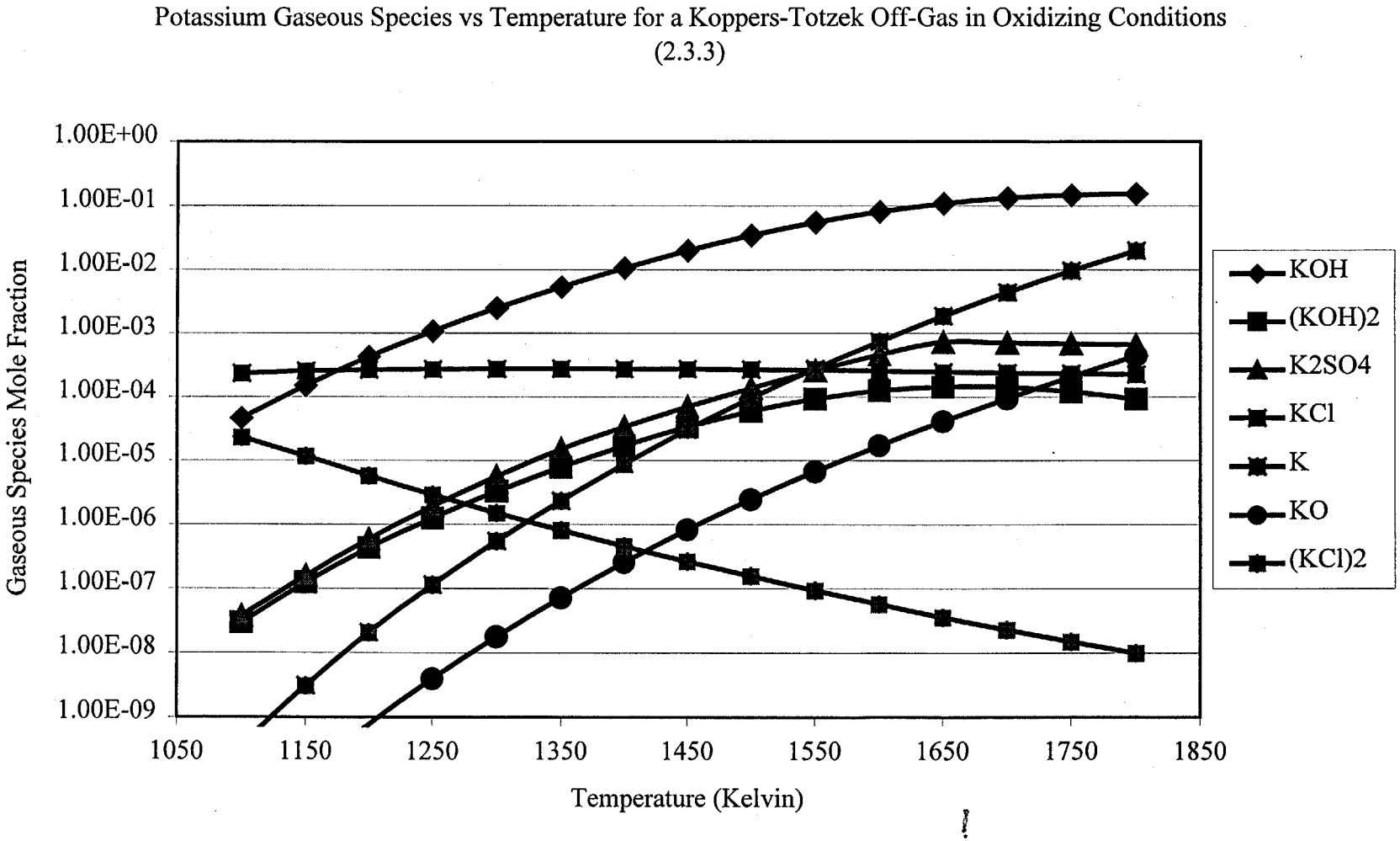

Figure A.8 Potassium Gaseous Species Mole Fraction for K_2CO_3 and a Koppers-Totzek Off-Gas with ZrO_2 under Oxidizing Conditions (2.3.3).

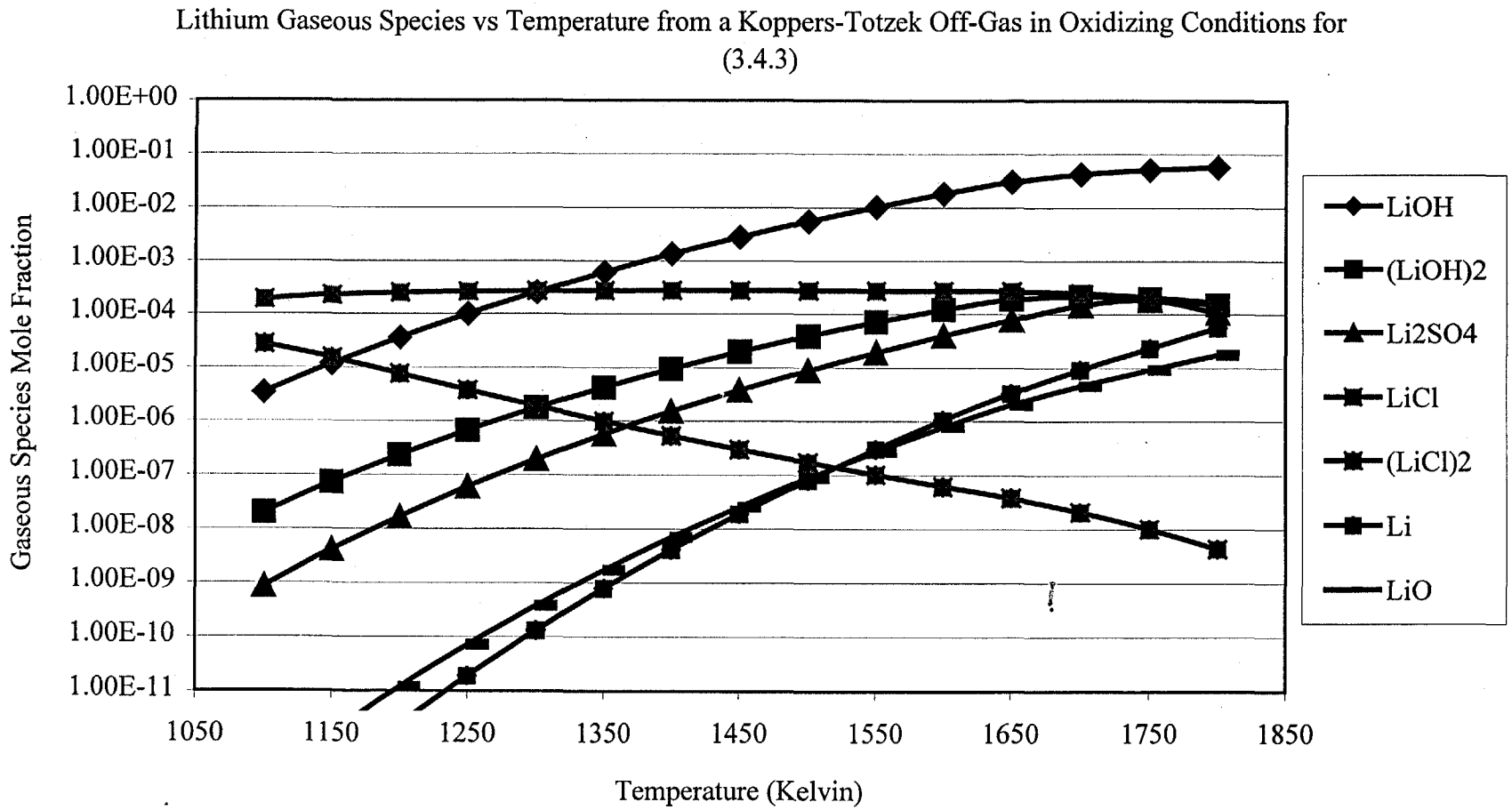

Figure A.9 Lithium Gaseous Species Mole Fraction for Li_2CO_3 and a Koppers-Totzek Off-Gas with NiO under Oxidizing Conditions (3.4.3).

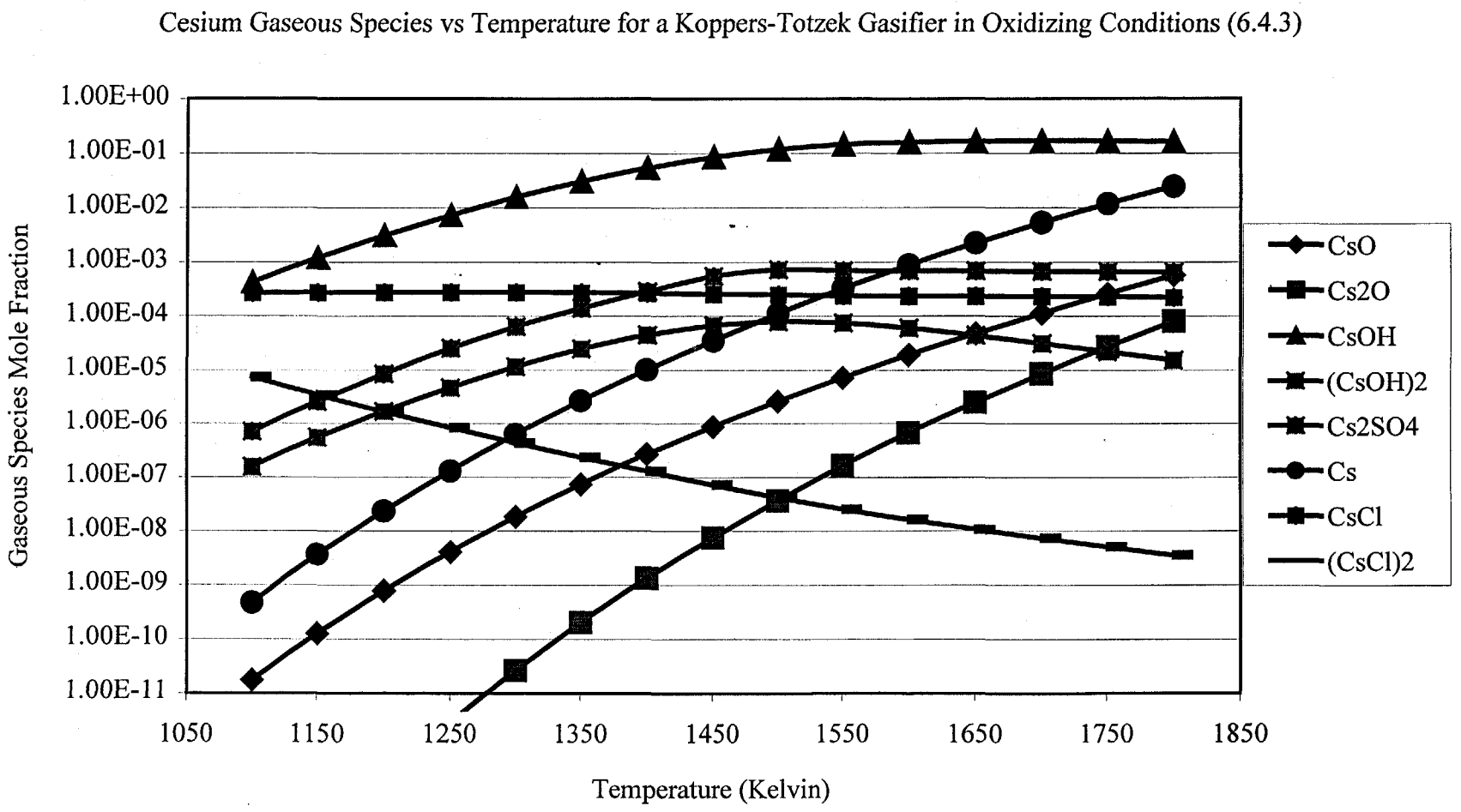

Figure A.10 Cesium Gaseous Species Mole Fraction for Cs_2CO_3 a Koppers-Totzek Off-Gas with NiO under Oxidizing Conditions (6.4.3).

Since K_2CO_3 was the most effective salt for capturing the sulfur, the next logical step was to see how this salt behaved with the other supports. K_2CO_3 was run with all supports listed in Table A.1. Even the supports that reacted with K_2CO_3, as seen in Table A.4, were used to demonstrate some of the undesirable characteristics of these systems. The FACT entering molar ratios are listed in Table A.8. Figure A.11 shows the SO_2 concentrations for K_2CO_3 simulations with different supports. K_2CO_3 reacts with all of the supports shown in yellow and green, but, it does not react with the supports shown in red and blue. For all of the non-reactive supports (ZrO_2, NiO, Fe_2O_3, CaO, $Ca_3(PO_4)_2$) the SO_2 concentration is essentially the same.

There is an exception for Fe_2O_3 at temperatures above 1700 K. Just above 1700 K, Fe_2O_3 is no longer stable and decomposes into oxygen and iron. The large amount of oxygen released when iron oxide decomposes dramatically dilutes the gas phase concentration of SO_2. The actual number of moles of SO_2 present in the gas phase remains the same.

The reactive supports failed to capture any of the sulfur in the liquid or solid phase with the exception of TiO_2 at low temperatures. In the case of TiO_2, a limited amount of sulfur was captured as K_2SO_4 (s) up until 1250 K. At 1250 K, K_2SO_4 (s) in this system is no longer stable. The reason the SO_2 concentration for the reactive systems is lower compared to the systems where no salt or support was present is because the potassium carbonate decomposes into CO_2 when the potassium carbonate reacts with the support to form a glassy compound. The decomposition of potassium carbonate dilutes the gas phase with CO_2. CO_2's mole fraction in the gas phase for the reactive supports is approximately 0.99, except when the support is WC. In general, the carbonates are unstable with SiO_2, Al_2O_3, TiO_2, and WC, as shown earlier in Table A.4.

Initially, from Figure A.11, it appears that WC captures a great deal of sulfur in the gas phase even at elevated temperatures. The reason the SO_2 concentration is so low stems from the fact that oxygen reacts with a small portion of WC to form $O^2W(OH)^2$ (g). This causes the system to behave is if under reduced conditions. Under reducing conditions, the sulfur would remain as hydrogen sulfide, which is what is observed in this case. The fact that, H_2S's mole fraction was around 10^{-4} in the lower temperature region of this system, along with the absence of K_2SO_4 in either the liquid or solid phase, demonstrates that this system is ineffective for capturing sulfur even though the SO_2 concentration is extremely low.

Figures A.12-A.15 give significant gaseous species concentrations for the non-reactive support systems. From these plots, the increased production of NO_x with increasing temperature is observed. The concentration levels are consistent with those found for the cases where no salt or support was present. There are high concentrations of nitrogen, carbon dioxide, and water present in all of the systems, which is indicative of the products of a combustion reaction. There also is an appreciable amount of oxygen present, which is expected based on the system being designed for 10% excess oxygen. Unfortunately, mercury is not present in either the solid or liquid phase. Its concentration is consistent with that seen for when no salt or support is present. Mercury at high temperature does remain in its zero oxidation state, which is consistent with the literature on the subject.

Figures A.15-18 show the salt related gaseous species for the non-reactive support systems. There are two important trends to take away from these figures. First, the amount of the undesirable salt species, in general, increases with temperature. The second very important concept is that for the non-reactive systems the salt speciation in the gas phase is not a function of the support material used. This concept will reduce the amount of data that needs to be reported for simulations run at lower temperatures with the nitrates in the following section.

Table A.8 FACT entering Molar Ratios for K_2CO_3 and a Koppers-Totzek Off-Gas with various Supports under High Temperature Oxidizing Conditions.

	(2.1.3)	(2.2.3)	(2.4.3)	(2.5.3)
Support	1.000E+00	1.000E+00	1.000E+00	1.000E+00
Salt	4.830E-02	8.197E-02	6.005E-02	1.284E-01
CO	5.366E-05	5.664E-05	5.467E-05	6.119E-05
CH_4	9.414E-08	9.937E-08	9.591E-08	1.074E-07
H_2	2.702E-05	2.852E-05	2.753E-05	3.081E-05
COS	2.824E-08	2.981E-08	2.877E-08	3.221E-08
H_2S	1.883E-07	1.987E-07	1.918E-07	2.147E-07
NH_3	0.000E+00	0.000E+00	0.000E+00	0.000E+00
CO_2	1.176E-05	1.241E-05	1.198E-05	1.341E-05
N_2	1.690E-04	1.784E-04	1.722E-04	1.927E-04
O_2	4.463E-05	4.711E-05	4.547E-05	5.089E-05
Ar	1.883E-07	1.987E-07	1.918E-07	2.147E-07
Hg	4.910E-12	5.183E-12	5.002E-12	5.599E-12
HCl	7.365E-08	7.774E-08	7.504E-08	8.399E-08
	(2.6.3)	**(2.7.3)**	**(2.8.3)**	**(2.9.3)**
Support	1.000E+00	1.000E+00	1.000E+00	1.000E+00
Salt	1.575E-01	6.422E-02	4.508E-02	2.494E-01
CO	6.435E-05	5.504E-05	5.339E-05	7.617E-05
CH_4	1.129E-07	9.656E-08	9.366E-08	1.336E-07
H_2	3.240E-05	2.771E-05	2.688E-05	3.835E-05
COS	3.387E-08	2.897E-08	2.810E-08	4.009E-08
H_2S	2.258E-07	1.931E-07	1.873E-07	2.673E-07
NH_3	0.000E+00	0.000E+00	0.000E+00	0.000E+00
CO_2	1.410E-05	1.206E-05	1.170E-05	1.669E-05
N_2	2.027E-04	1.733E-04	1.681E-04	2.399E-04
O_2	5.351E-05	4.577E-05	4.440E-05	6.335E-05
Ar	2.258E-07	1.931E-07	1.873E-07	2.673E-07
Hg	5.888E-12	5.036E-12	4.885E-12	6.970E-12
HCl	8.831E-08	7.554E-08	7.327E-08	1.045E-07

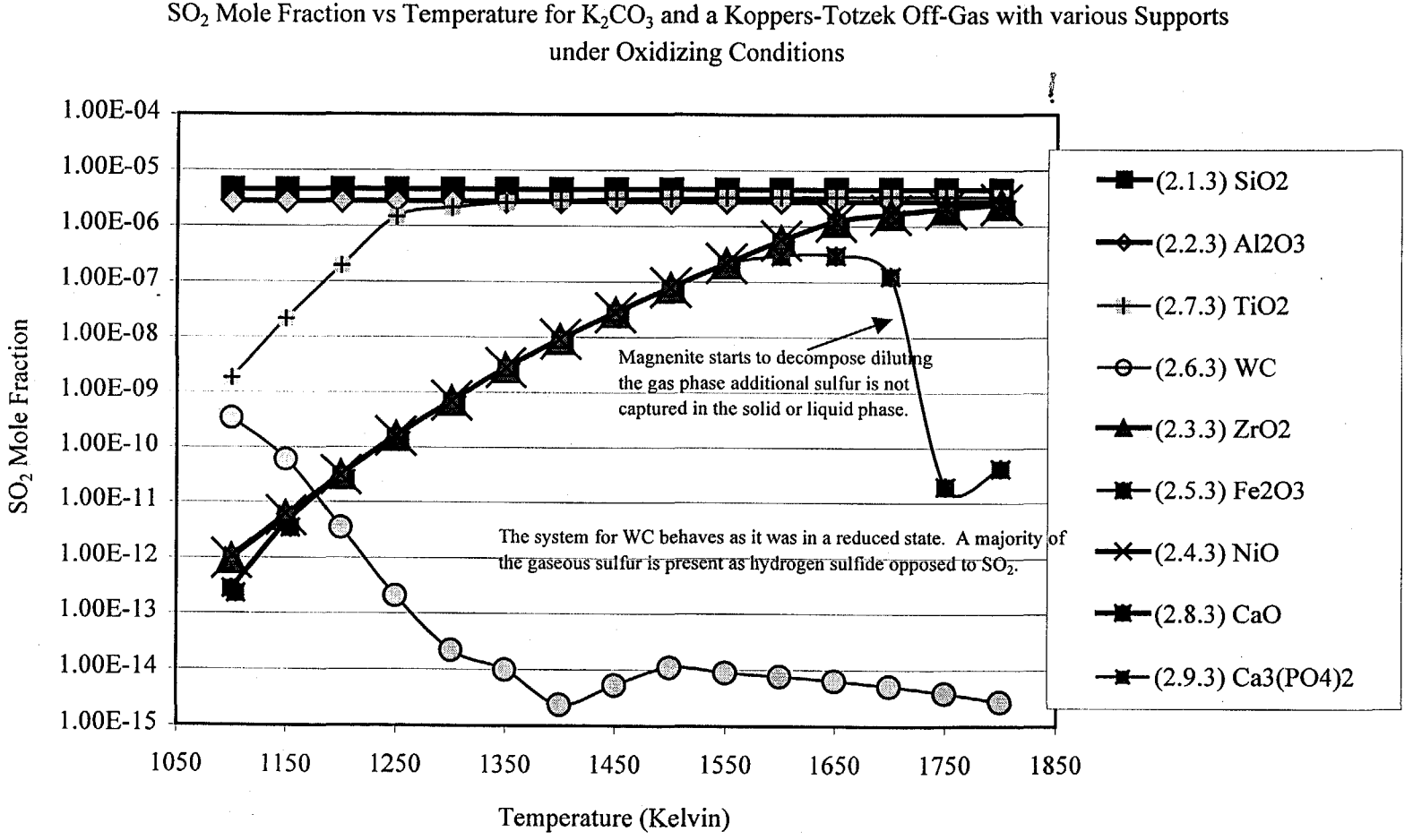

Figure A.11 SO_2 Mole Fraction for K_2CO_3 and a Koppers-Totzek Off-Gas with various Supports under High Temperature Oxidizing Conditions.

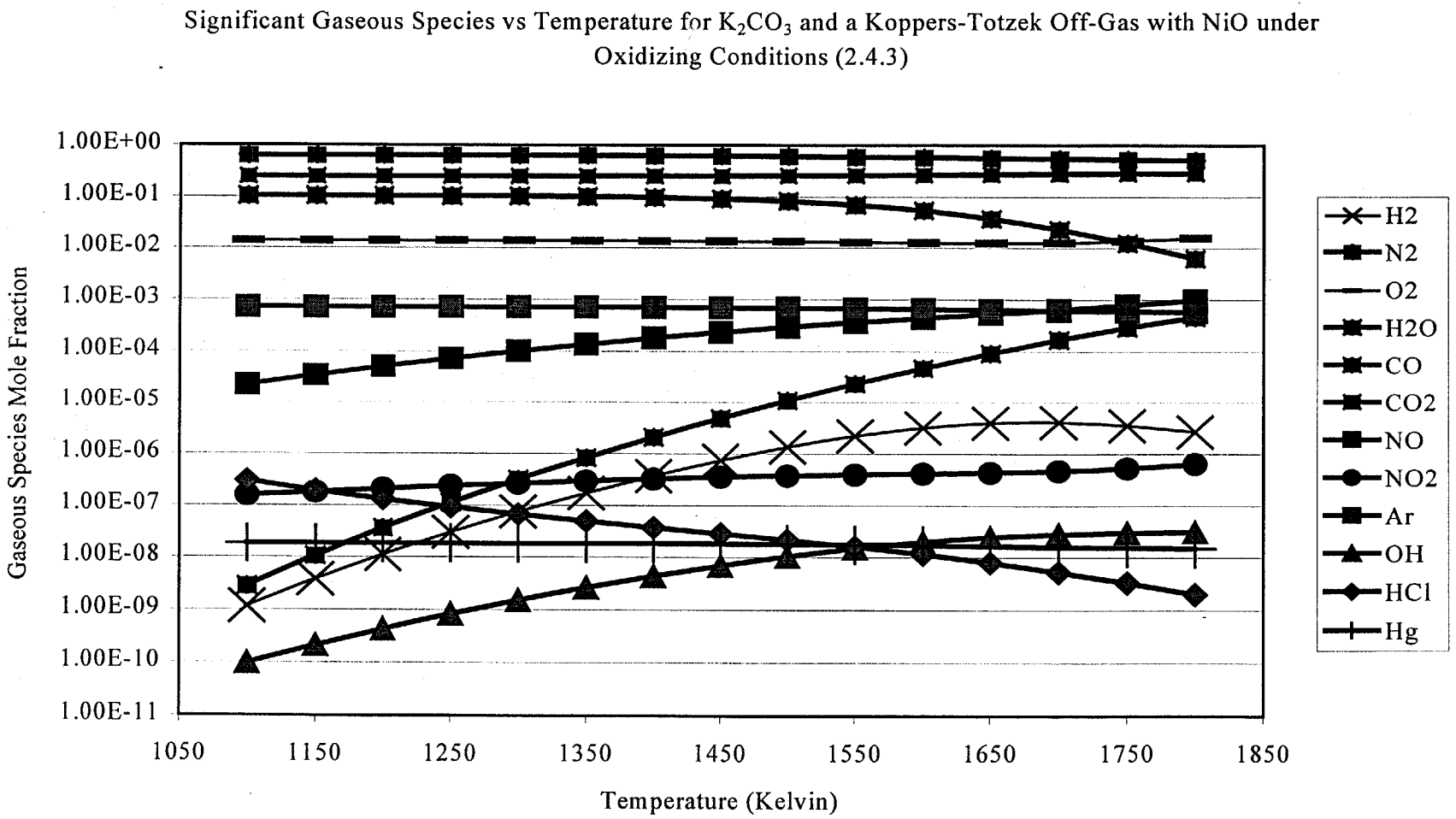

Figure A.12 Significant Gaseous Species Mole Fraction for K_2CO_3 and a Koppers-Totzek Off-Gas with NiO under Oxidizing Conditions (2.4.3).

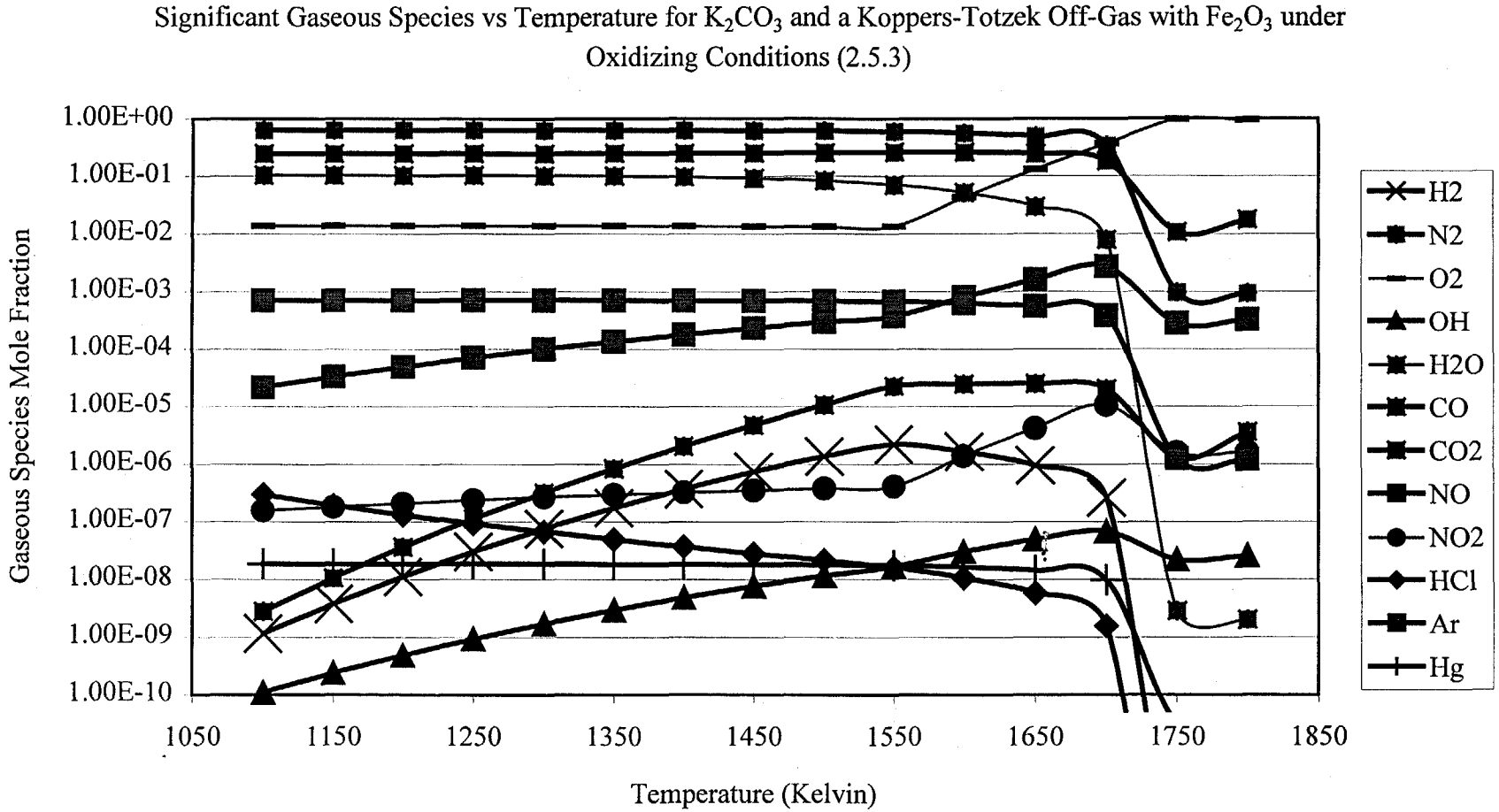

Figure A.13 Significant Gaseous Species Mole Fraction for K_2CO_3 and a Koppers-Totzek Off-Gas with Fe_2O_3 under Oxidizing Conditions (2.5.3).

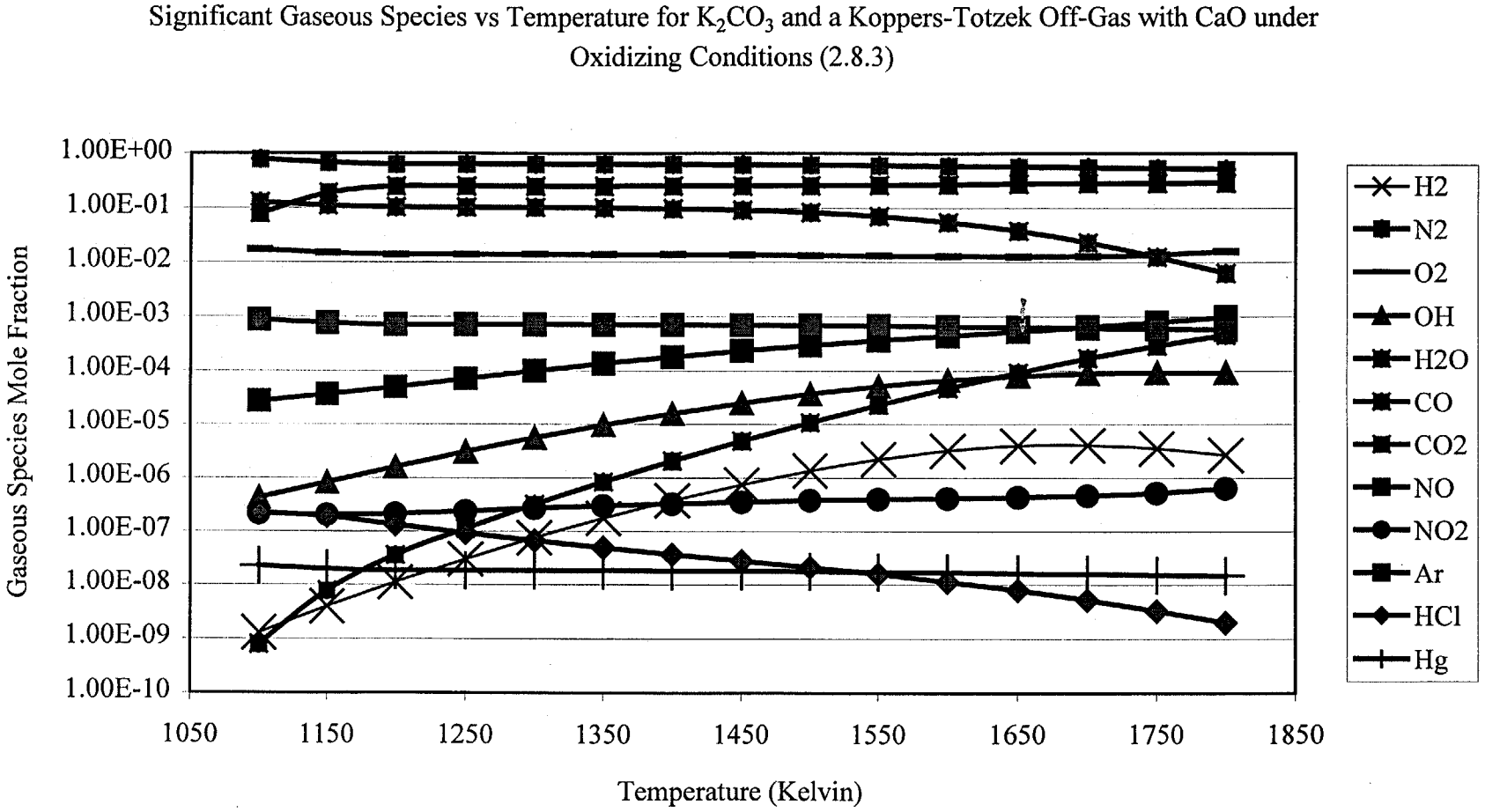

Figure A.14 Significant Gaseous Species Mole Fraction for K_2CO_3 and a Koppers-Totzek Off-Gas with CaO under Oxidizing Conditions (2.8.3).

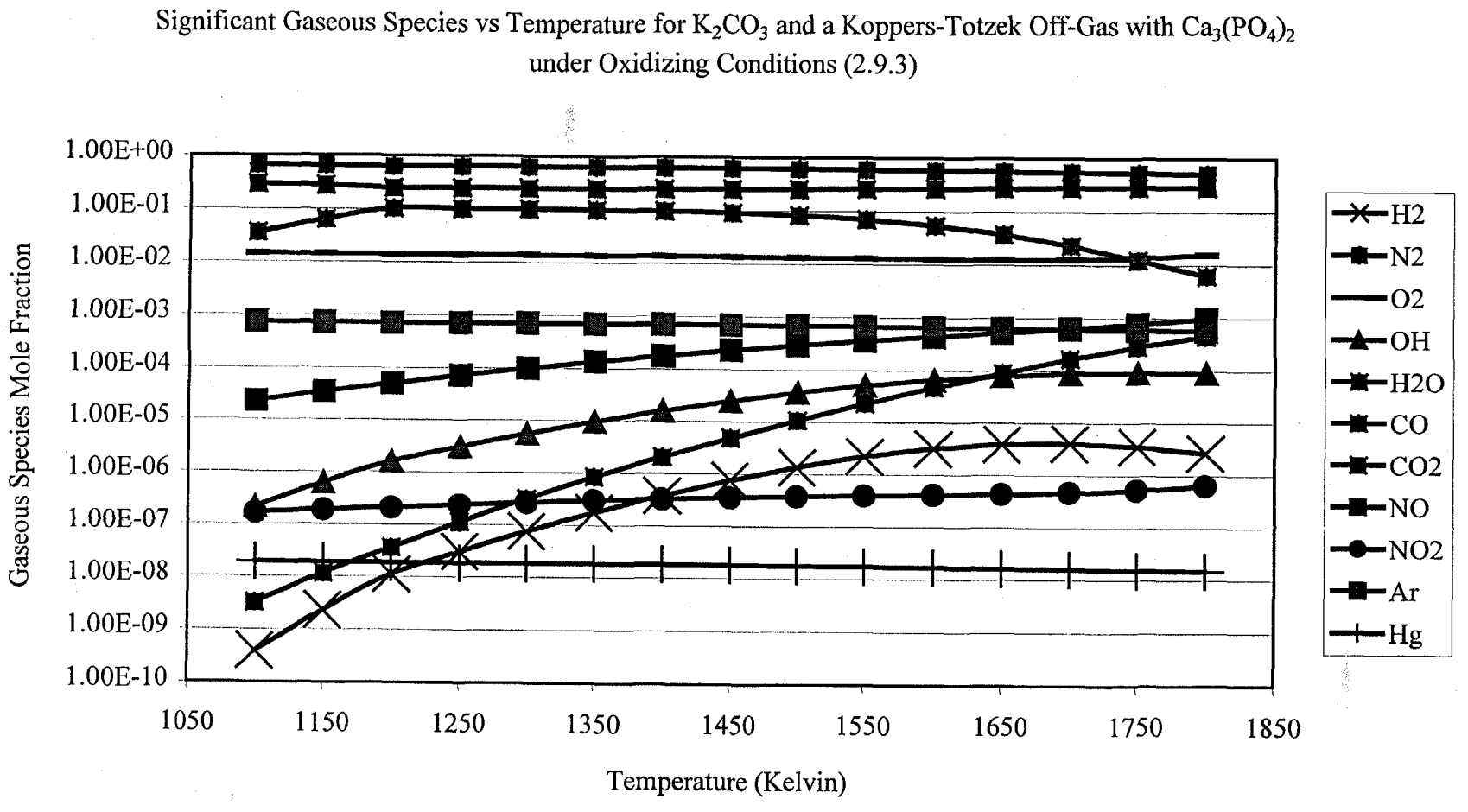

Figure A.15 Significant Gaseous Species Mole Fraction for K_2CO_3 and a Koppers-Totzek Off-Gas with $Ca_3(PO_4)_2$ under Oxidizing Conditions (2.9.3).

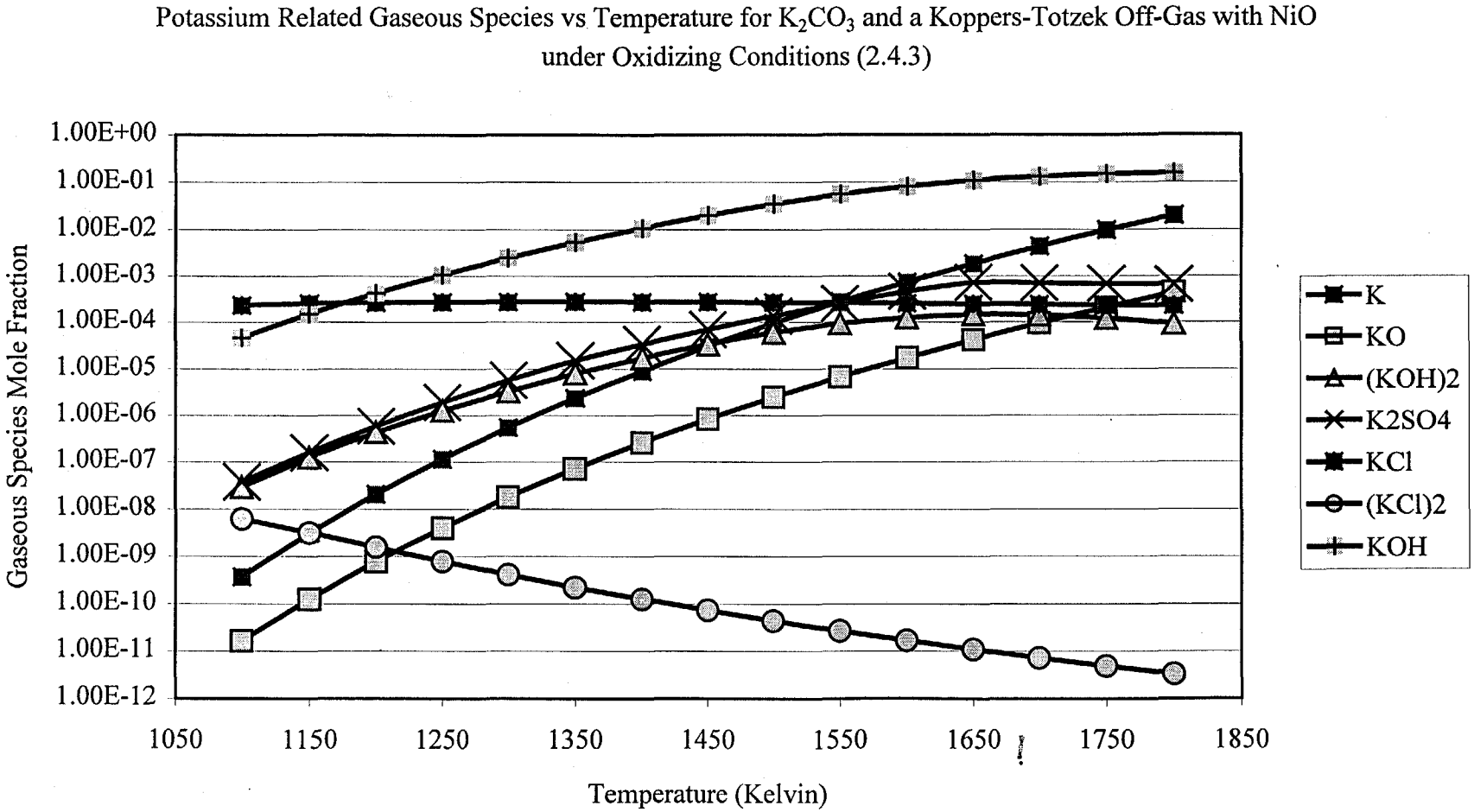

Figure A.16 Potassium Gaseous Species Mole Fraction for K_2CO_3 and a Koppers-Totzek Off-Gas with NiO under Oxidizing Conditions (2.4.3).

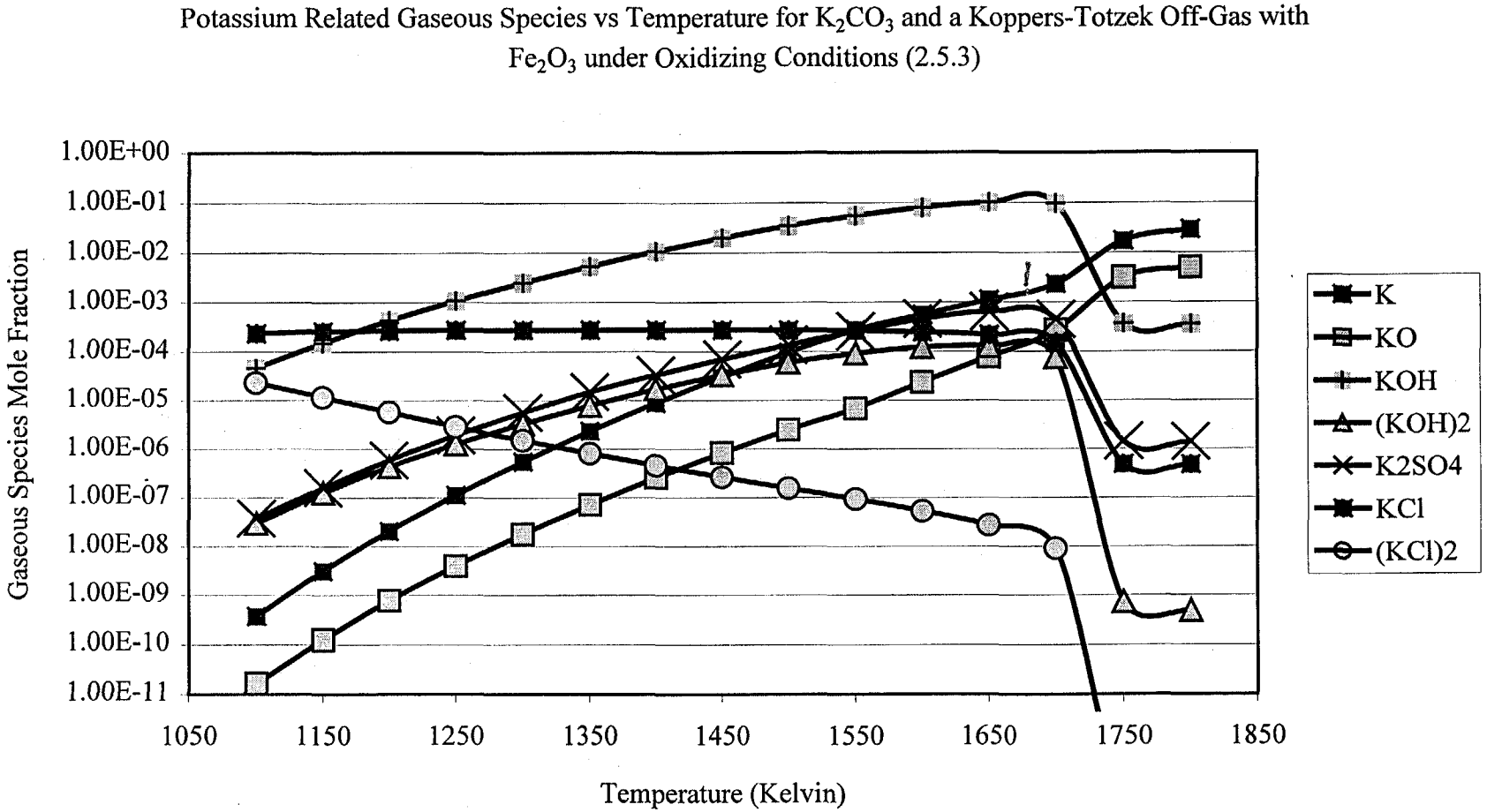

Figure A.17 Potassium Gaseous Species Mole Fraction for K_2CO_3 and a Koppers-Totzek Off-Gas with Fe_2O_3 under Oxidizing Conditions (2.5.3).

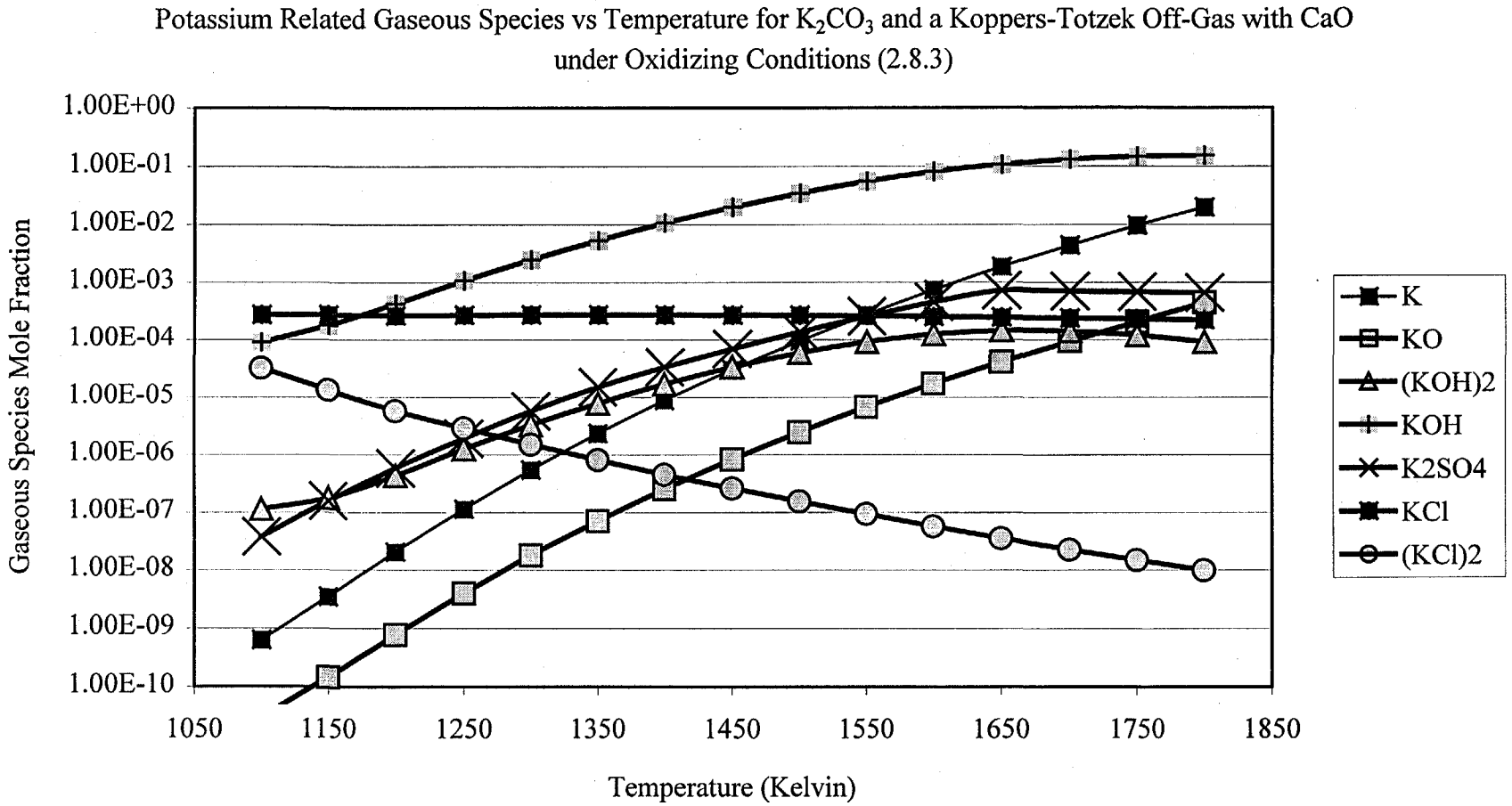

Figure A.18 Potassium Gaseous Species Mole Fraction for K_2CO_3 and a Koppers-Totzek Off-Gas with CaO under Oxidizing Conditions (2.8.3).

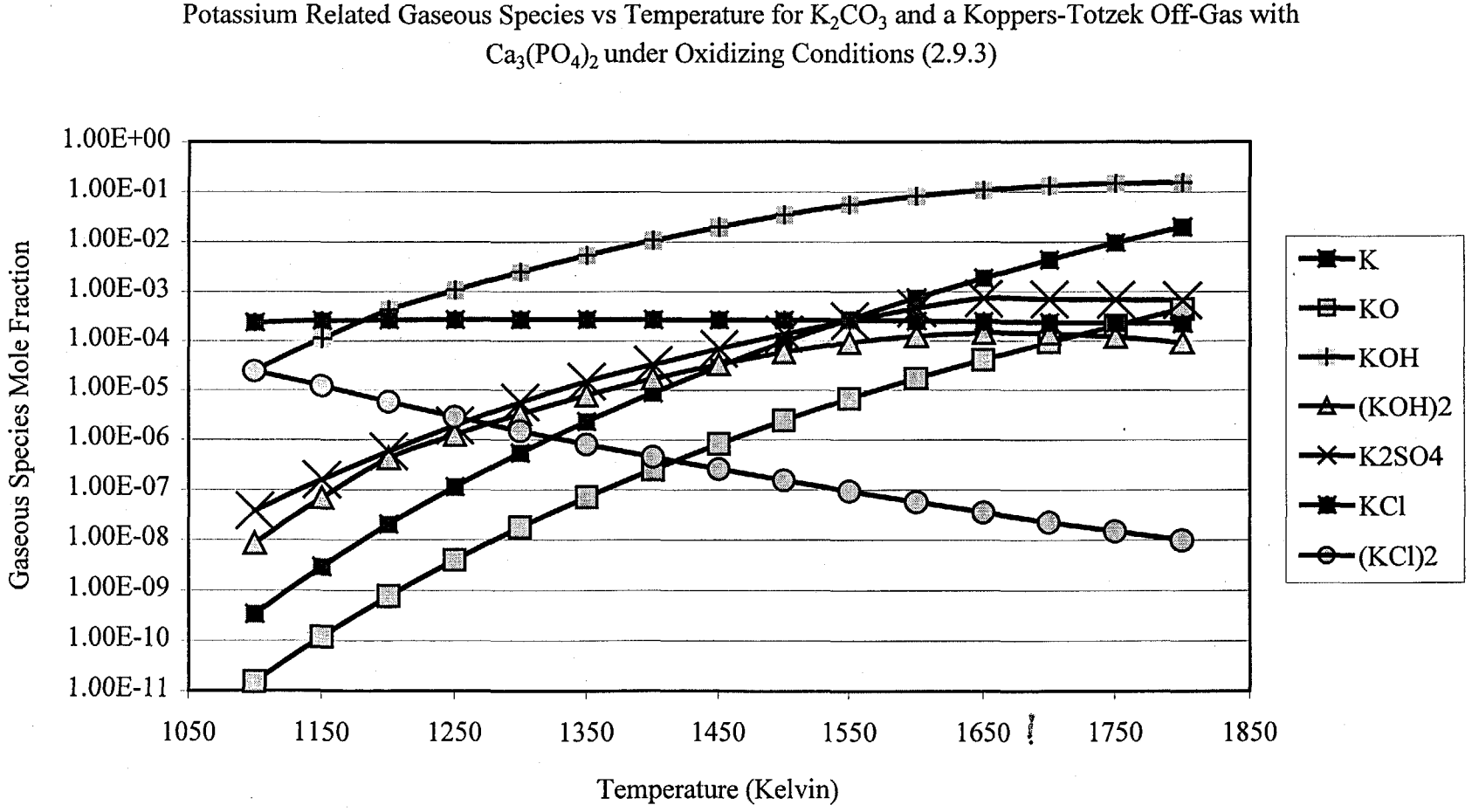

Figure A.19 Potassium Gaseous Species Mole Fraction for K_2CO_3 and a Koppers-Totzek Off-Gas with $Ca_3(PO_4)_2$ under Oxidizing Conditions (2.9.3).

A.6b) High Temperature/Reducing Condition Simulations

Sulfur capture in the liquid and solid phases still occurred at high temperature even without the addition of oxygen to the system. In the cases where molten carbonates were used small amounts of K_2SO_4 formed reducing the overall amount of sulfur left in the gas phase. For this series of simulations, the off-gas from a Lurgi gasifier was used to generate the entering FACT molar ratio inputs, listed in Table A.9.

Initially, all of the salts and a non-reactive support were reacted with to determine what happened to the sulfur, NO_x, and mercury. Figures A.20 and A.21 give H_2S and SO_2 mole fractions as a function of the different high temperature salts. Due to the oxygen deficiency, there was still a large amount of hydrogen sulfide present in the gas along with significant amounts of SO_2. Similar to the results for high temperature in an oxygen rich environment the salts: Na_2WO_4, Na_2SO_4, and B_2O_3 fail to capture sulfur in the solid or liquid phase. The carbonates on the other hand do indeed capture sulfur as a sulfate, except Li_2CO_3 In this case, a majority of the sulfur in fact reacts with the support to form Ni_3S_2 (liquid) up until 1250 K. After 1250 K, Li_2SO_4 does form for about another 50 K until it is no longer stable and sulfur is no longer found in the liquid or solid phase. This accounts for the large increase of SO_2 in Figure A.21 for Li_2CO_3. K_2CO_3 appears to do the best job capturing the sulfur in light of the suspect thermodynamic data for Cs_2CO_3. Even though some of the sulfur is captured, the H_2S and SO_2 concentrations are greater than the ppm-v level except for K_2CO_3 below 1150K.

The other concern with these systems arises from the low CO and H_2 concentrations. Figure A.22 shows significant gaseous species concentrations as a function of temperature for system (2.3.1). It looks like a significant portion of the H_2 and CO was oxidized to form H_2O and CO_2. Unless these oxidation reactions are somehow kinetically limited, there is no point in using this system in conjunction with a molten carbonate fuel cell. In the following section discussion will focus on where the oxygen comes from that causes the gas streams' oxidation. This same phenomenon was observed for all of the carbonate salts tested. For Na_2WO_4, Na_2SO_4, and B_2O_3, the main gas phase constituents were still CO and H_2, but as previously mentioned these salts failed to capture any sulfur. Figure A.23 gives the salt related gaseous species output for system (2.3.1) Again, the amount of salt species present in the gas phase increases with temperature, and is essentially the same for all of the K_2CO_3 systems in this section. K_2SO_4 (g) reaches the ppm level around 1250 K.

Table A.9 FACT entering Molar Ratios for High Temperature Salts, a Lurgi Off-Gas, and a Non-Reactive Support under Reducing Conditions.

	(1.3.1)	(2.3.1)	(3.4.1)	(4.3.1)
Support	1.000E+00	1.000E+00	1.000E+00	1.000E+00
Salt	1.770E-01	8.916E-02	1.011E-01	4.194E-02
CO	4.396E-05	3.783E-05	3.858E-05	3.506E-05
CH_4	4.054E-05	3.488E-05	3.557E-05	3.233E-05
H_2	1.642E-04	1.413E-04	1.441E-04	1.310E-04
COS	5.710E-07	4.913E-07	5.010E-07	4.554E-07
H_2S	1.142E-06	9.826E-07	1.002E-06	9.108E-07
NH_3	0.000E+00	0.000E+00	0.000E+00	0.000E+00
CO_2	1.252E-04	1.077E-04	1.098E-04	9.982E-05
N_2	9.516E-07	8.188E-07	8.351E-07	7.590E-07
O_2	0.000E+00	0.000E+00	0.000E+00	0.000E+00
Ar	5.710E-07	4.913E-07	5.010E-07	4.554E-07
Hg	4.023E-12	3.461E-12	3.530E-12	3.208E-12
HCl	6.034E-08	5.192E-08	5.295E-08	4.813E-08

	(5.3.1)	(6.4.1)	(7.3.1)
Support	1.000E+00	1.000E+00	1.000E+00
Salt	8.675E-02	2.292E-02	1.770E-01
CO	3.768E-05	3.404E-05	4.396E-05
CH_4	3.474E-05	3.139E-05	4.054E-05
H_2	1.408E-04	1.272E-04	1.642E-04
COS	4.893E-07	4.421E-07	5.710E-07
H_2S	9.787E-07	8.841E-07	1.142E-06
NH_3	0.000E+00	0.000E+00	0.000E+00
CO_2	1.073E-04	9.690E-05	1.252E-04
N_2	8.156E-07	7.368E-07	9.516E-07
O_2	0.000E+00	0.000E+00	0.000E+00
Ar	4.893E-07	4.421E-07	5.710E-07
Hg	3.448E-12	3.115E-12	4.023E-12
HCl	5.172E-08	4.672E-08	6.034E-08

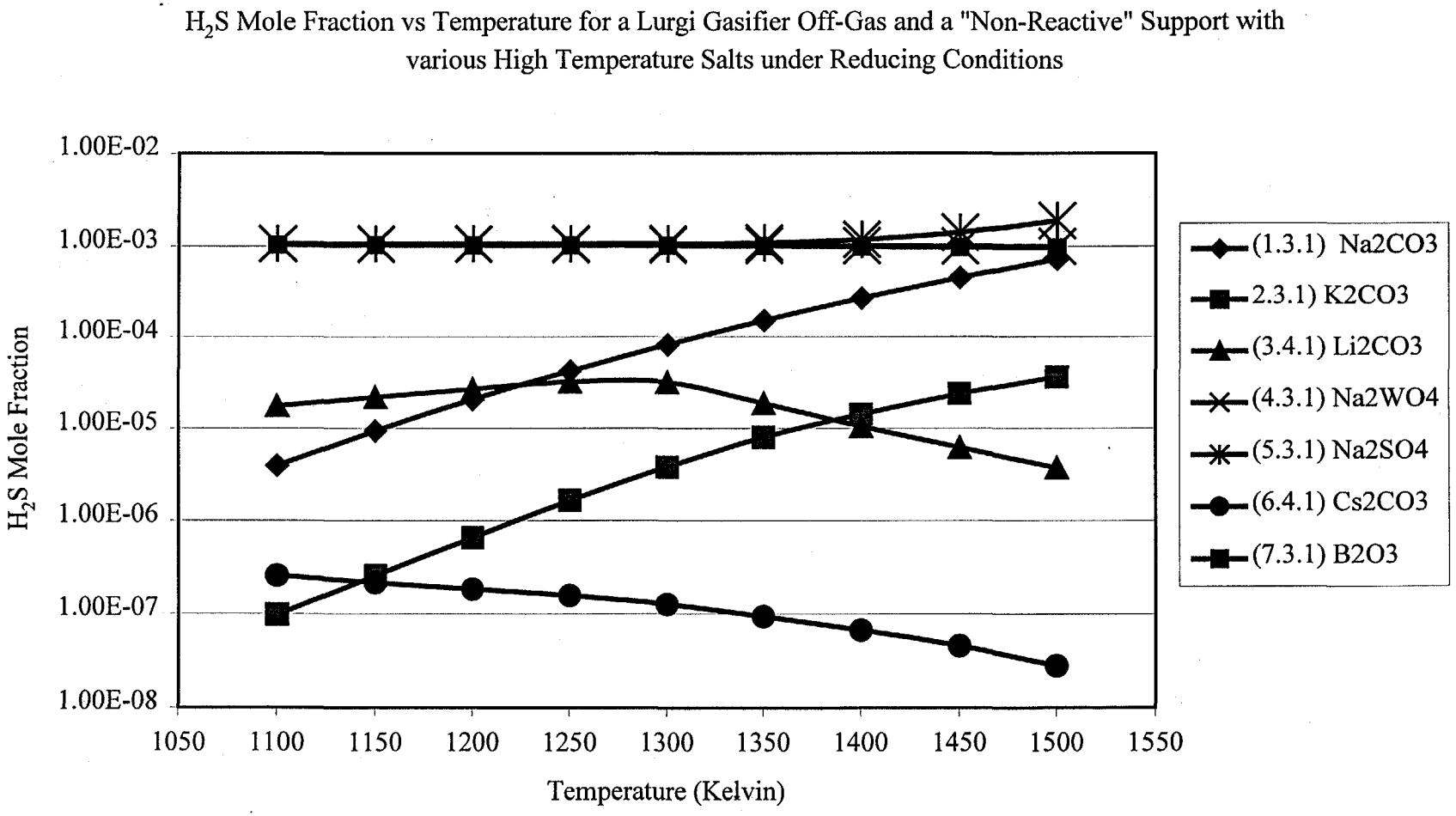

Figure A.20 H_2S Mole Fraction for a Lurgi Gasifier Off-Gas and a "Non-Reactive" Support with various High Temperature Salts under Reducing Conditions.

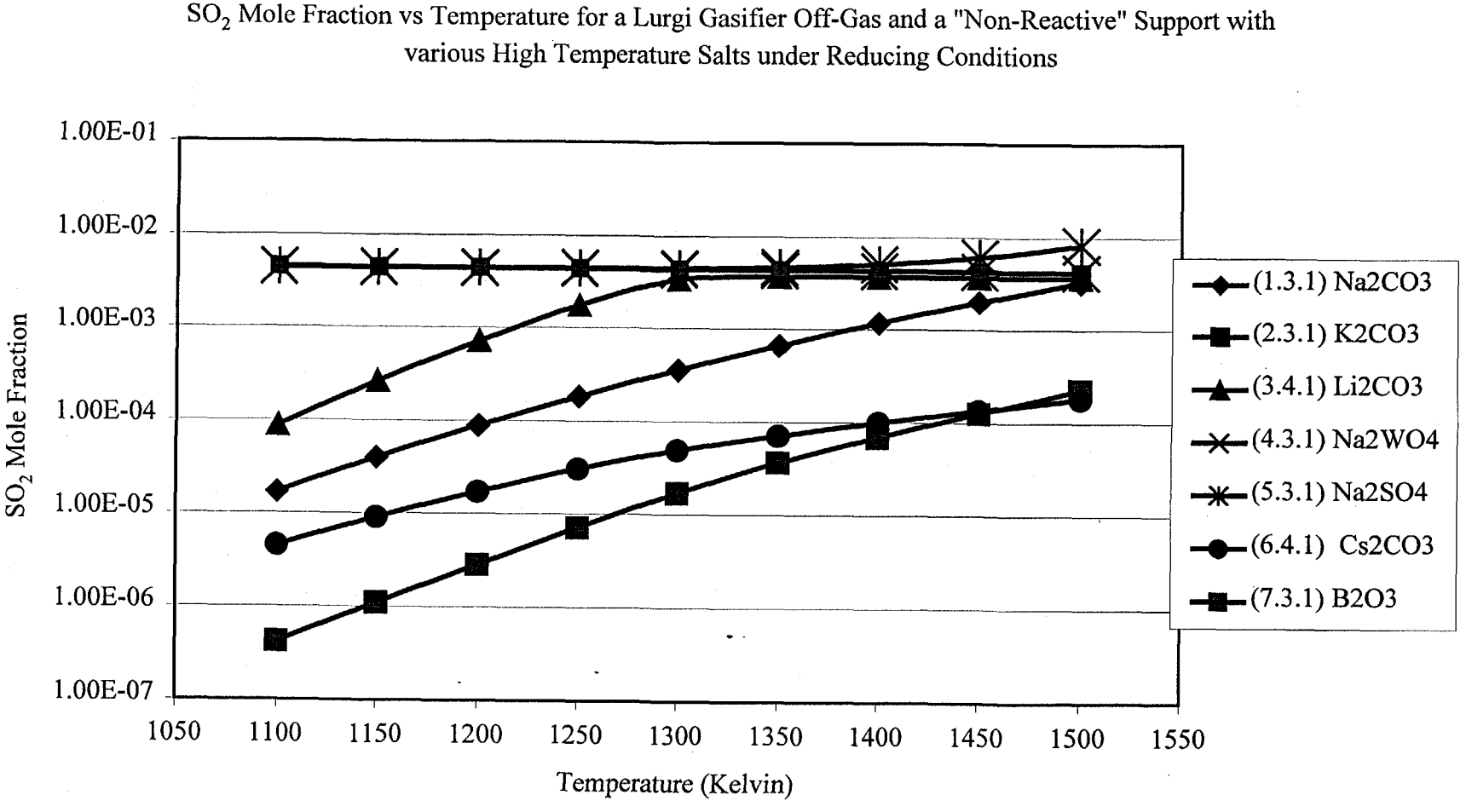

Figure A.21 SO_2 Mole Fraction for a Lurgi Gasifier Off-Gas and a "Non-Reactive" Support with various High Temperature Salts under Reducing Conditions.

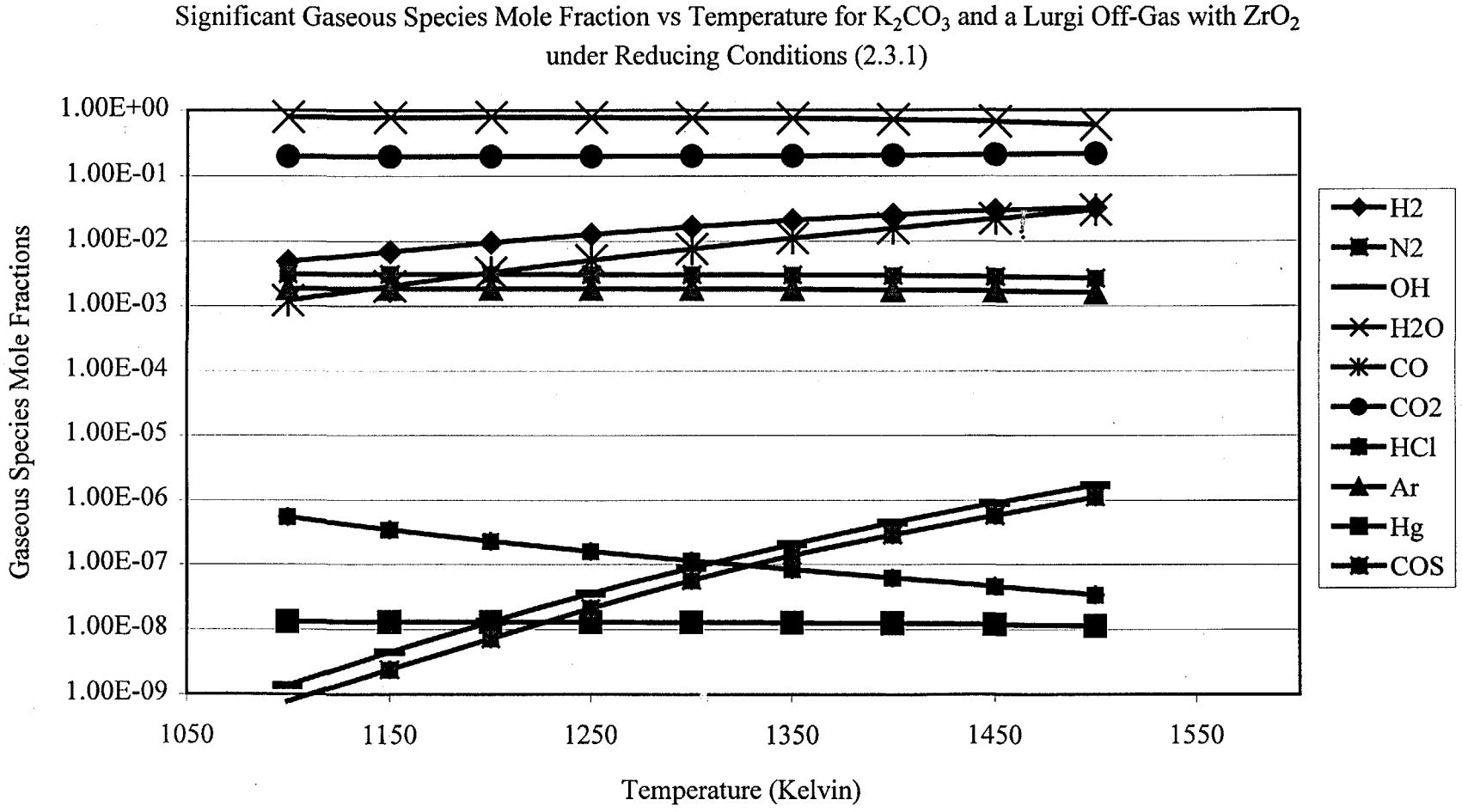

Figure A.22 Significant Gaseous Species Mole Fraction vs Temperature for K_2CO_3 and Lurgi Off-Gas with ZrO_2 under Reducing Conditions (2.3.1).

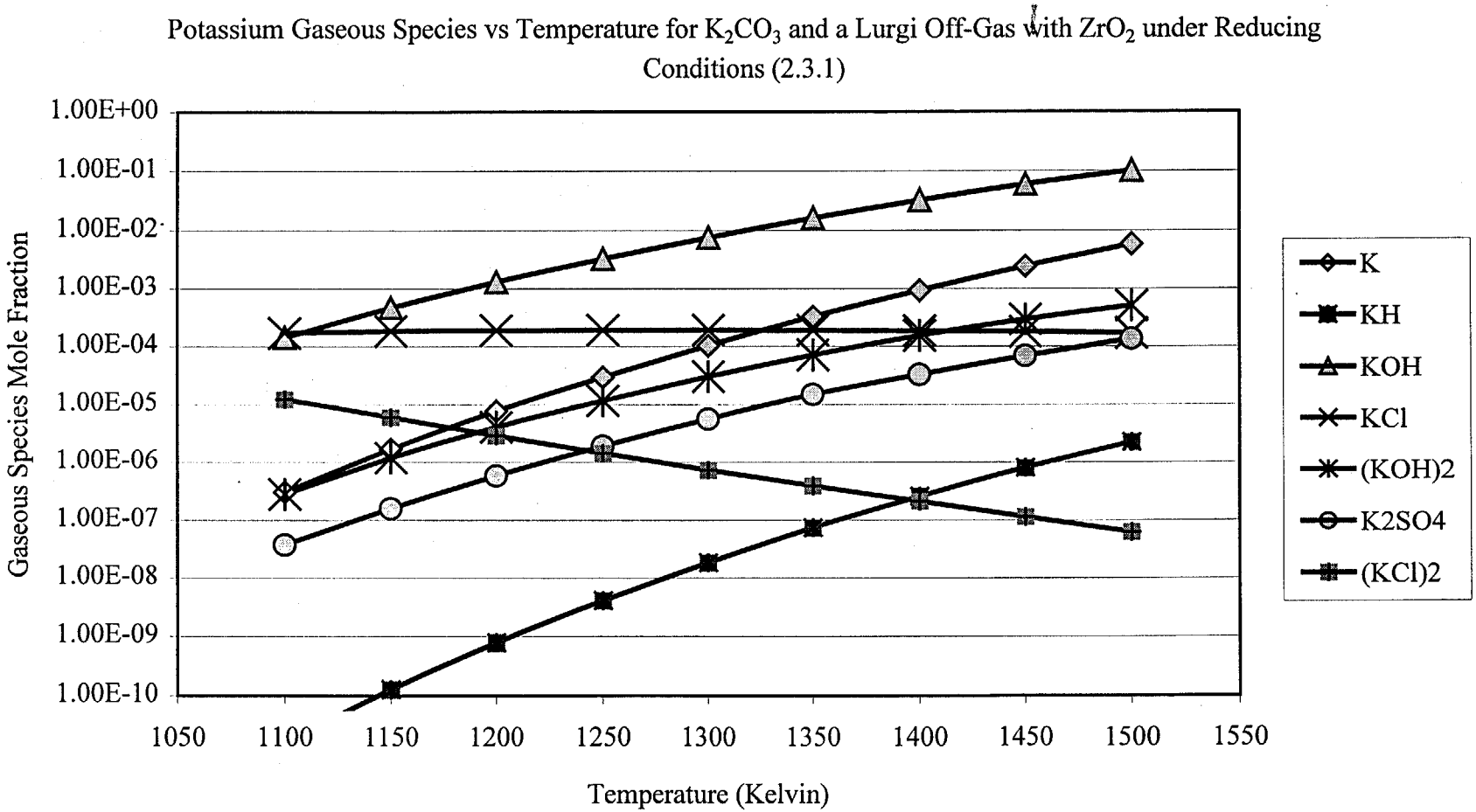

Figure A.23 Potassium Gaseous Species Mole Fractions for K_2CO_3 and a Lurgi Off-Gas with ZrO_2 under Reducing Conditions (2.3.1).

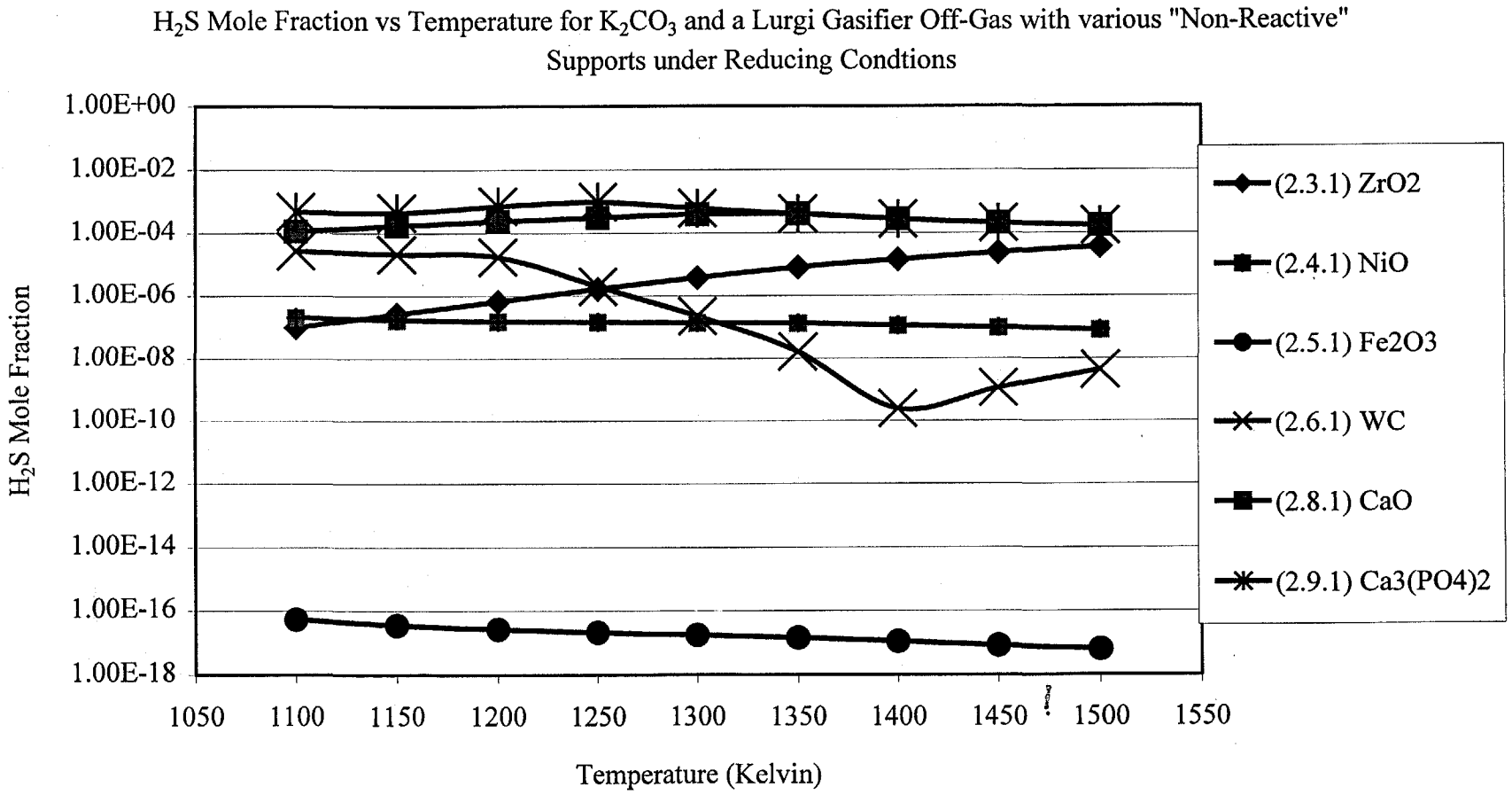

Figure A.24 H_2S Mole Fraction for K_2CO_3 and a Lurgi Gasifier Off-Gas with various "Non-Reactive" Supports under Reducing Conditions.

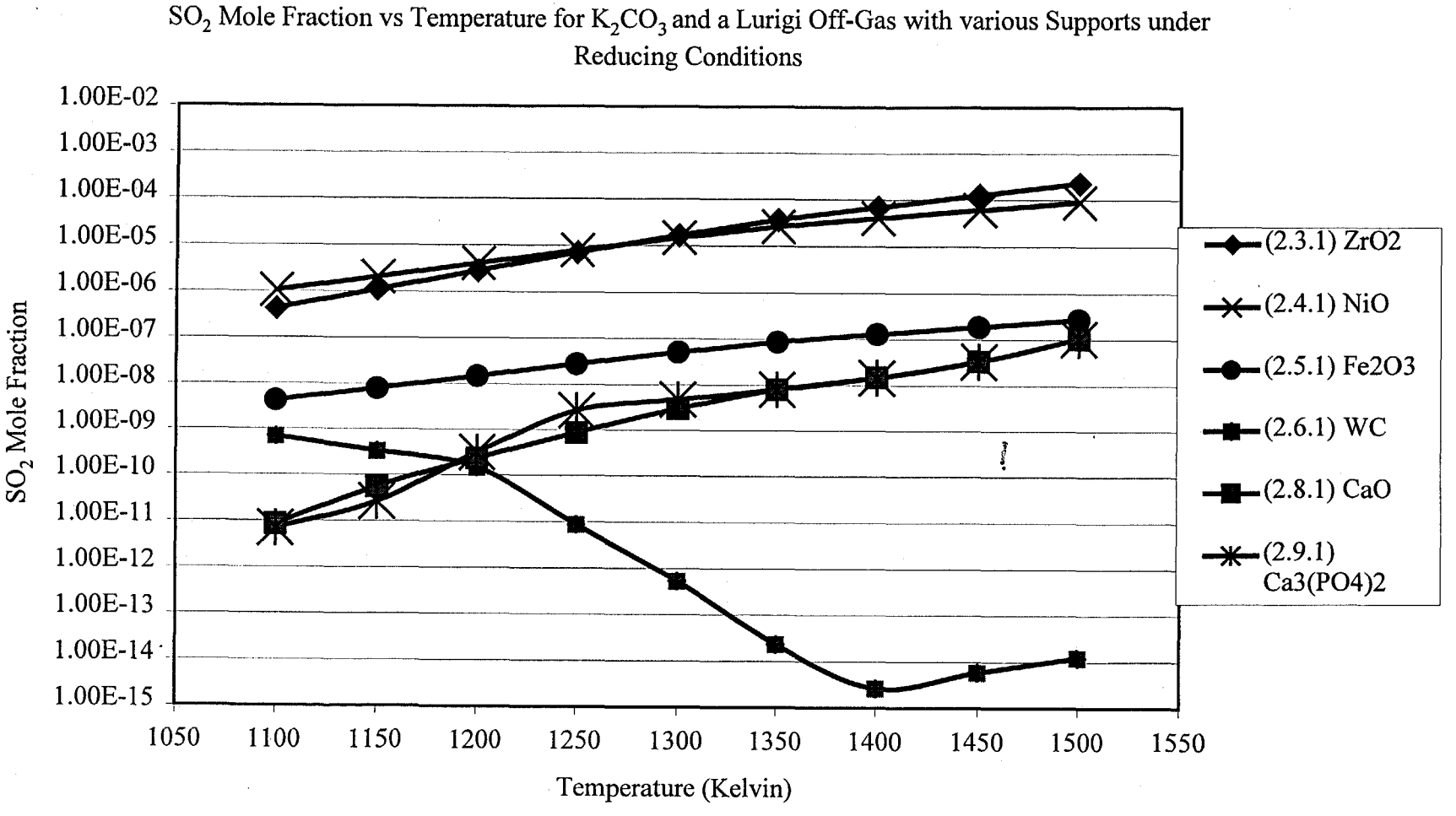

Figure A.25 SO_2 Mole Fraction for K_2CO_3 and a Lurgi Off-Gas with "Non-Reactive" Supports under Reducing Conditions.

Figures A.24 and A.25 show H_2S and SO_2 concentrations, respectively, for systems with K_2CO_3 supported on what were thought to be "non-reactive" supports. The entering molar ratios for the equilibrium simulations are listed in Table A.10. Surprisingly, the degree of sulfur capture is a function of the type of support used. The system with Fe_2O_3 by far does the best in terms of sulfur capture with extremely low concentrations of H_2S and SO_2 below the ppm-v level over the entire temperature range explored

In these systems, again two distinct types of behavior are seen. ZrO_2, NiO, and Fe_2O_3 all partially react, releasing oxygen to the system. This causes these systems to behave as if they were under weakly oxidized conditions, which accounts for the significant concentrations of SO_2 seen in Figure A.25. The presence of oxygen also accounts for the low concentrations of H_2 and CO and high concentrations of CO_2 and water vapor present for these three systems seen in Figures A.23, A.26 and A.27. Under these weak oxidizing conditions, the sulfur was captured as K_2SO_4. The amount of sulfur captured in these three systems is highest for the iron oxide support. Unfortunately, this system also has H_2 and CO concentrations two orders of magnitude lower than the either NiO or ZrO_2.

For WC, CaO, and $Ca_3(PO_4)_2$, the situation was entirely different. These three systems behaved like they were under reducing conditions. Their respective SO_2 concentrations were all very low, but their H_2S concentrations were much higher, which indicates a reduced environment. For these three supports, the sulfur captured was in a reduced form, like K_2S or CaS. Figures A.28-30 show the main gaseous constituents as H_2 and CO for all three systems, opposed to CO_2 and H_2O like the previous supports. An important note regarding the WC system; around 1350 K the remaining K_2CO_3 dissociates diluting the gas phase, which causes the sudden drop in gaseous species concentrations. Another important aspect of the reduced system is the high concentrations of COS still present in the systems seen Figure A.28-A.30. For WC from 1100-1200 K there is a COS concentration on the order of 100 ppm-v, which explains where the sulfur resides. The other two reducing supports (CaO and $Ca_3(PO_4)_2$) have COS concentrations an order of magnitude lower than the WC system over the entire temperature range.

The amount of gaseous potassium species follows the same temperature trend seen for the high temperature oxidizing section. Figure A.31-A.33 show that the potassium gaseous species are essentially the same for the "oxidizing" supports. Figures A.34-A.36 show that the potassium gaseous species are the same for the "reducing" supports up until the point where K_2CO_3 breaks down in the WC system. The primary difference between the two groups of support gaseous species' concentrations is the presence of K_2SO_4 (g) in the "oxidized" systems and higher K (g) concentrations in the "reduced" systems.

Equilibrium shows that not one of the supports investigated is truly stable under reduced conditions at high temperature. The supports do not necessarily react with the salt as seen in the high temperature oxidizing environment, but do react to a small extent. It is entirely possible for a system such as (2.4.1), with NiO as the

support, that the reaction that forms the small amount Ni (s) seen in the equilibrium products is kinetically limited. If it was kinetically limited, the support would be non-reactive and the system as a whole should behave as if under reduced conditions. Even if this scenario was possible the sulfur capture seen in the other "reduced" systems was not to the extent to warrant using the high temperature fluidized bed as a gas clean up system for carbonate fuel cells. The H_2S concentrations are around 100 ppm-v at the lower temperatures for the three reducing supports, which are one to two orders of magnitude higher than acceptable levels for a fuel cell system. In the end, the high temperature region under reducing conditions does not possess sufficient sulfur or mercury capturing capability to justify its implementation.

Table A.10 FACT entering Molar Ratios for K_2CO_3 and a Lurgi Off-Gas with various Supports under Reducing Conditions.

	(2.1.1)	(2.2.1)	(2.4.1)	(2.5.1)
Support	1.000E+00	1.000E+00	1.000E+00	1.000E+00
Salt	4.347E-02	7.378E-02	5.404E-02	1.155E-01
CO	3.515E-05	3.689E-05	3.574E-05	3.952E-05
CH_4	3.241E-05	3.402E-05	3.296E-05	3.644E-05
H_2	1.313E-04	1.378E-04	1.335E-04	1.477E-04
COS	4.565E-07	4.791E-07	4.642E-07	5.133E-07
H_2S	9.130E-07	9.582E-07	9.284E-07	1.027E-06
NH_3	0.000E+00	0.000E+00	0.000E+00	0.000E+00
CO_2	1.001E-04	1.050E-04	1.017E-04	1.125E-04
N_2	7.608E-07	7.985E-07	7.736E-07	8.555E-07
O_2	0.000E+00	0.000E+00	0.000E+00	0.000E+00
Ar	4.565E-07	4.791E-07	4.642E-07	5.133E-07
Hg	3.216E-12	3.376E-12	3.270E-12	3.616E-12
HCl	4.824E-08	5.063E-08	4.906E-08	5.425E-08
	(2.6.1)	**(2.7.1)**	**(2.8.1)**	**(2.9.1)**
Support	1.000E+00	1.000E+00	1.000E+00	1.000E+00
Salt	1.417E-01	5.780E-02	4.057E-02	2.244E-01
CO	4.133E-05	3.596E-05	3.499E-05	4.795E-05
CH_4	3.811E-05	3.315E-05	3.226E-05	4.422E-05
H_2	1.544E-04	1.343E-04	1.307E-04	1.791E-04
COS	5.367E-07	4.670E-07	4.544E-07	6.227E-07
H_2S	1.073E-06	9.339E-07	9.088E-07	1.245E-06
NH_3	0.000E+00	0.000E+00	0.000E+00	0.000E+00
CO_2	1.176E-04	1.024E-04	9.961E-05	1.365E-04
N_2	8.945E-07	7.783E-07	7.573E-07	1.038E-06
O_2	0.000E+00	0.000E+00	0.000E+00	0.000E+00
Ar	5.367E-07	4.670E-07	4.544E-07	6.227E-07
Hg	3.781E-12	3.290E-12	3.201E-12	4.388E-12
HCl	5.672E-08	4.935E-08	4.802E-08	6.581E-08

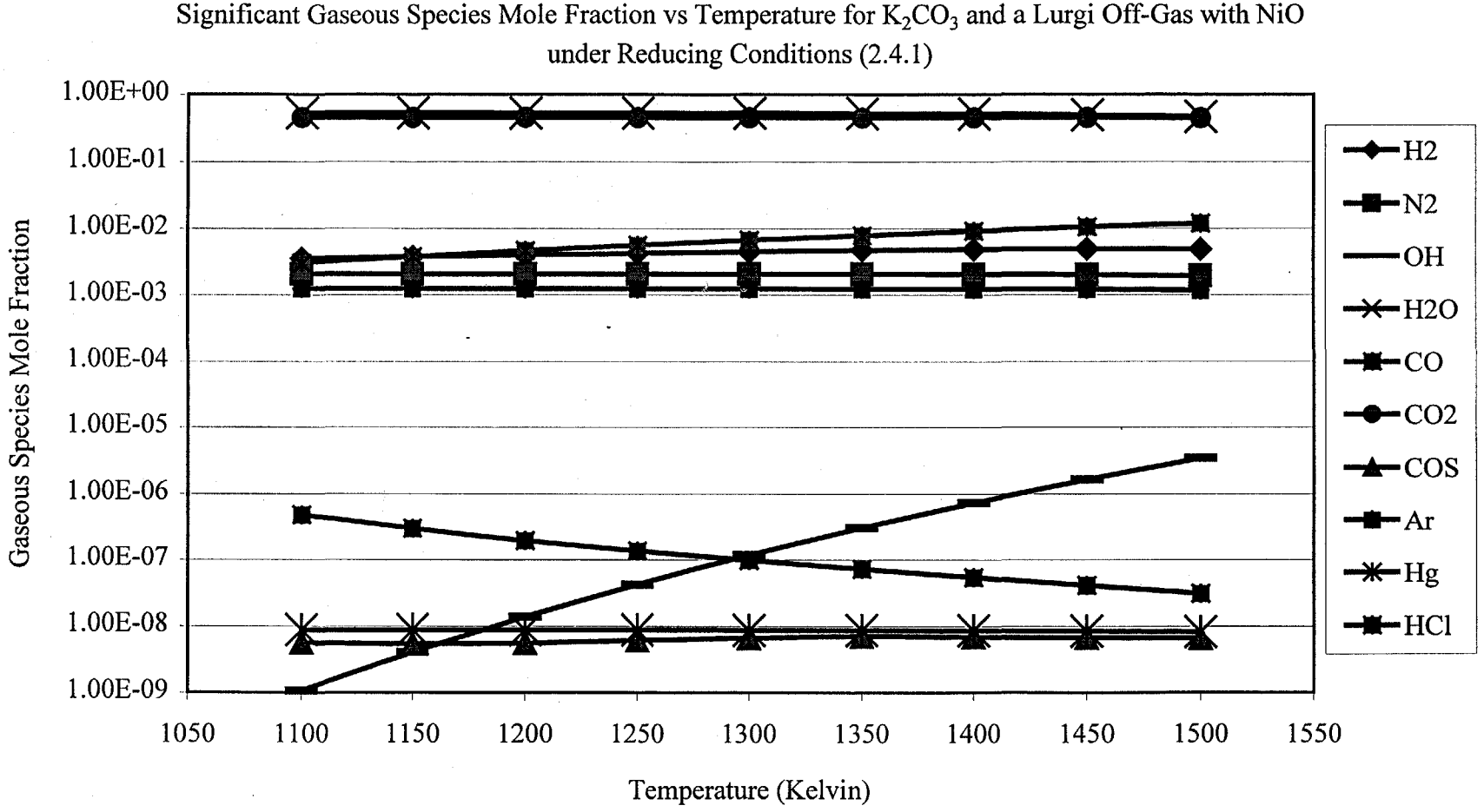

Figure A.26 Significant Gaseous Species Mole Fraction for K_2CO_3 and a Lurgi Off-Gas with NiO under Reducing Conditions (2.4.1).

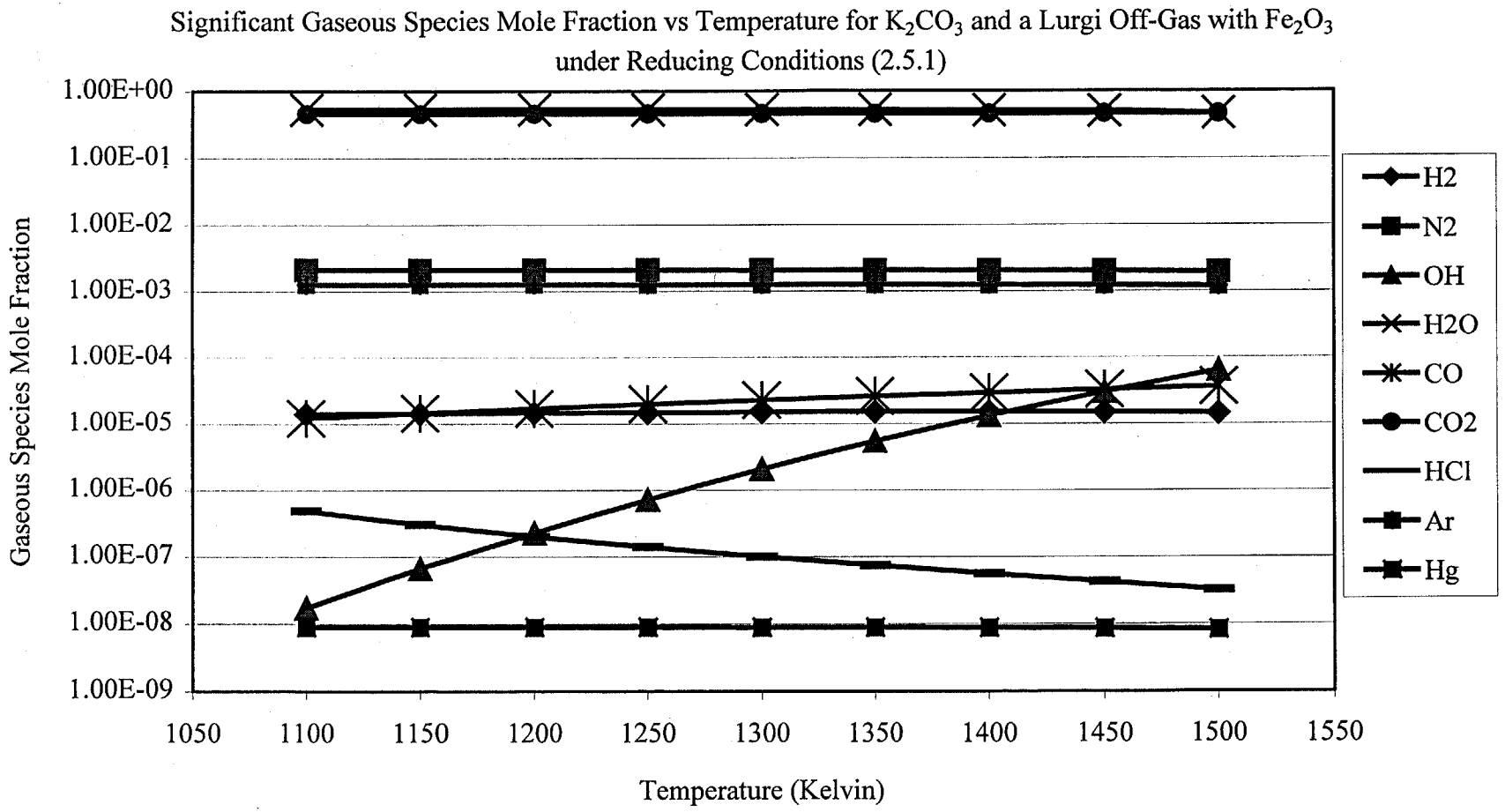

Figure A.27 Significant Gaseous Species Mole Fraction for K_2CO_3 and a Lurgi Off-Gas with Fe_2O_3 under Reducing Conditions (2.5.1).

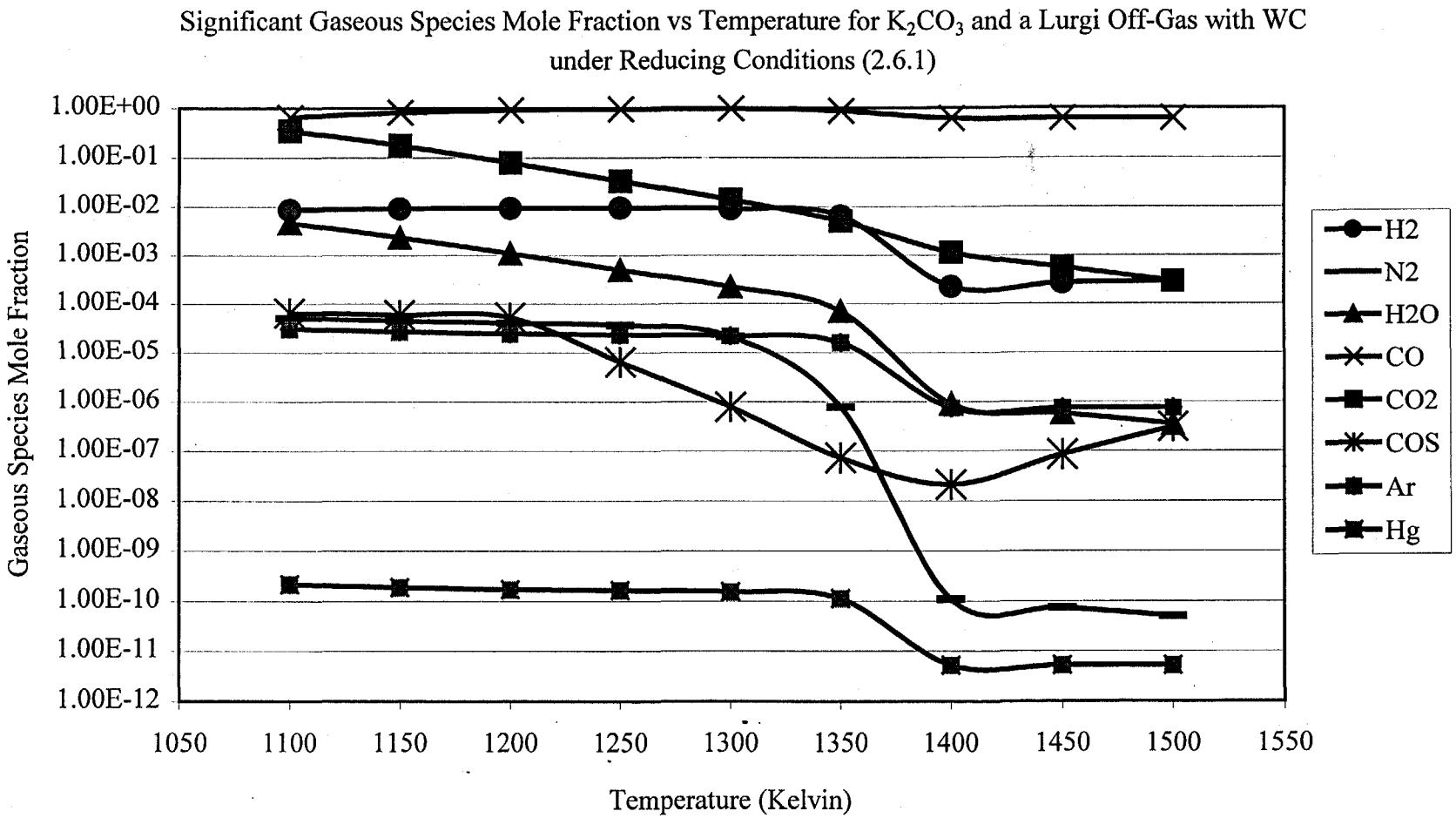

Figure A.28 Significant Gaseous Species Mole Fraction for K_2CO_3 and a Lurgi Off-Gas with WC under Reducing Conditions (2.6.1).

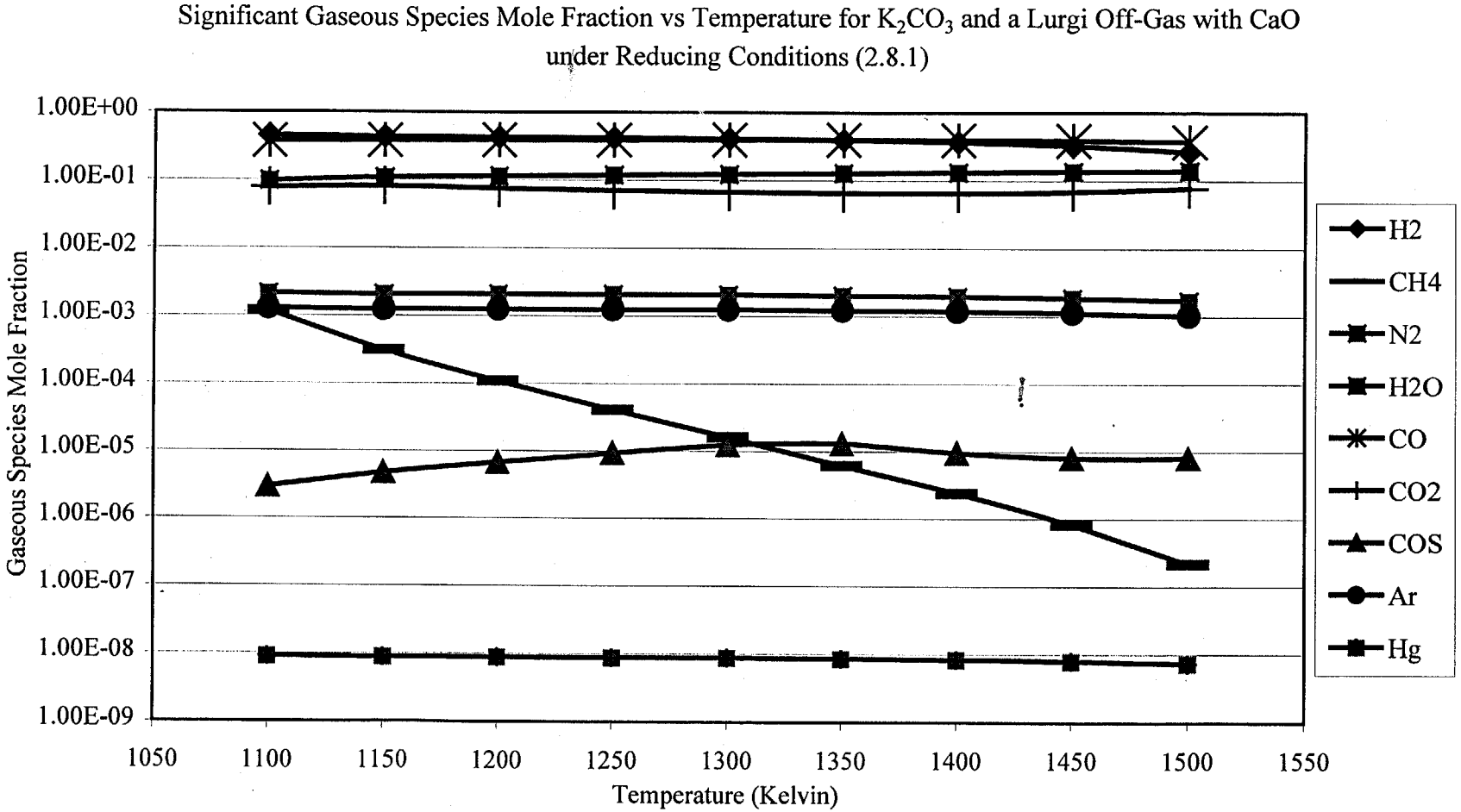

Figure A.29 Significant Gaseous Species Mole Fraction for K_2CO_3 and a Lurgi Off-Gas with CaO under Reducing Conditions (2.8.1).

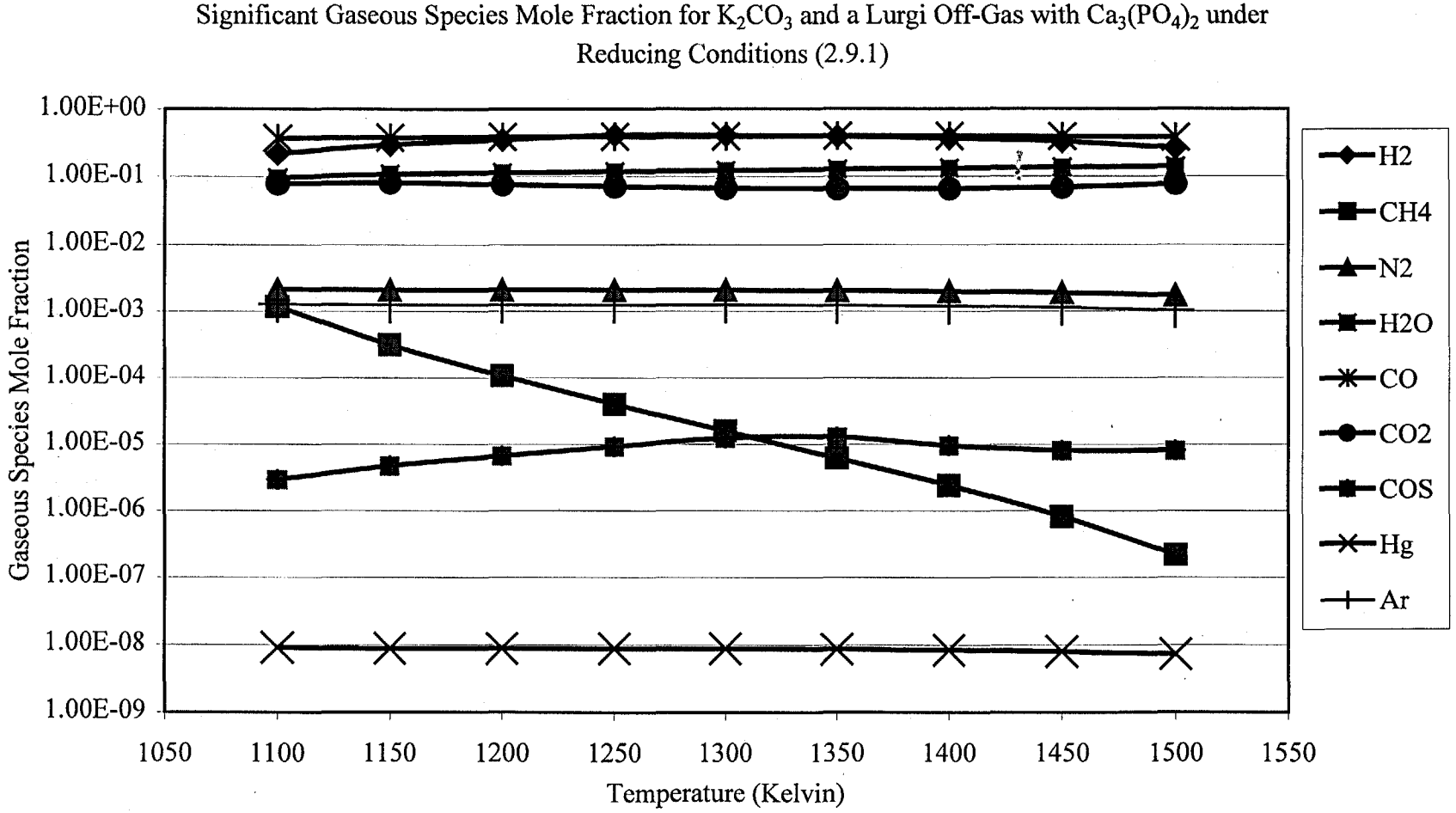

Figure A.30 Significant Gaseous Species Mole Fraction for K_2CO_3 and a Lurgi Off-Gas with $Ca_3(PO_4)_2$ under Reducing Conditions (2.9.1).

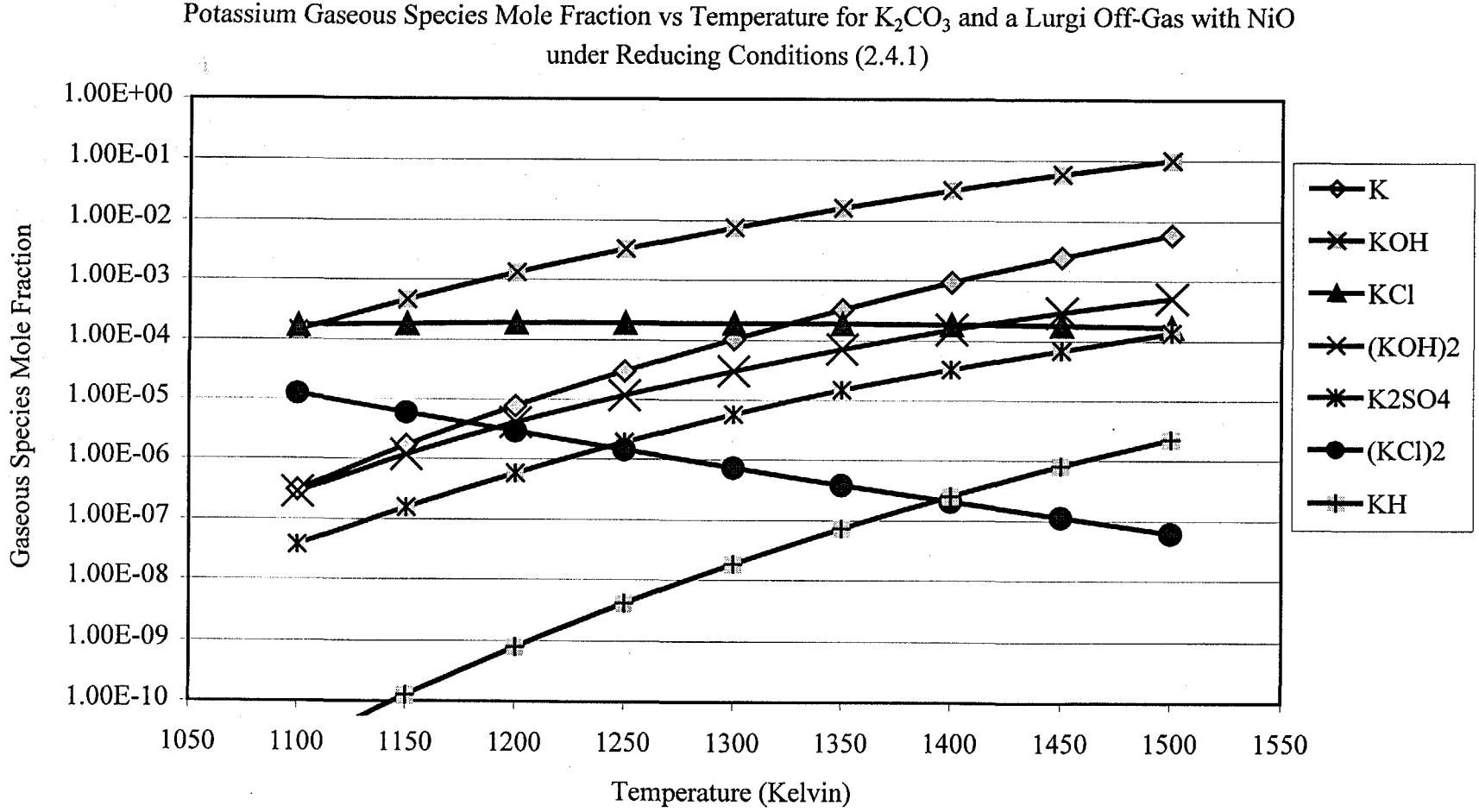

Figure A.31 Potassium Gaseous Species Mole Fraction for K_2CO_3 and a Lurgi Off-Gas with NiO under Reducing Conditions (2.4.1).

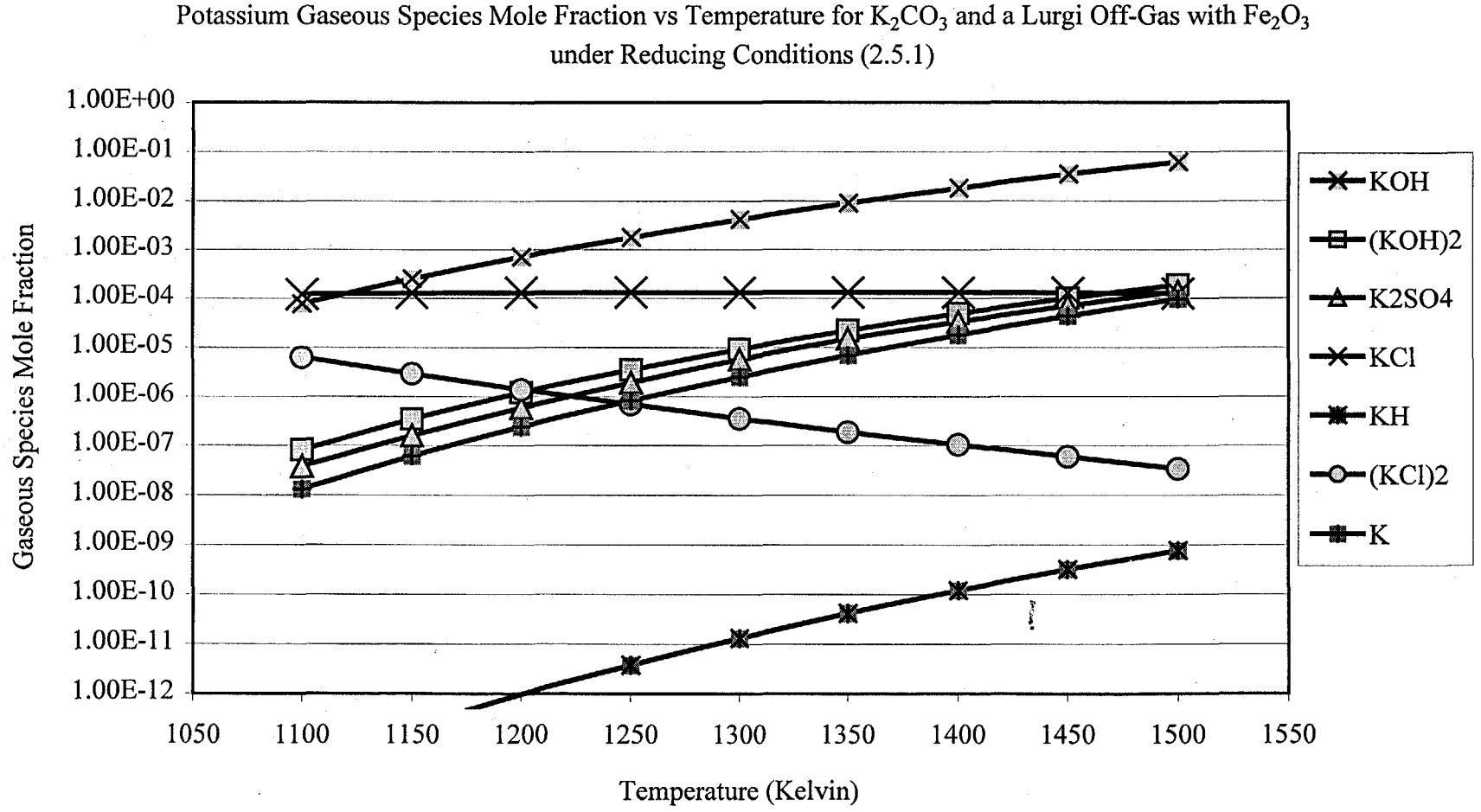

Figure A.32 Potassium Gaseous Species Mole Fraction for K_2CO_3 and a Lurgi Off-Gas with Fe_2O_3 under Reducing Conditions (2.5.1).

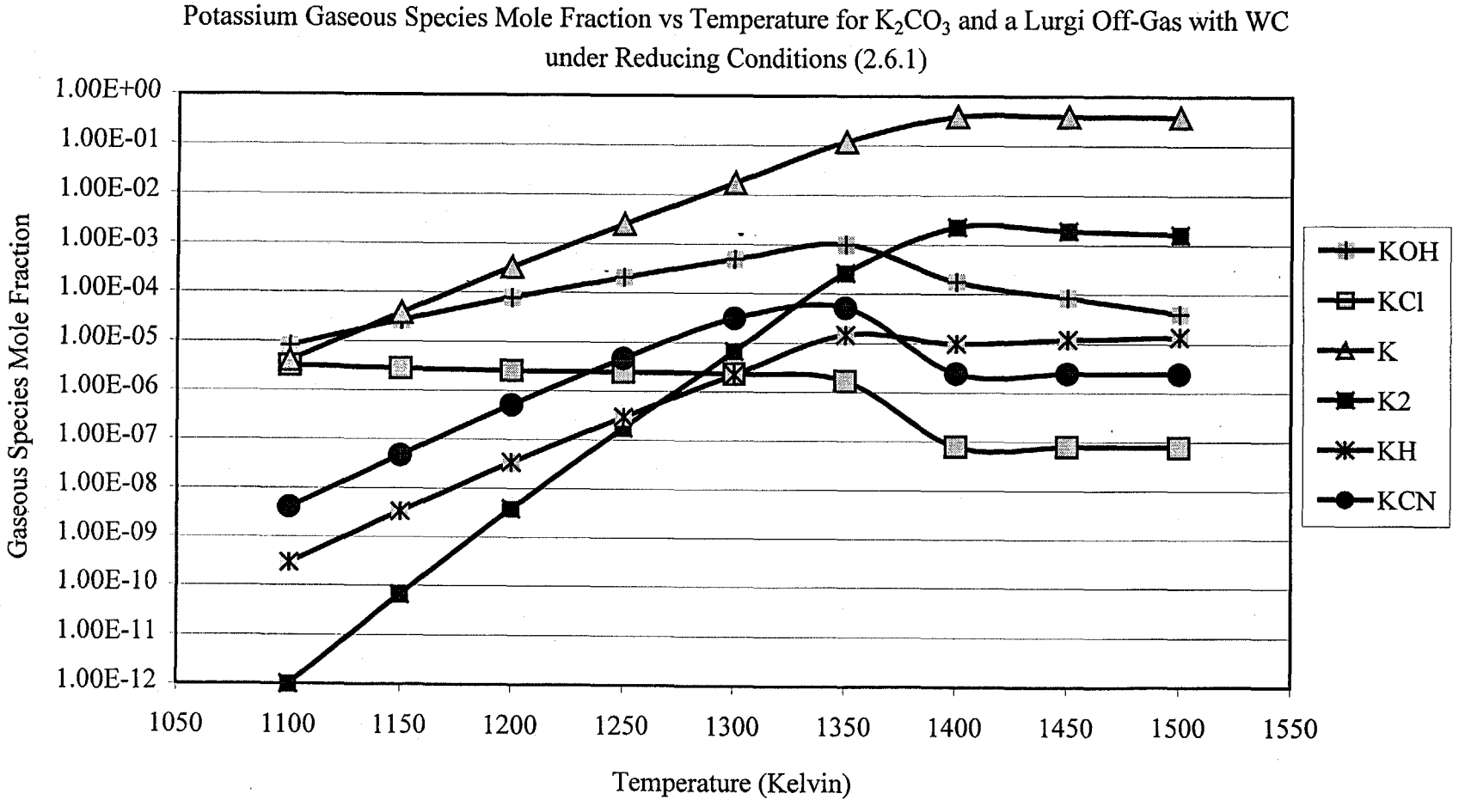

Figure A.33 Potassium Gaseous Species Mole Fraction for K_2CO_3 and a Lurgi Off-Gas with WC under Reducing Conditions (2.6.1).

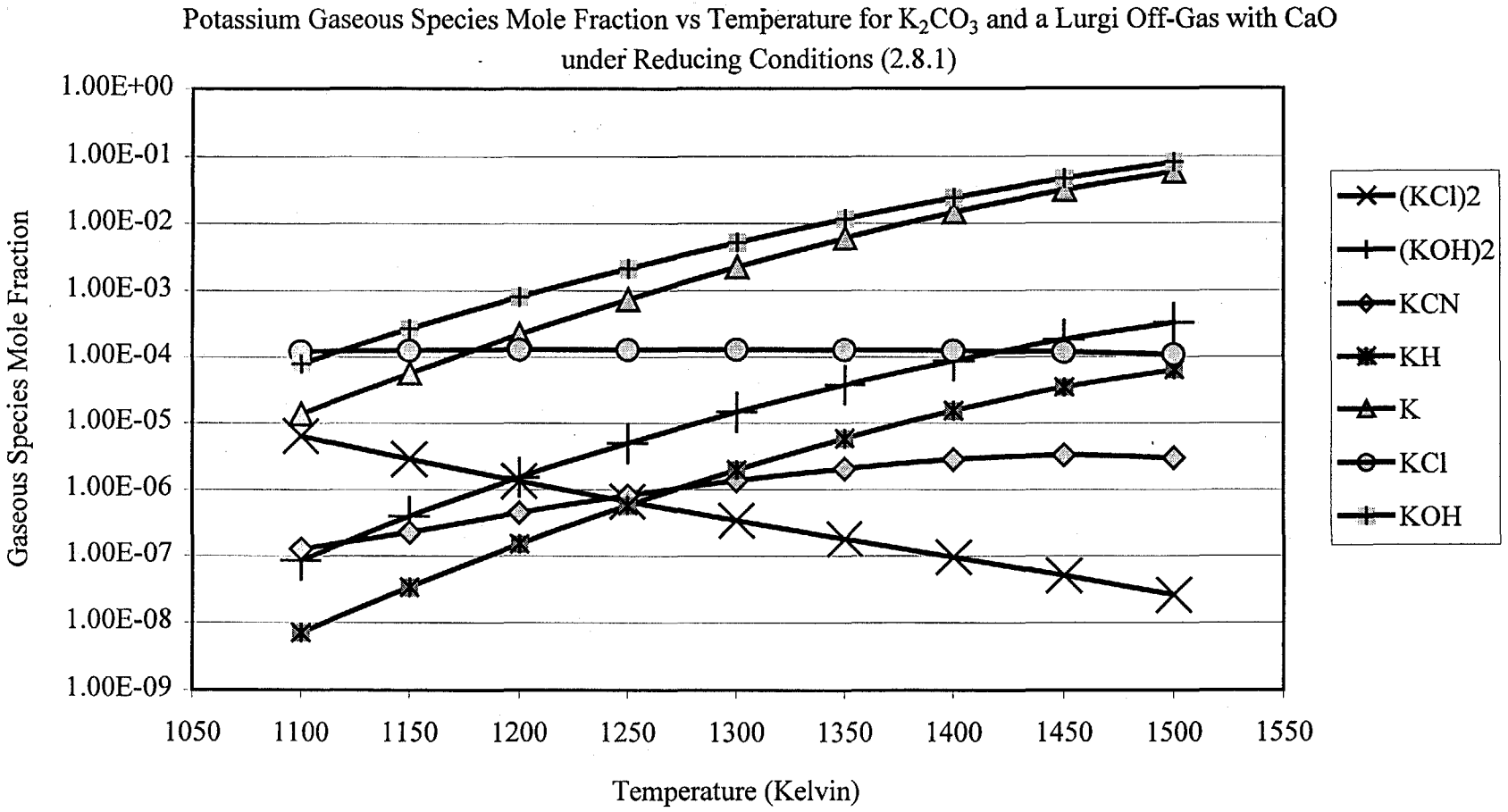

Figure A.34 Potassium Gaseous Species Mole Fraction for K_2CO_3 and a Lurgi Off-Gas with CaO under Reducing Conditions (2.8.1).

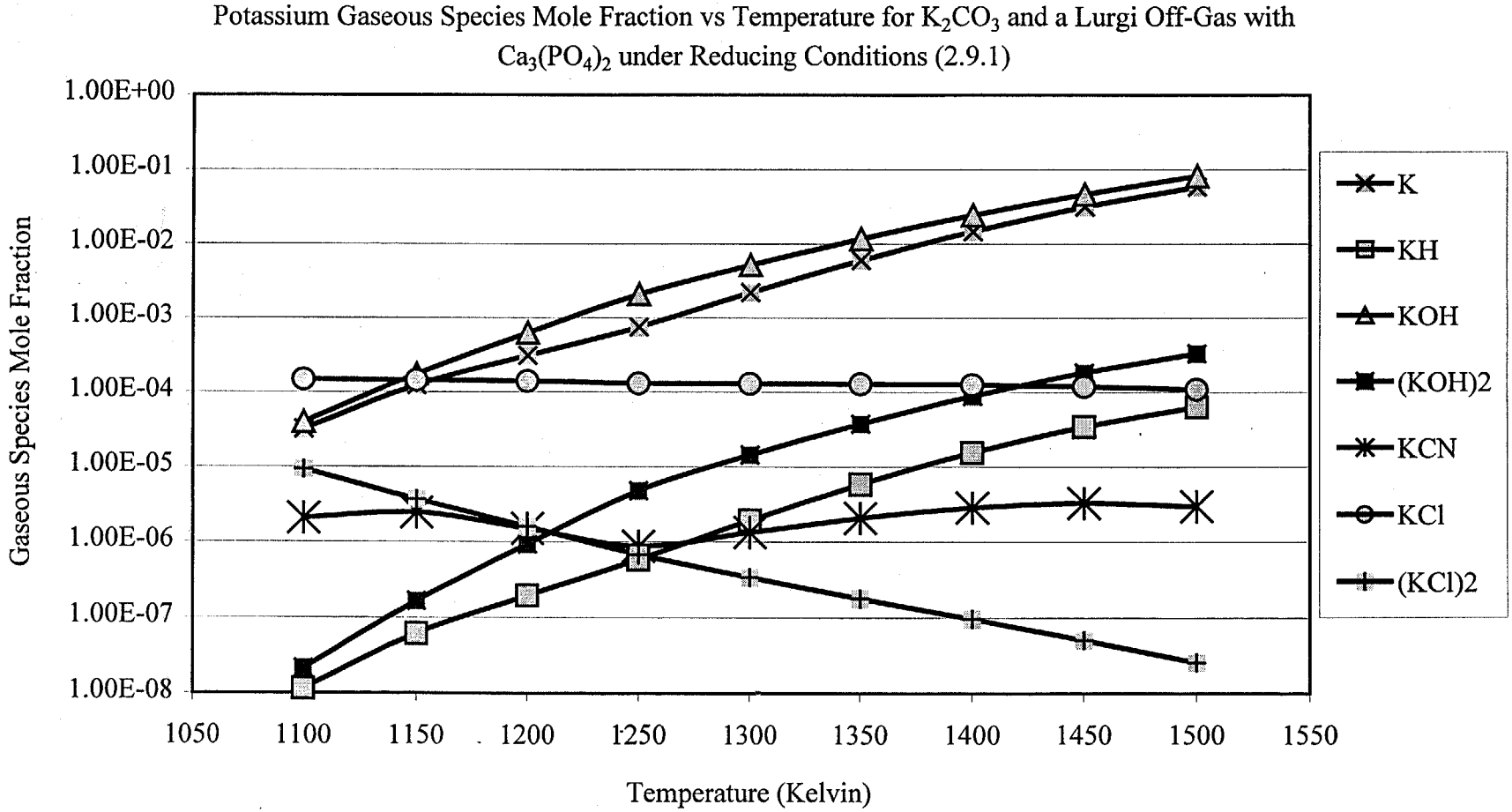

Figure A.35 Potassium Gaseous Species Mole Fraction for K_2CO_3 and a Lurgi Off-Gas with $Ca_3(PO_4)_2$ under Reducing Conditions (2.9.1).

A.6c) Low Temperature/Oxidizing Condition Simulations

This section examines various nitrates' ability to capture sulfur under oxidizing conditions at low temperature. The simulations were performed for two specific areas. The first step determined which of the nitrates did the best job capturing sulfur. After completing that section, the designated salt was combined with the set of supports in Table A. 1 to see if sulfur capture was a function of a "non-reactive" support. Table A.11 contains the reactant molar ratios inputted into the Equilib program. The simulations were run from 500-1100 K, taking equilibrium species information every 50 K.

Figure A.36 contains the SO_2 mole fraction versus temperature for these simulations. The SO_2 concentration for all of the salts at the lower end of the temperature range is extremely low, but clearly $NaNO_3$ and KNO_3 are the most effective. Around 950 K there is a distinct change in the $NaNO_3$ curve caused by it dissociating. $AgNO_3$ is unstable immediately and only captures sulfur up to 950 K, while $LiNO_3$ dissociates around 650 K. All of the nitrates capture sulfur as either a solid or liquid sulfate.

Both $NaNO_3$ and KNO_3 do roughly the same job removing the sulfur from the gas phase, except at the upper end of the temperature range tested. KNO_3 does have the advantage that it is stable over the entire temperature range. From this perspective it appears that KNO_3 is the logical choice to test with the remainder of the supports. Before proceeding it is important to compare the remainder of the gaseous species associated with these two salts found in Figures A.37-A.40. Figure A.37 and A.38 show the significant non-salt related gaseous species for $NaNO_3$ and KNO_3 respectively. In both cases, there are very high levels of N_2 and O_2, due to the nitrates partially dissociating into these components. There also were significant amounts of CO_2 and H_2O, which are products of the oxidation of CO and H_2. The NO_X concentration for both salts crossed the 1 ppm-v level around 850 K and topped out at 100 ppm-v around 1100 K, which is slightly higher than one would expect. In the case of $NaNO_3$, the actual molar amount of NO_x present after it dissociates at 950 K was still greater than the system with KNO_3. The concentration remains roughly the same due to diluting the gas phase with additional N_2 and O_2.

Figures A.39 and A.40 describe the salt related gaseous species for the two salts. Both figures show a general increasing trend with temperature for the gaseous salt species. The figures look identical in terms of the shape of the curves and place in regards to the respective gaseous species, but the gas concentrations for the $NaNO_3$ system is in general two orders of magnitude lower than KNO_3. In the end, KNO_3 was selected to test with the remainder of the supports due to its stability over the entire temperature range.

None of the low temperature oxidizing nitrate systems captured any mercury in the solid or liquid phase. The mercury remains primarily in its elemental form in the gas phase with only a small amount present as HgO.

Table A.11 FACT entering Molar Ratios for a Koppers-Totzek Off-Gas and Low Temperature Salts with Non-Reactive Supports.

	(8.4.3)	(9.3.3)	(10.3.3)	(11.3.3)
Support	1.000E+00	1.000E+00	1.000E+00	1.000E+00
Salt	1.204E-01	1.611E-01	1.354E-01	8.060E-02
CO	6.037E-05	6.476E-05	6.193E-05	5.651E-05
CH_4	1.059E-07	1.136E-07	1.087E-07	9.915E-08
H_2	3.040E-05	3.260E-05	3.118E-05	2.846E-05
COS	3.177E-08	3.408E-08	3.260E-08	2.974E-08
H_2S	2.118E-07	2.272E-07	2.173E-07	1.983E-07
NH_3	0.000E+00	0.000E+00	0.000E+00	0.000E+00
CO_2	1.323E-05	1.419E-05	1.357E-05	1.238E-05
N_2	1.901E-04	2.040E-04	1.951E-04	1.780E-04
O_2	5.020E-05	5.385E-05	5.151E-05	4.700E-05
Ar	2.118E-07	2.272E-07	2.173E-07	1.983E-07
Hg	5.524E-12	5.925E-12	5.667E-12	5.171E-12
HCl	8.285E-08	8.888E-08	8.500E-08	7.756E-08

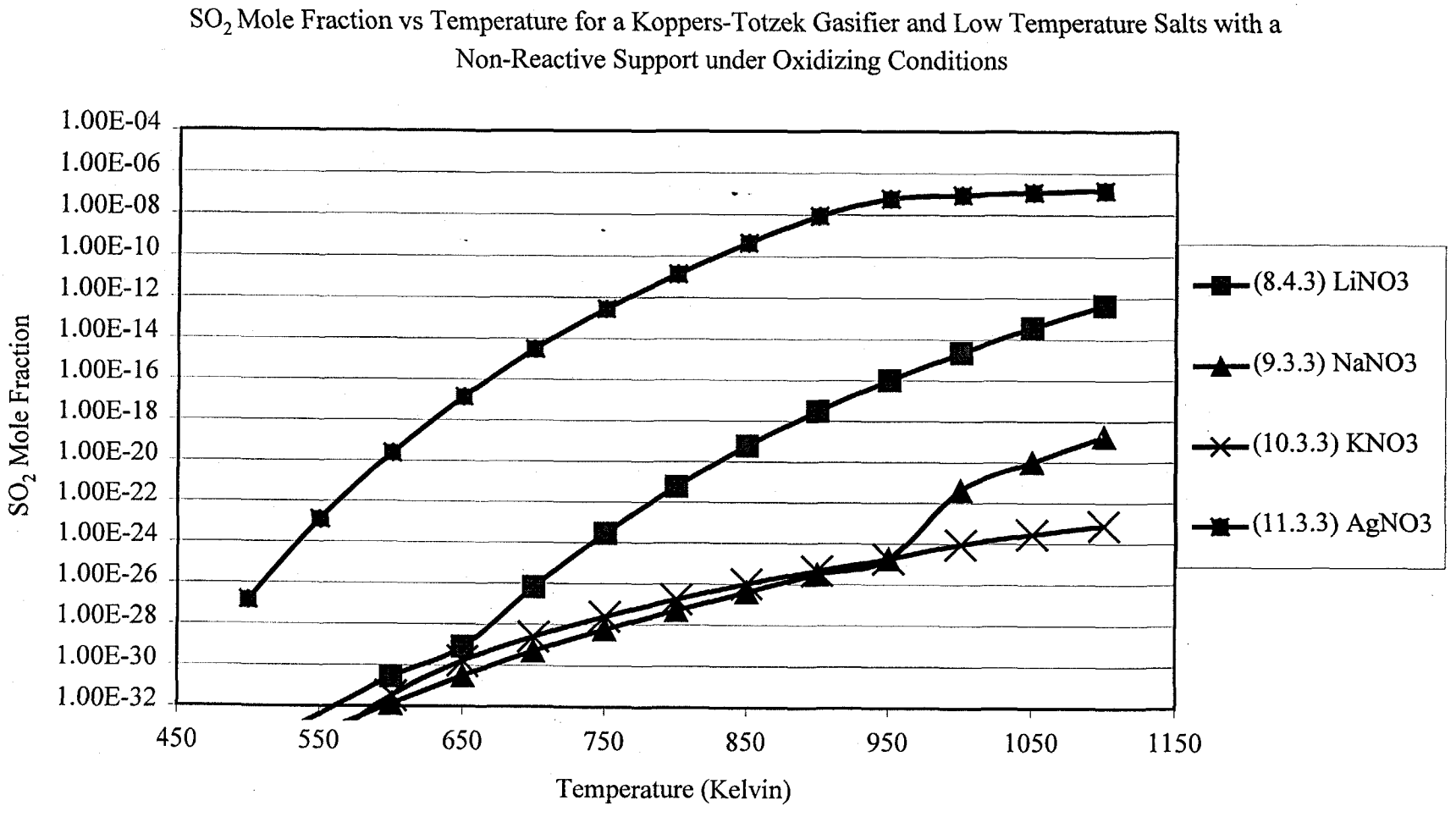

Figure A.36 SO_2 Mole Fraction for a Koppers-Totzek Off-Gas and Low Temperature Salts with a Non-Reactive Support under Oxidizing Conditions.

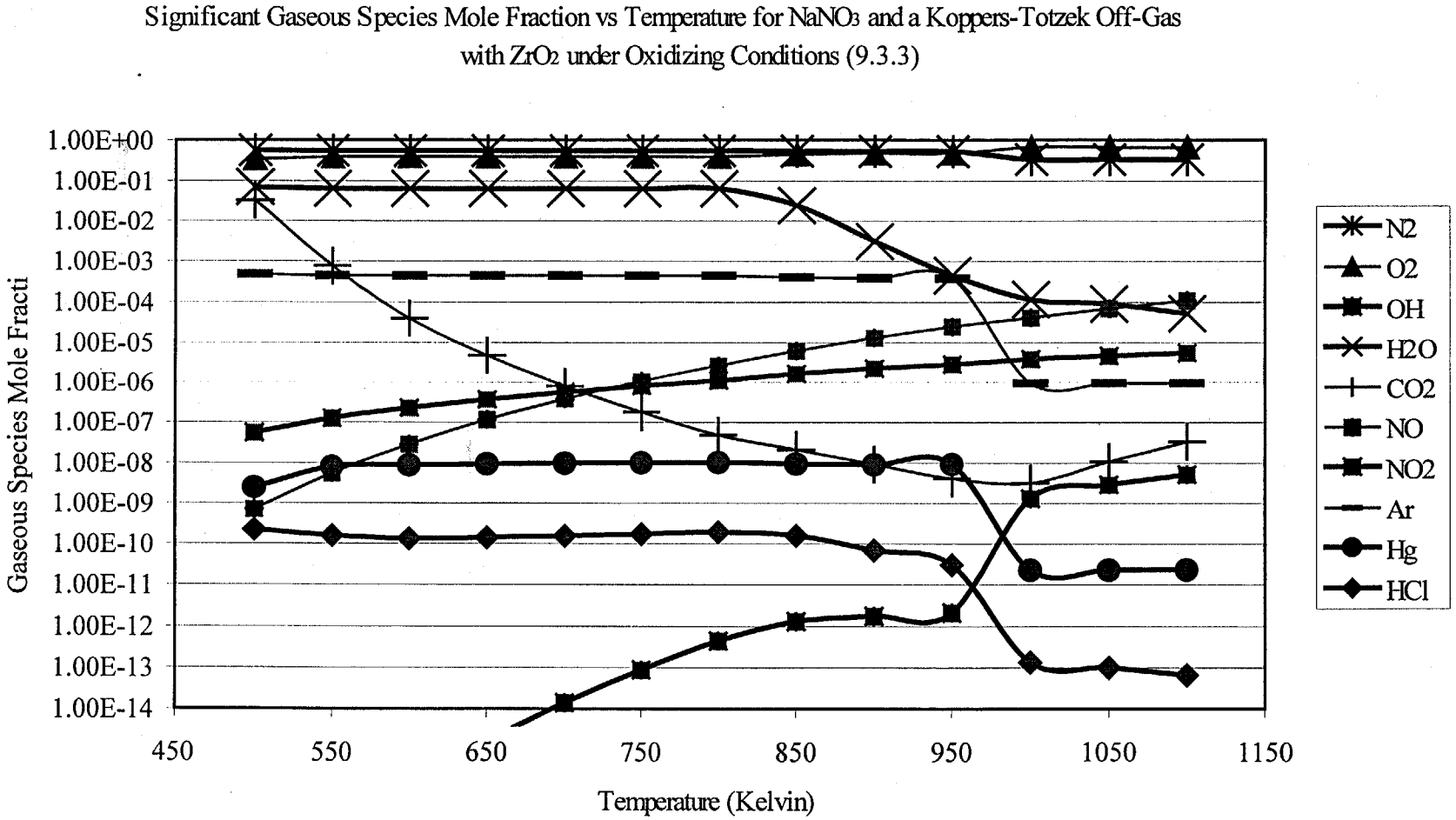

Figure A.37 Significant Gaseous Species Mole Fraction for $NaNO_3$ and a Koppers-Totzek Off-Gas with ZrO_2 under Oxidizing Conditions (9.3.3).

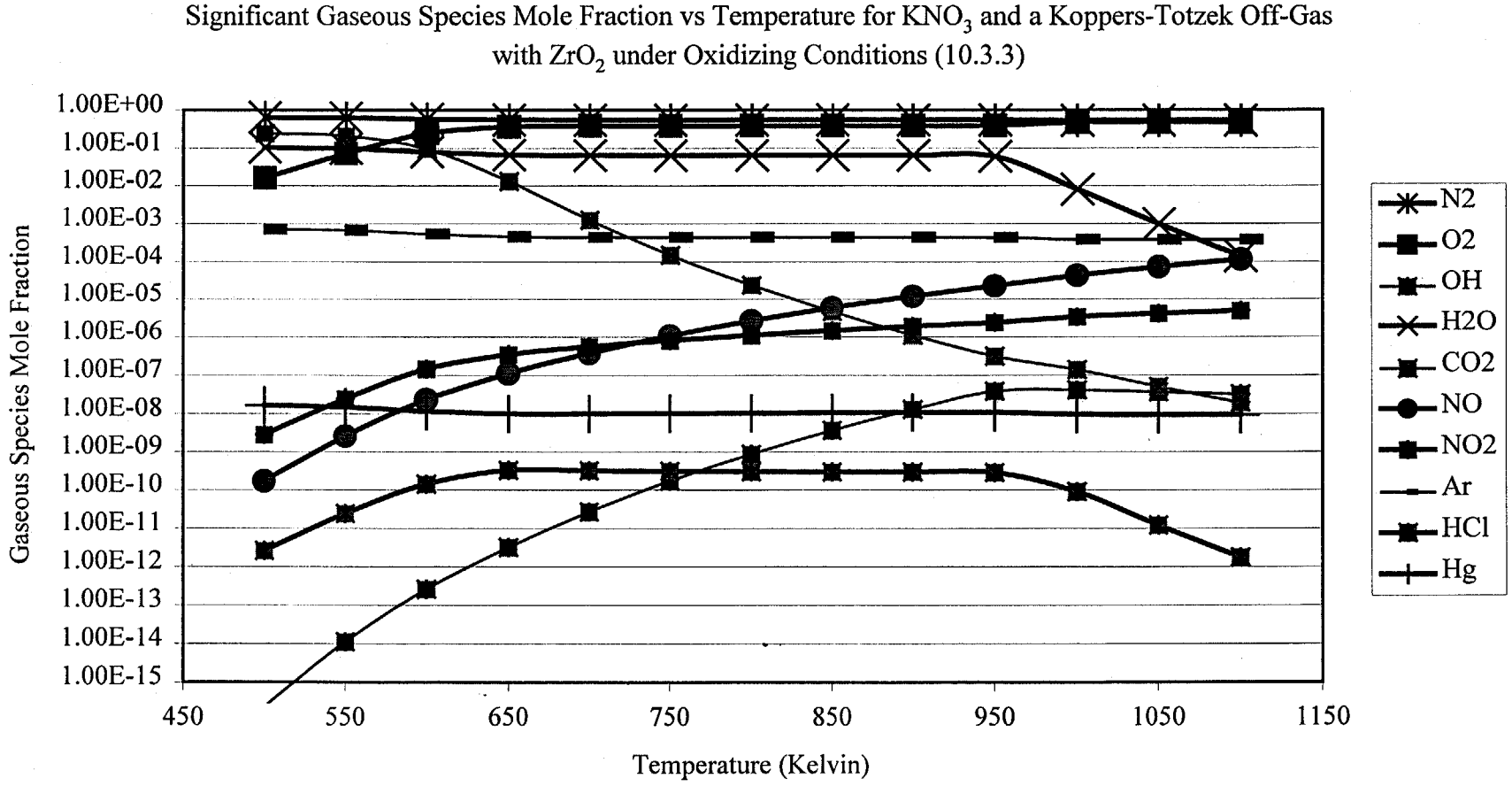

Figure A.38 Significant Gaseous Species Mole Fraction for KNO_3 and a Koppers-Totzek Off-Gas with ZrO_2 under Oxidizing Conditions (10.3.3).

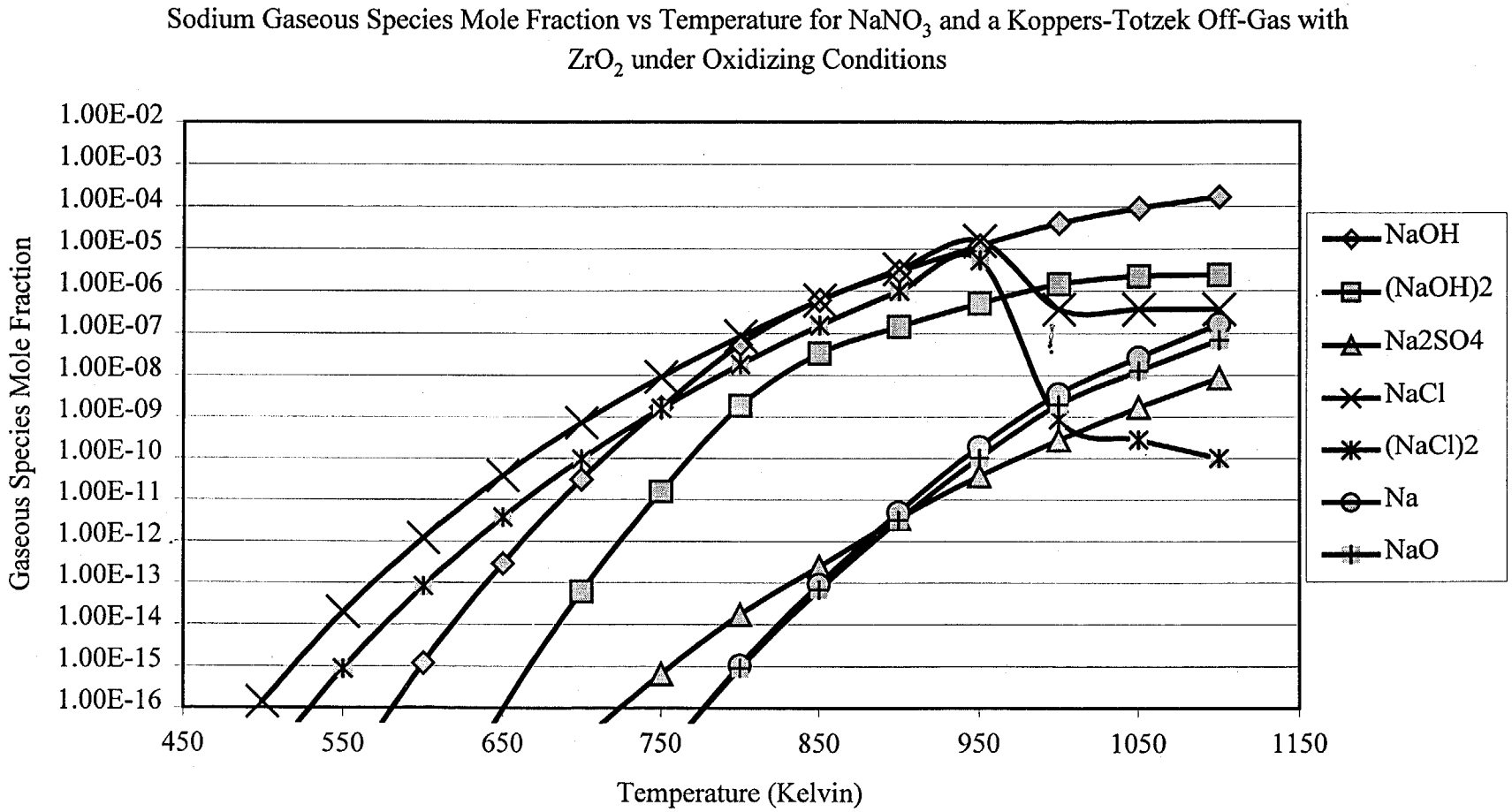

Figure A.39 Sodium Gaseous Species Mole Fraction for $NaNO_3$ and a Koppers-Totzek Off-Gas with ZrO_2 under Oxidizing Conditions (9.3.3).

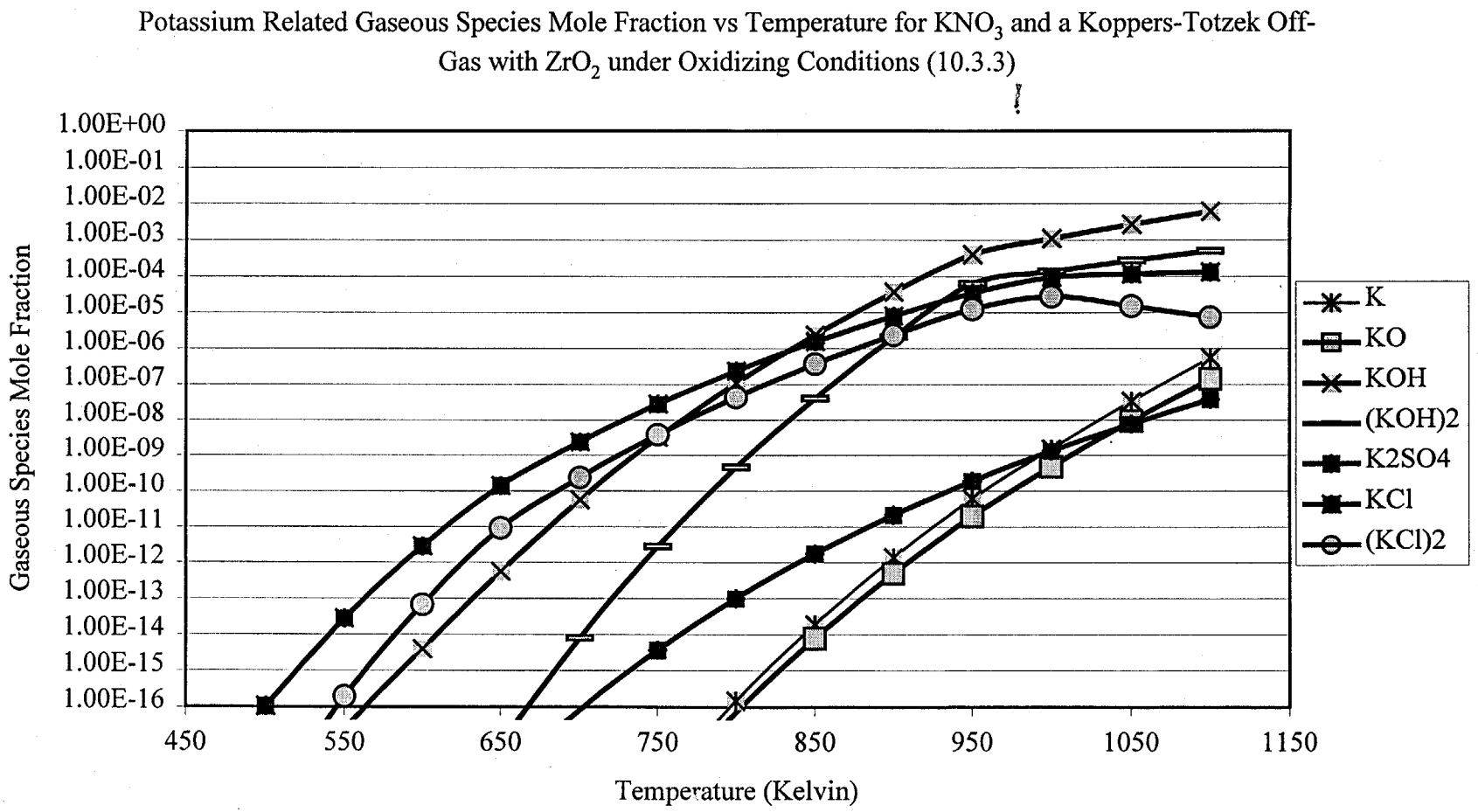

Figure A.40 Potassium Gaseous Species Mole Fraction for KNO_3 and a Koppers-Totzek Off-Gas with ZrO_2 under Oxidizing Conditions (10.3.3).

In this section, KNO_3 was run with each support to determine if there were any significant differences in sulfur capture for systems where the salt and the support do not react and to examine what products form in the solid and liquid phase for all of the systems tested. Table A.12 contains the reactant molar ratios inputted into the Equilib program for this section.

Figure A.41 plots the SO_2 concentration for the various systems tested. Initially, it appears that all of the systems expected to be non-reactive, from earlier results found in Table A.4, captured the same amount of sulfur. The reactive supports still captured a significant amount of sulfur as a solid sulfate but the formation of glassy compounds such as $K_2Si_4O_9$, KAl_9O_{14}, and $K_2Ti_6O_{13}$ would further complicate their practical implementation in a high temperature fluidized bed. All of the supports captured sulfur as a sulfate, except WC. Entering this section, it was first thought that both CaO and $Ca_3(PO_4)_2$ were not going to react with the KNO_3. For CaO, small amounts of $Ca(OH)_2$ and $CaCO_3$ are formed from 500-700 K. For $Ca_3(PO_4)_2$, a small amount of K_2HPO_4 (s) is formed over the entire temperature range. The sulfur capture in these systems is still the same when compared to the completely non-reactive supports: ZrO_2, NiO, and Fe_2O_3.

Important gaseous species are plotted in Figures A.42-A.46 for NiO, Fe_2O_3, WC, CaO, and $Ca_3(PO_4)_2$ respectively. All of the systems resemble each other with the exception of WC. In the WC system, oxygen reacted with WC to form WO_2. This reaction used up a majority of the oxygen present in the system causing it to behave as if in a reduced state. For this system, there actually was no sulfur capture in the liquid or solid phase. The reason the SO_2 concentration in Figure A.41 was lower in this system compared to the systems using SiO_2, Al_2O_3, and TiO_2 was a result of the sulfur remaining in its reduced form, H_2S. Appropriately, Figure A.44 shows a high H_2S concentration. As stated previously, the remainder of supports all exhibited similar gaseous species concentration. Moderate levels of NO_x and significant combustion products were present. Again, all of the mercury entering the system remained in the gas phase.

Figures A.47-50 show the significant salt related species for the non-reactive supports. There was very little difference in the salt speciation for the various supports tested. For low temperature oxidizing conditions, KNO_3 and $NaNO_3$ capture significant amounts of sulfur in the solid phase. As a whole, sulfur capture is not a function of the support particle used when the support did not react substantially with the salt or oxygen present in the system. Based on the very low equilibrium concentrations of SO_2 and only moderate levels of NO_x, the low temperature oxidation of an off-gas from a gasifier in the presence of KNO_3 or $NaNO_3$ demonstrates the necessary qualities for its implementation as a hot gas clean-up strategy.

Table A.12 FACT entering Molar Ratios for KNO_3 and a Koppers-Totzek Off Gas with various Supports under Oxidizing Conditions.

	(10.1.3)	(10.2.3)	(10.4.3)	(10.5.3)
Support	1.00E+0	1.000E+00	1.000E+00	1.000E+00
Salt	6.603E-2	1.121E-01	8.209E-02	1.755E-01
CO	5.520E-5	5.953E-05	5.665E-05	6.643E-05
CH_4	9.684E-8	1.044E-07	9.939E-08	1.165E-07
H_2	2.779E-5	2.997E-05	2.852E-05	3.345E-05
COS	2.905E-8	3.133E-08	2.982E-08	3.496E-08
H_2S	1.937E-7	2.089E-07	1.988E-07	2.331E-07
NH_3	0.00E+0	0.000E+00	0.000E+00	0.000E+00
CO_2	1.209E-5	1.304E-05	1.241E-05	1.456E-05
N_2	1.739E-4	1.875E-04	1.784E-04	2.092E-04
O_2	4.591E-5	4.951E-05	4.711E-05	5.525E-05
Ar	1.937E-7	2.089E-07	1.988E-07	2.331E-07
Hg	5.051E-12	5.447E-12	5.184E-12	6.078E-12
HCl	7.576E-8	8.170E-08	7.775E-08	9.117E-08
	(10.6.3)	**(10.7.3)**	**(10.8.3)**	**(10.9.3)**
Support	1.000E+00	1.000E+00	1.000E+00	1.000E+00
Salt	2.153E-01	8.779E-02	6.162E-02	3.409E-01
CO	7.141E-05	5.718E-05	5.481E-05	9.175E-05
CH_4	1.253E-07	1.003E-07	9.615E-08	1.610E-07
H_2	3.596E-05	2.879E-05	2.760E-05	4.620E-05
COS	3.759E-08	3.010E-08	2.885E-08	4.829E-08
H_2S	2.506E-07	2.006E-07	1.923E-07	3.219E-07
NH_3	0.00E+00	0.00E+00	0.00E+00	0.00E+00
CO_2	1.565E-05	1.253E-05	1.201E-05	2.010E-05
N_2	2.249E-04	1.801E-04	1.726E-04	2.890E-04
O_2	5.939E-05	4.756E-05	4.558E-05	7.630E-05
Ar	2.506E-07	2.006E-07	1.923E-07	3.219E-07
Hg	6.534E-12	5.232E-12	5.015E-12	8.395E-12
HCl	9.801E-08	7.848E-08	7.522E-08	1.259E-07

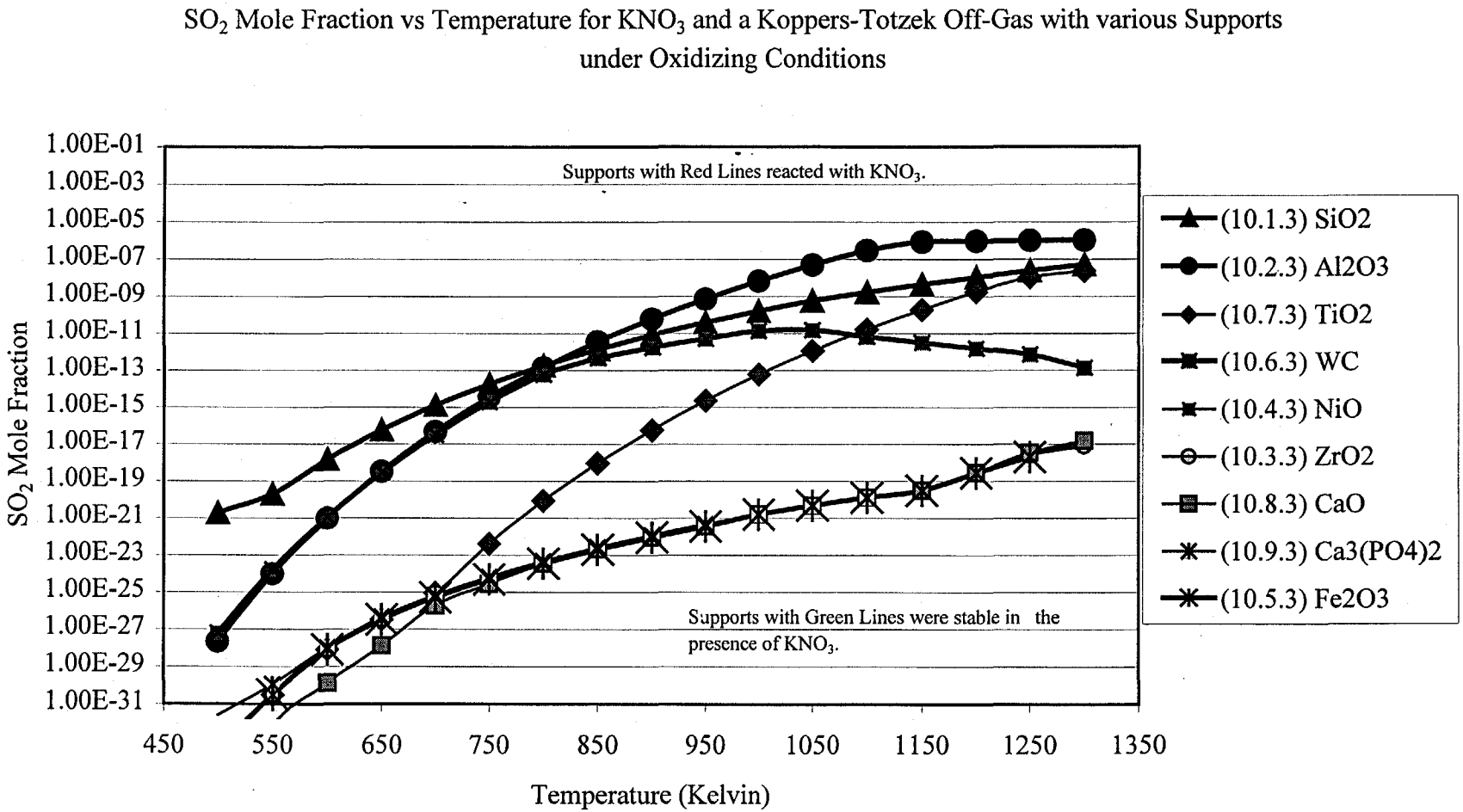

Figure A.41 SO_2 Mole Fraction for KNO_3 and a Koppers-Totzek Off-Gas with various Supports under Oxidizing Conditions.

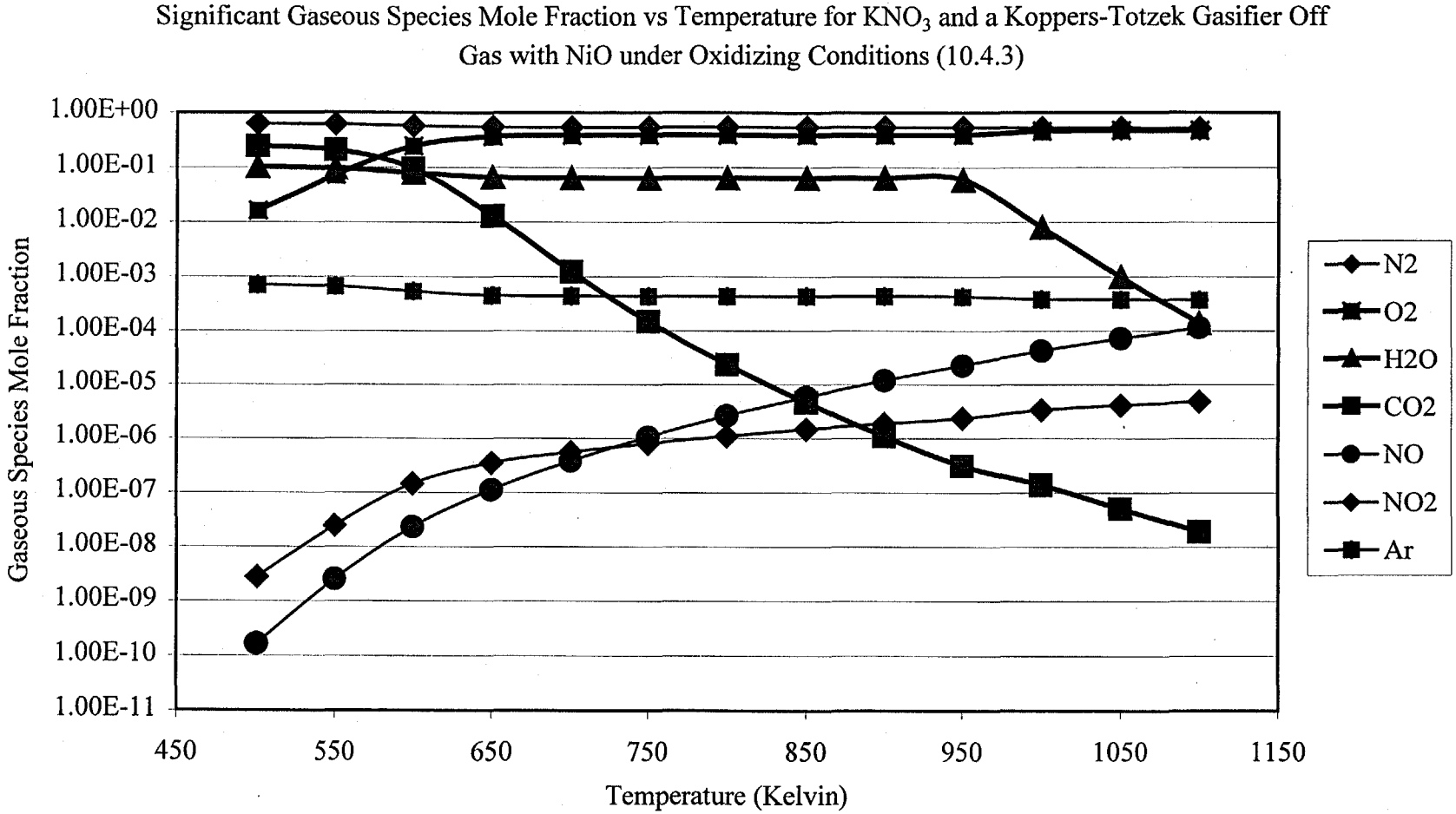

Figure A.42 Significant Gaseous Species Mole Fraction for KNO_3 and a Koppers-Totzek Off-Gas with NiO under Oxidizing Conditions (10.4.3).

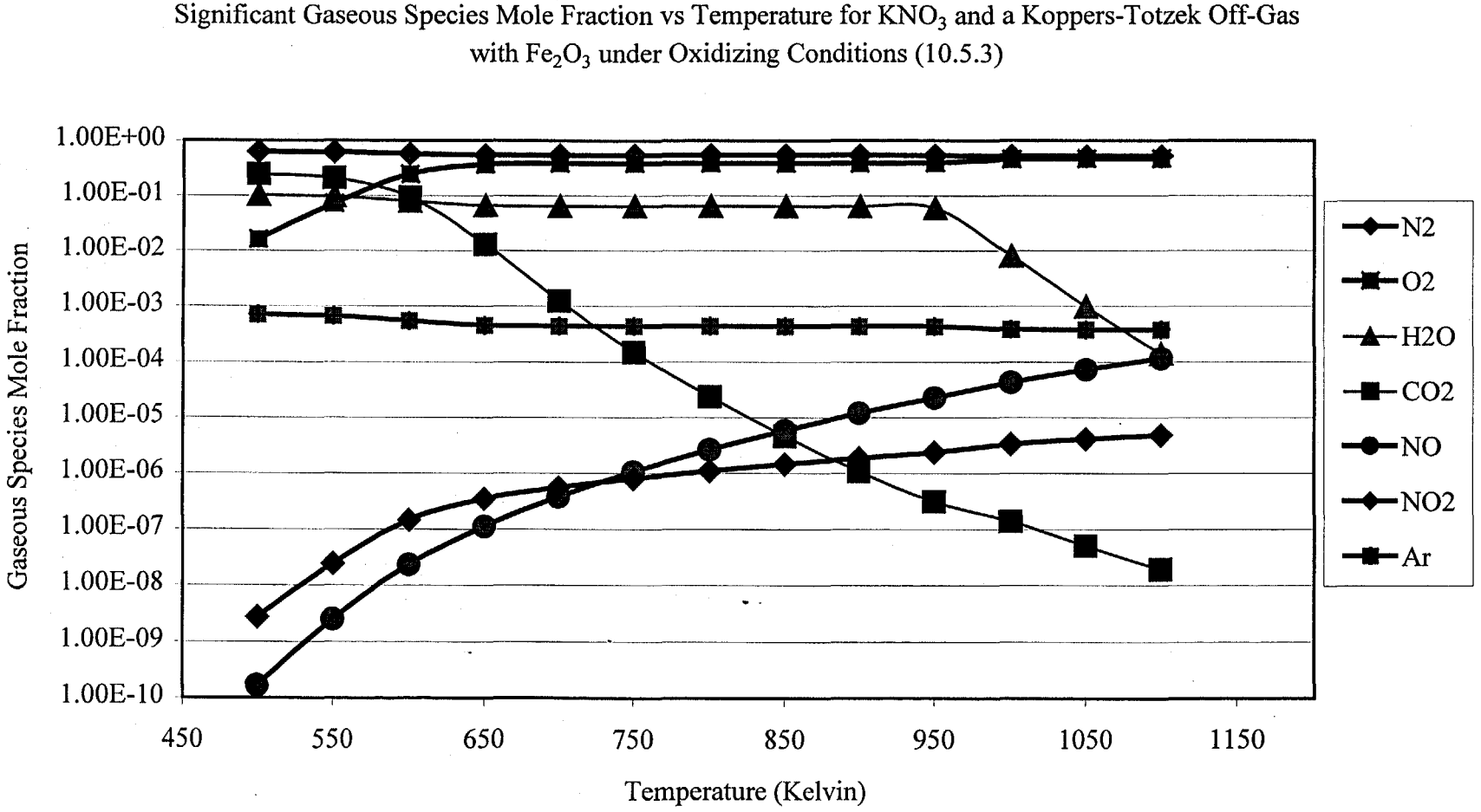

Figure A.43 Significant Gaseous Species Mole Fraction for KNO_3 and a Koppers-Totzek Off-Gas with Fe_2O_3 under Oxidizing Conditions (10.5.3).

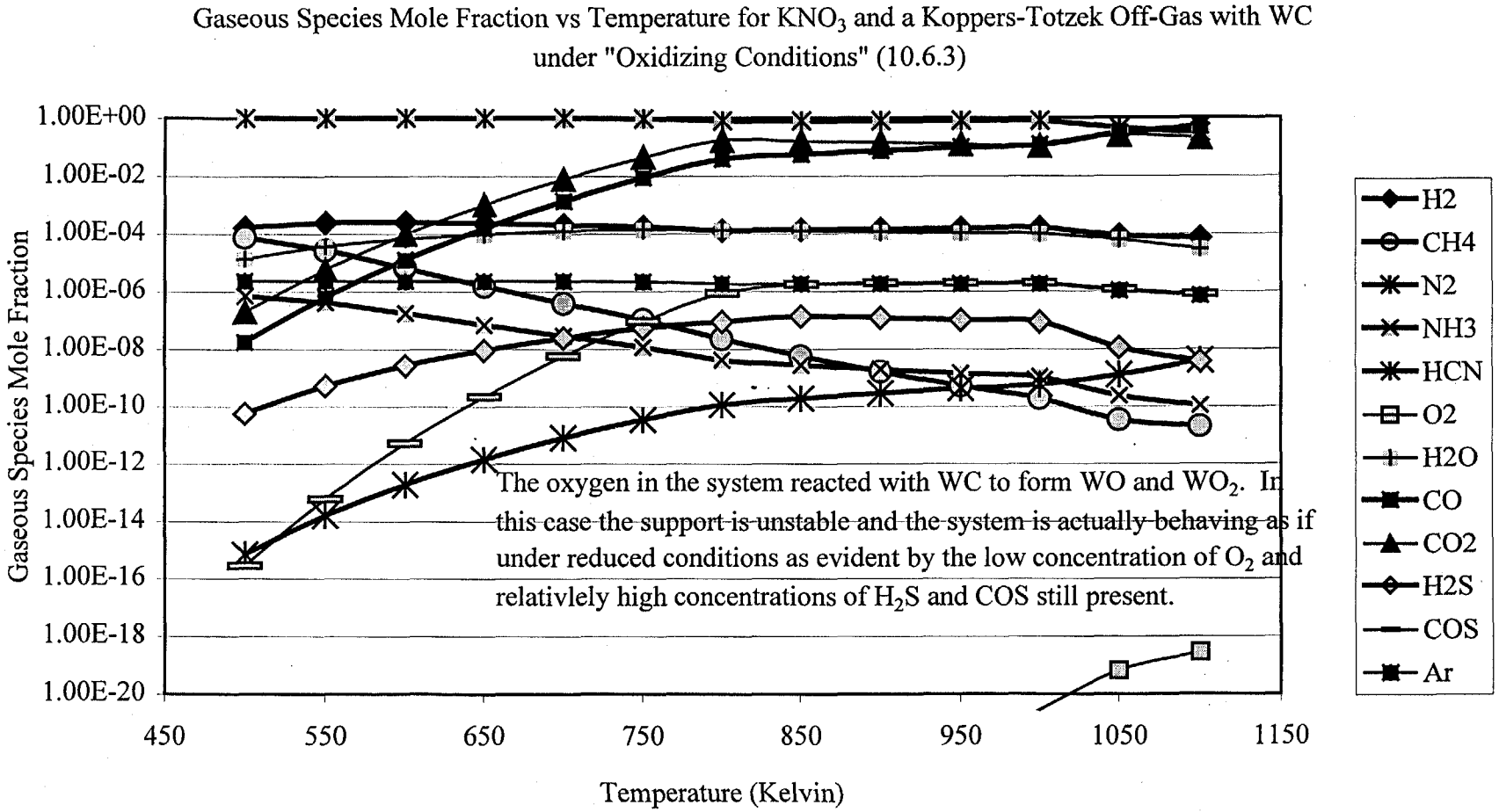

Figure A.44 Significant Gaseous Species Mole Fraction for KNO_3 and a Koppers-Totzek Off-Gas with WC under Oxidizing Conditions (10.6.3).

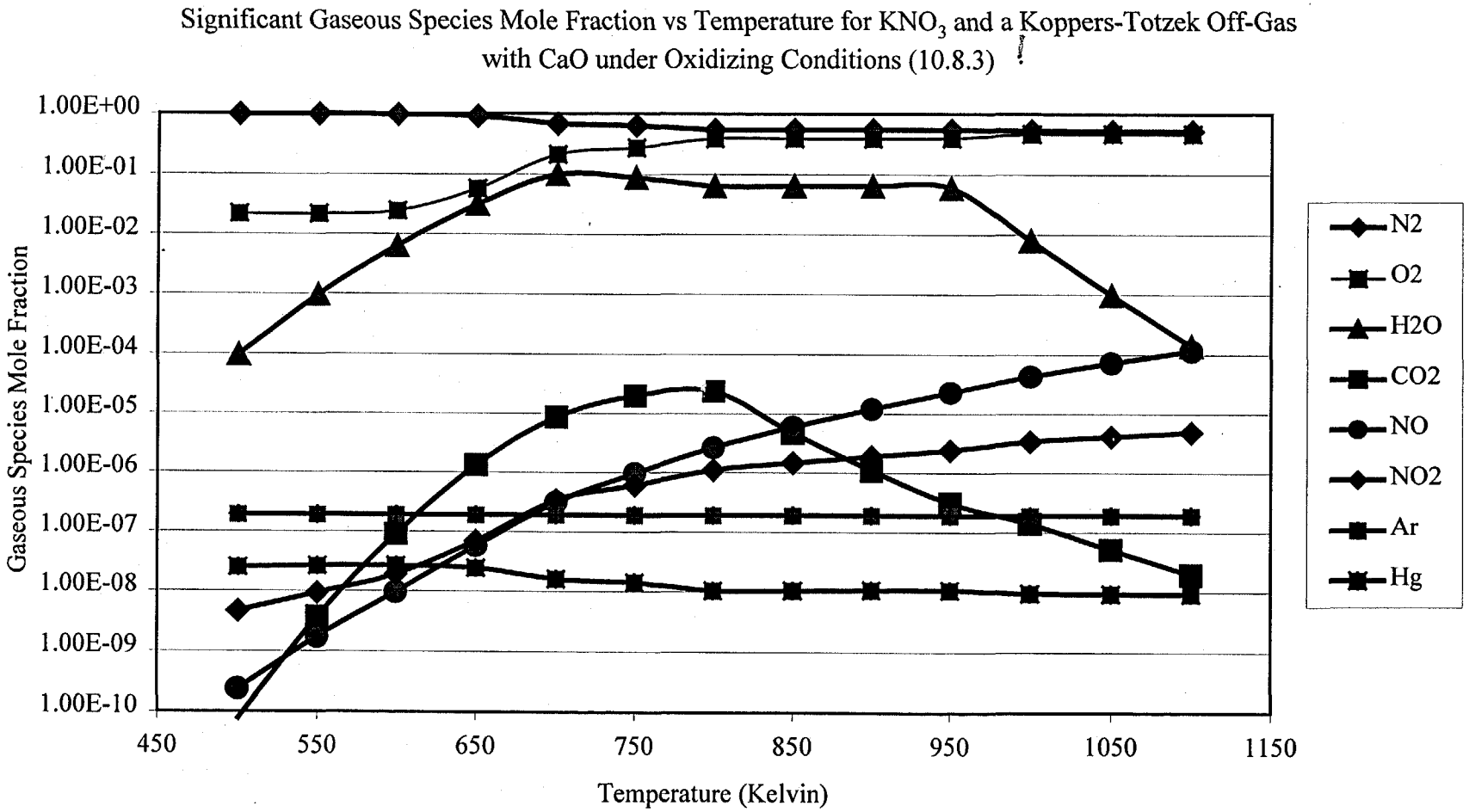

Figure A.45 Significant Gaseous Species Mole Fraction for KNO_3 and a Koppers-Totzek Off-Gas with CaO under Oxidizing Conditions (10.8.3).

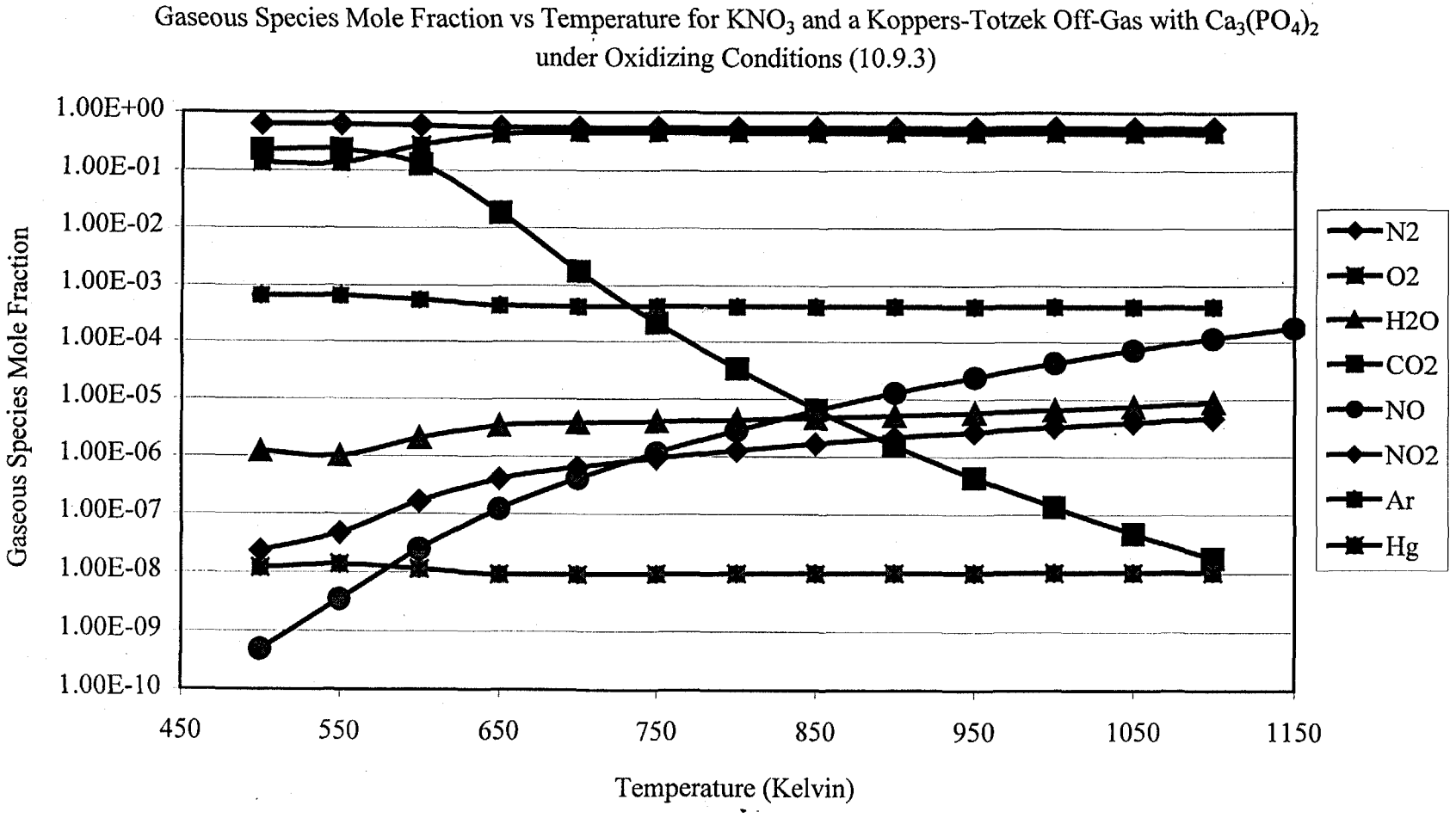

Figure A.46 Significant Gaseous Species Mole Fraction for KNO_3 and a Koppers-Totzek Off-Gas with $Ca_3(PO_4)_2$ under Oxidizing Conditions (10.9.3).

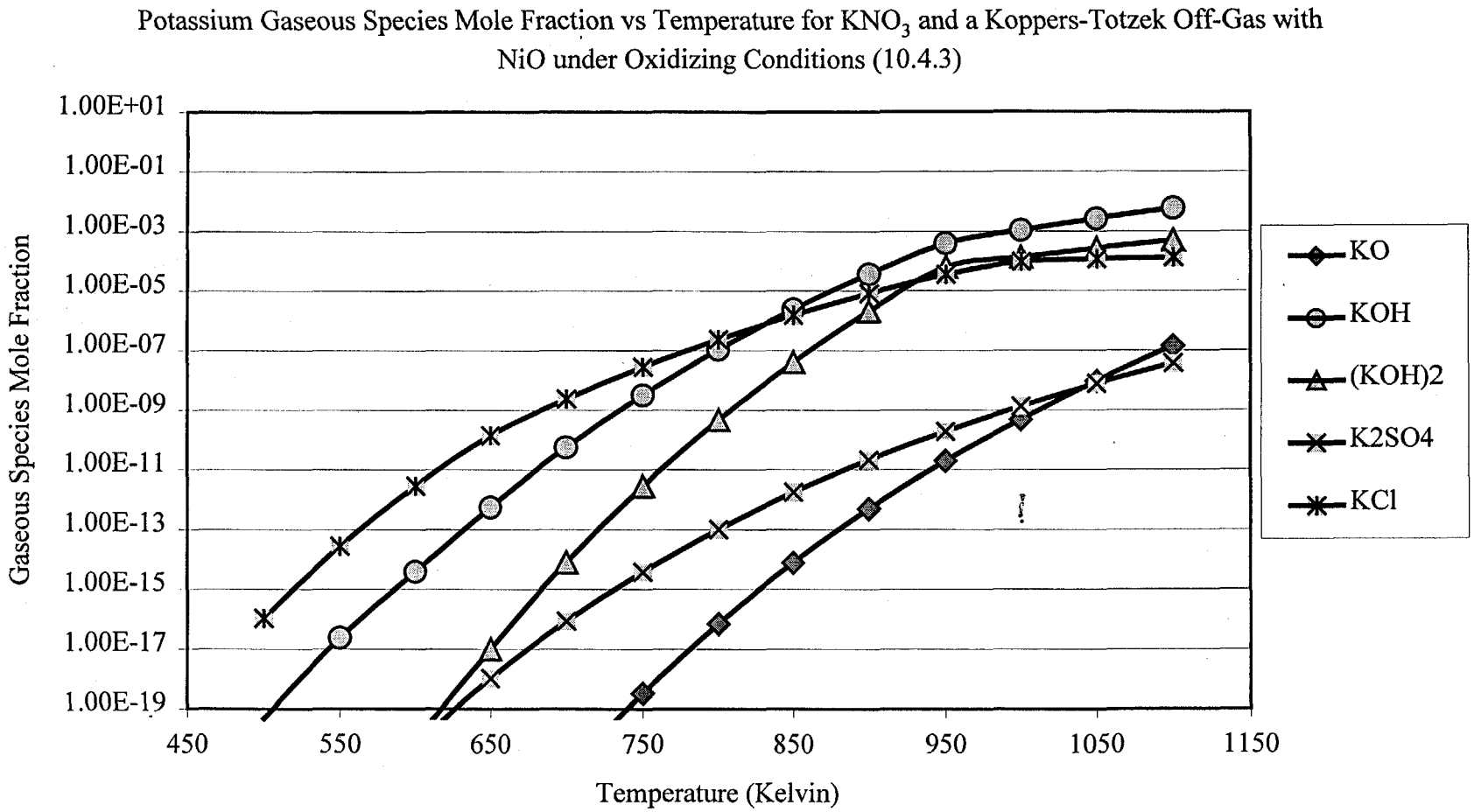

Figure A.47 Potassium Gaseous Species Mole Fraction for KNO_3 and a Koppers-Totzek Off-Gas with NiO under Oxidizing Conditions (10.4.3).

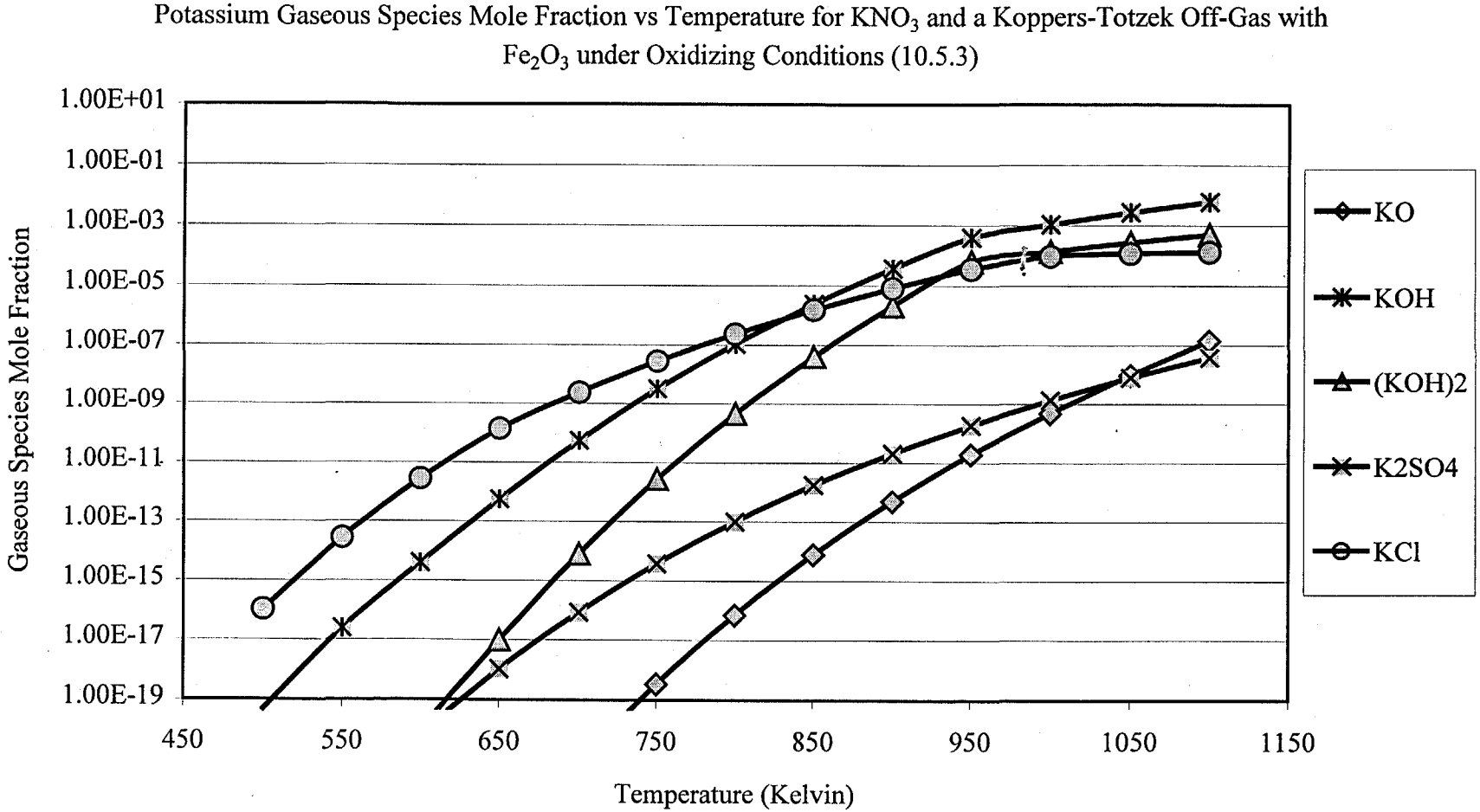

Figure A.48 Potassium Gaseous Species Mole Fraction for KNO_3 and a Koppers-Totzek Off-Gas with Fe_2O_3 under Oxidizing Conditions (10.5.3).

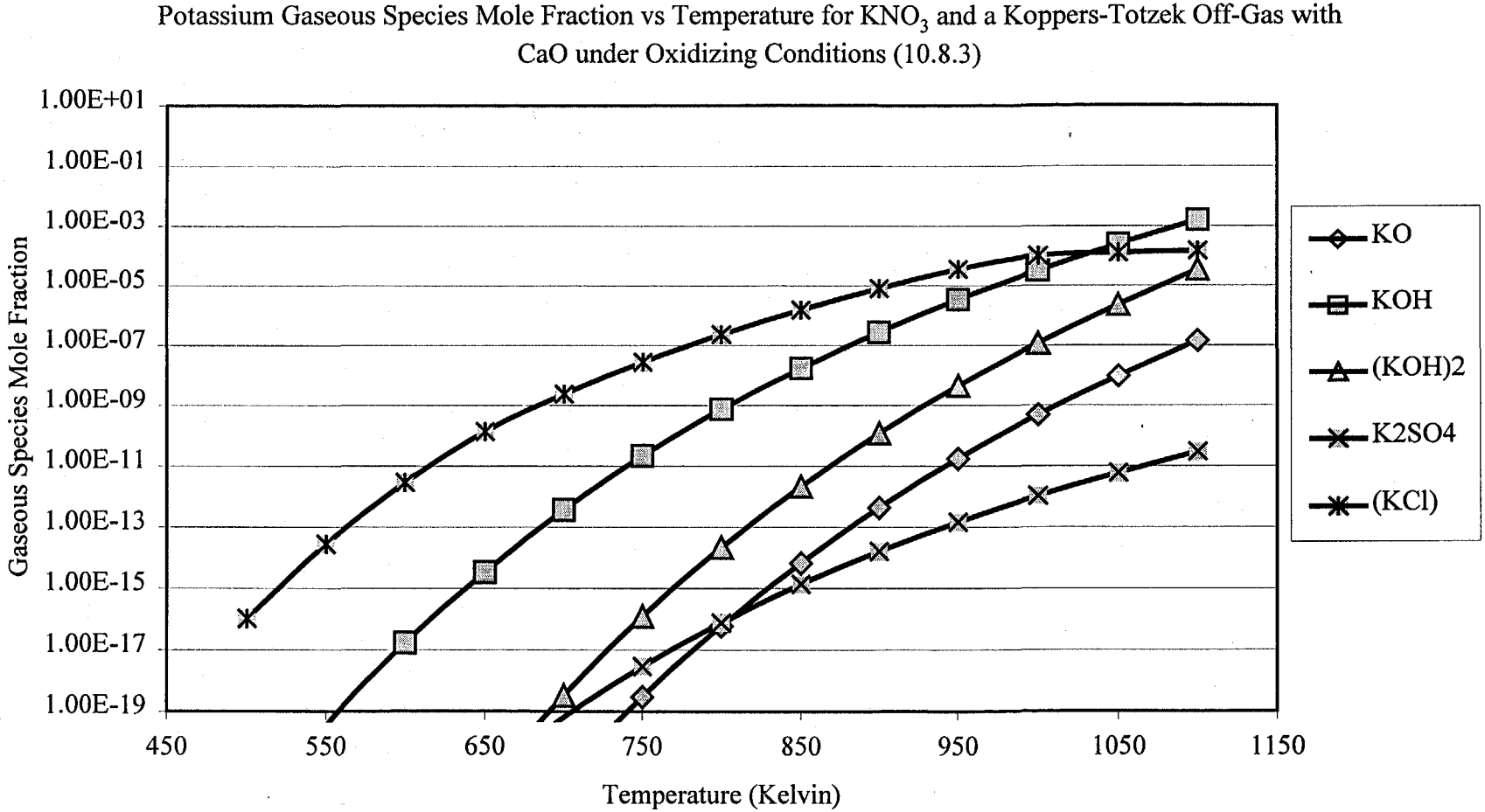

Figure A.49 Potassium Gaseous Species Mole Fraction for KNO_3 and a Koppers-Totzek Off-Gas with CaO under Oxidizing Conditions (10.8.3).

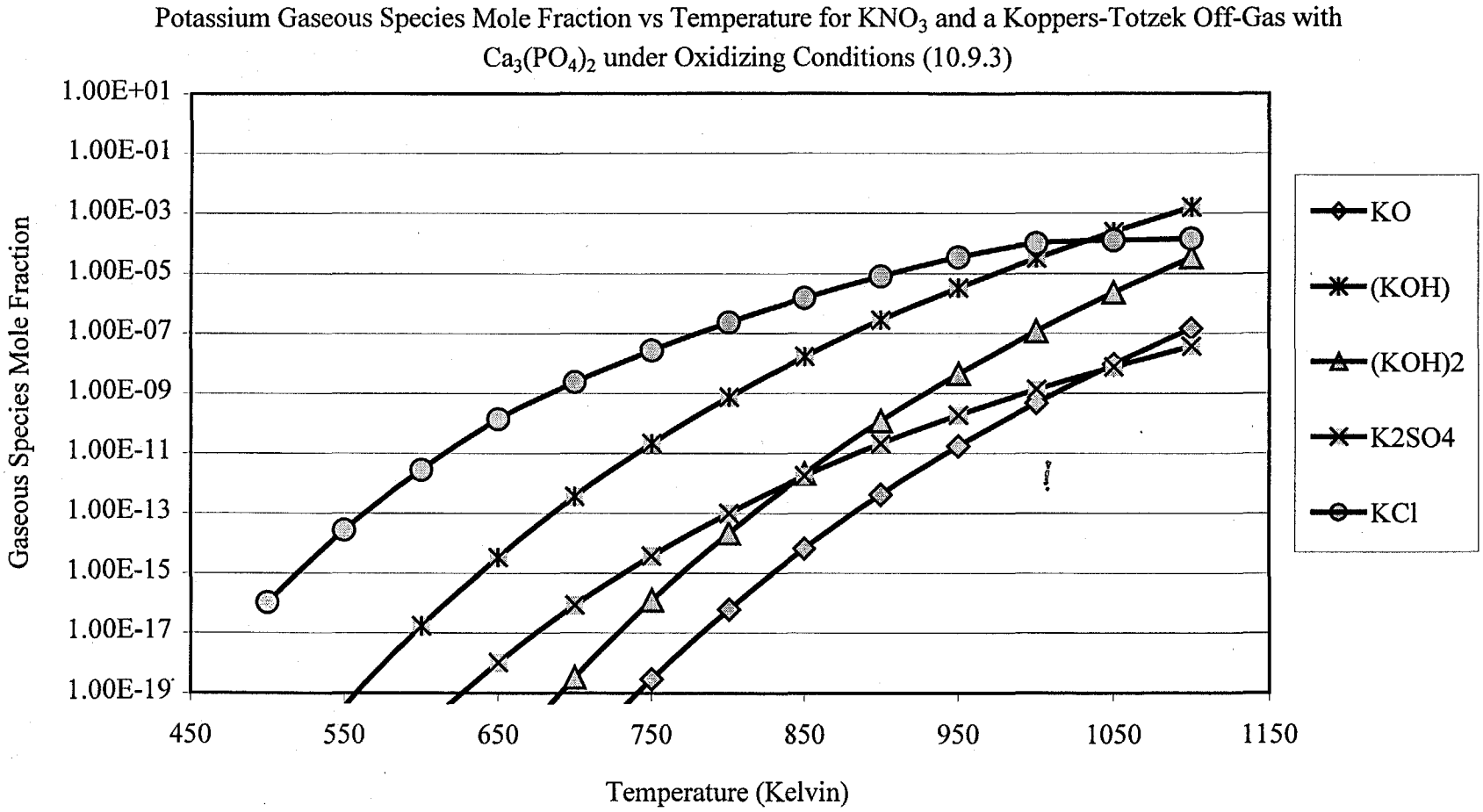

Figure A.50 Potassium Gaseous Species Mole Fraction for KNO_3 and a Koppers-Totzek Off-Gas with $Ca_3(PO_4)_2$ under Oxidizing Conditions (10.9.3).

A.6d) Low Temperature/Reducing Condition Simulations

This section looked at the nitrates' ability to capture sulfur under reducing conditions. Two main areas were tested, similar to the manner in which previous sections were studied. First, all of the applicable salts were tested with a non-reactive supports and the off-gas from a Winkler Gasifier to determine which salt does the best job as far as sulfur removal and overall stability. The next section ran the selected salt with the remainder of the supports to ascertain if there were any differences as far as sulfur capture for non-reactive systems and also determine the solid and liquid products for all of the systems tested.

The FACT entering molar ratios for the scenarios testing the various nitrates' sulfur capturing capabilities are listed in Table A.13.

The scenarios were run from 500-1100 K to cover the stable range for the different nitrates. Figures A.51-A.54 contain information on the sulfur containing gaseous species. The amount of sulfur containing species in the gas phase for these systems was extremely low. Both KNO_3 and $NaNO_3$ are far superior compared to $LiNO_3$ and $AgNO_3$ at keeping the sulfur species mole fraction below 10^{-20} over the entire temperature range. $AgNO_3$ is unstable over the entire temperature range tested, immediately forming silver sulfate and Ag (s). $LiNO_3$ is stable up to 650 K at which it completely dissociates releasing nitrogen and oxygen, thus diluting the gas phase. $NaNO_3$ is stable up to 950 K, while KNO_3 is stable over the entire temperature range tested. From a stability and sulfur capture standpoint KNO_3 is the best choice to test with the rest of the supports.

Initially, the potential for sulfur capture looks very promising, but an inspection of the other equilibrium gas phase constituents shows that a majority of the H_2 and CO was oxidized to CO_2 and H_2O. Although the systems were designed to operate under reduced conditions, small amounts of the nitrates dissociate and release nitrogen and oxygen into the gas phase. The sulfur is captured as a sulfate, which is not expected in a system truly operating in a reduced state. Figure A.55 shows the significant gaseous species for the KNO_3 system. CO and H_2 are at very low concentrations over the entire temperature range leaving virtually nothing left to oxidize for generating electricity in a molten carbonate fuel cell. Another concern with these systems is the high concentration of NO_x present at relatively low temperatures tested. At the upper end of the temperature range, NO_x values are on the order of 100 ppm-v, which is higher than expected in a reduced system. Again, the nitrate dissociation contributes to the formation of NO_x in systems where it is not expected.

Figure A.55 shows a mercury concentration just over 1E-2 ppm-v that slightly decreases with increasing temperature. The actual molar amount of elemental mercury present in the gas phase is equal to 2.5334E-11 moles. This amount is slightly less than the amount input into FACT of 2.651E-11 moles found in Table A.13. The "missing" mercury remains in the gas phase as HgO.

Figure A.56 shows the potassium gaseous species concentrations as a function of temperature. As expected there were very low levels of potassium gaseous species at the lower temperatures. Around 850 K, the first salt gaseous species

reached a concentration greater than 1 ppm-v and topped out at 10000 ppm-v at the upper end of the temperature range. The other salt species exhibit behavior similar to the potassium gaseous species in relation to the temperature trend. The sodium system curves look similar to those found in Figure A.56, but on average are two orders of magnitude lower than the potassium gaseous species. The highest sodium gaseous species concentration is around 100 ppm-v at 1100 K for NaOH. From this perspective $NaNO_3$ is the more attractive candidate.

Table A.13 FACT entering Molar Ratios for Low Temperature Salts and a Winkler Off-Gas with a Non-Reactive Support under Reducing Conditions.

	(8.4.2)	(9.3.2)	(10.3.2)	(11.3.2)
Support	1.000E+00	1.000E+00	1.000E+00	1.000E+00
Salt	1.204E-01	1.611E-01	1.354E-01	8.060E-02
CO	2.826E-04	3.024E-04	2.897E-04	2.652E-04
CH_4	9.421E-06	1.008E-05	9.656E-06	8.841E-06
H_2	2.415E-04	2.584E-04	2.475E-04	2.266E-04
COS	3.140E-07	3.360E-07	3.219E-07	2.947E-07
H_2S	9.421E-07	1.008E-06	9.656E-07	8.841E-07
NH_3	0.000E+00	0.000E+00	0.000E+00	0.000E+00
CO_2	8.786E-05	9.401E-05	9.006E-05	8.245E-05
N_2	4.396E-06	4.704E-06	4.506E-06	4.126E-06
O_2	0.000E+00	0.000E+00	0.000E+00	0.000E+00
Ar	6.281E-07	6.720E-07	6.438E-07	5.894E-07
Hg	2.586E-11	2.767E-11	2.651E-11	2.427E-11
HCl	3.879E-07	4.150E-07	3.976E-07	3.640E-07

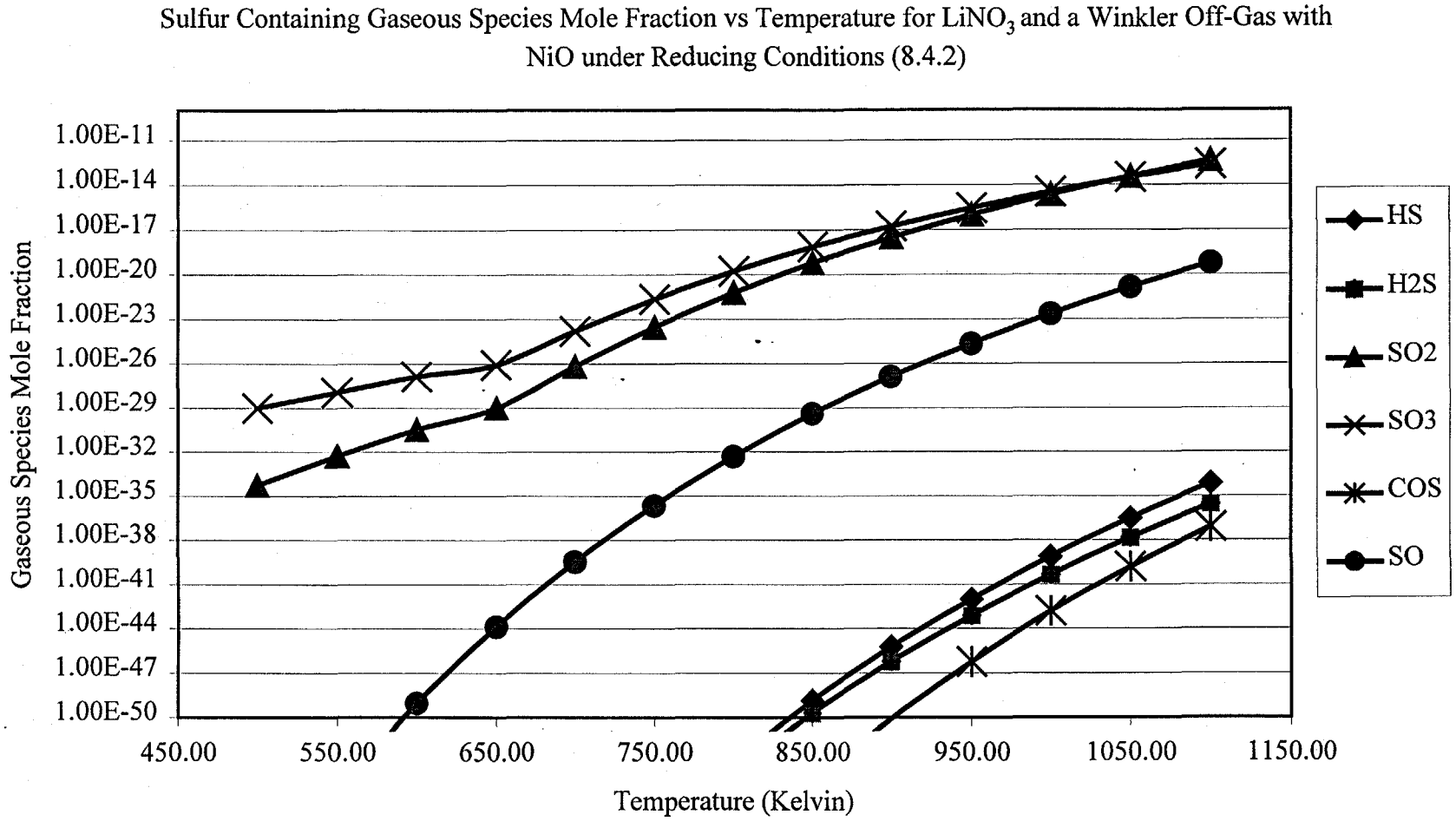

Figure A.51 Sulfur Containing Gaseous Species Mole Fraction for $LiNO_3$ and a Winkler Off-Gas with NiO under Reducing Conditions (8.4.2).

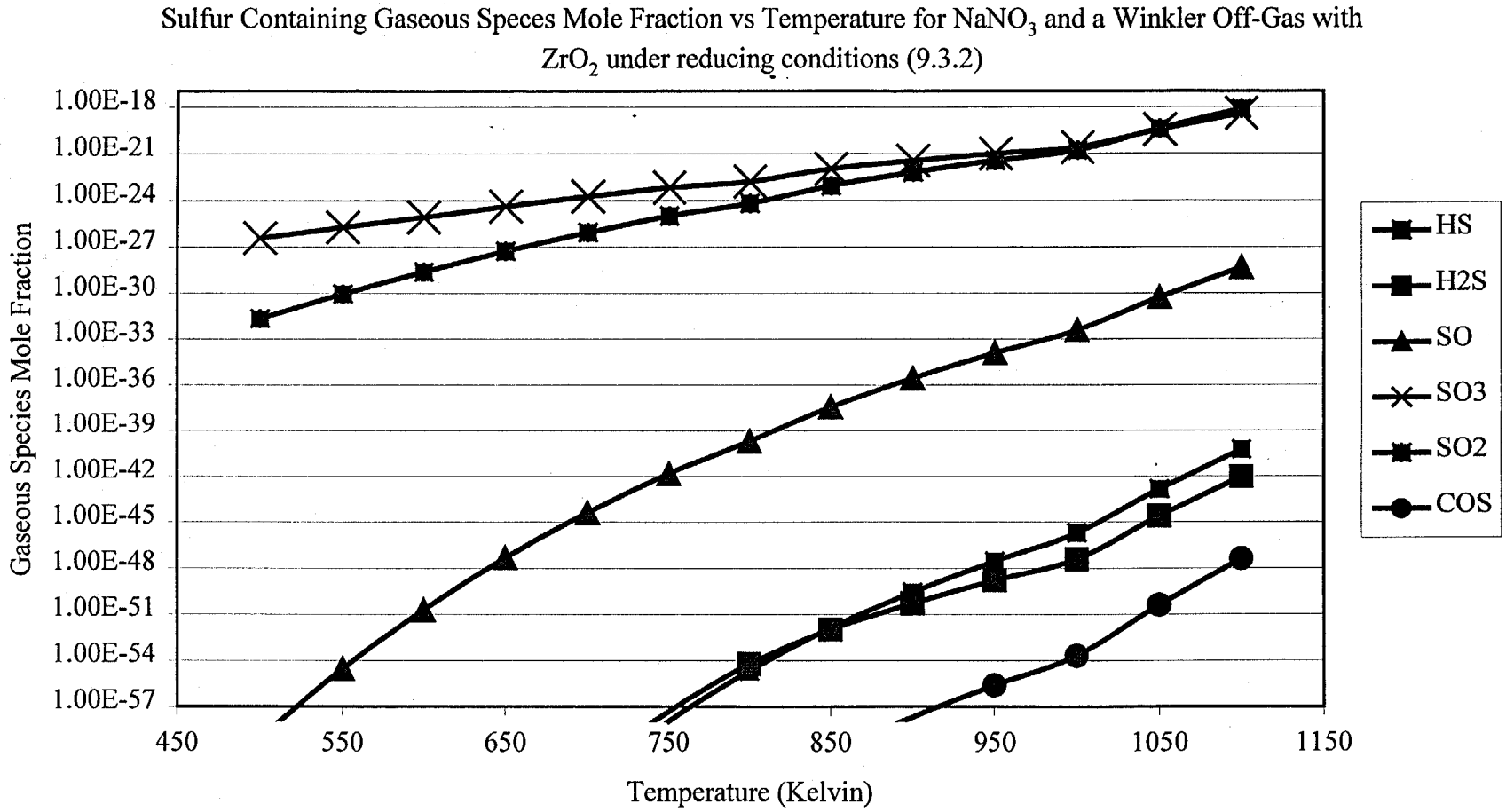

Figure A.52 Sulfur Containing Gaseous Species Mole Fraction for $NaNO_3$ and a Winkler Off-Gas with ZrO_2 under Reducing Conditions (9.3.2).

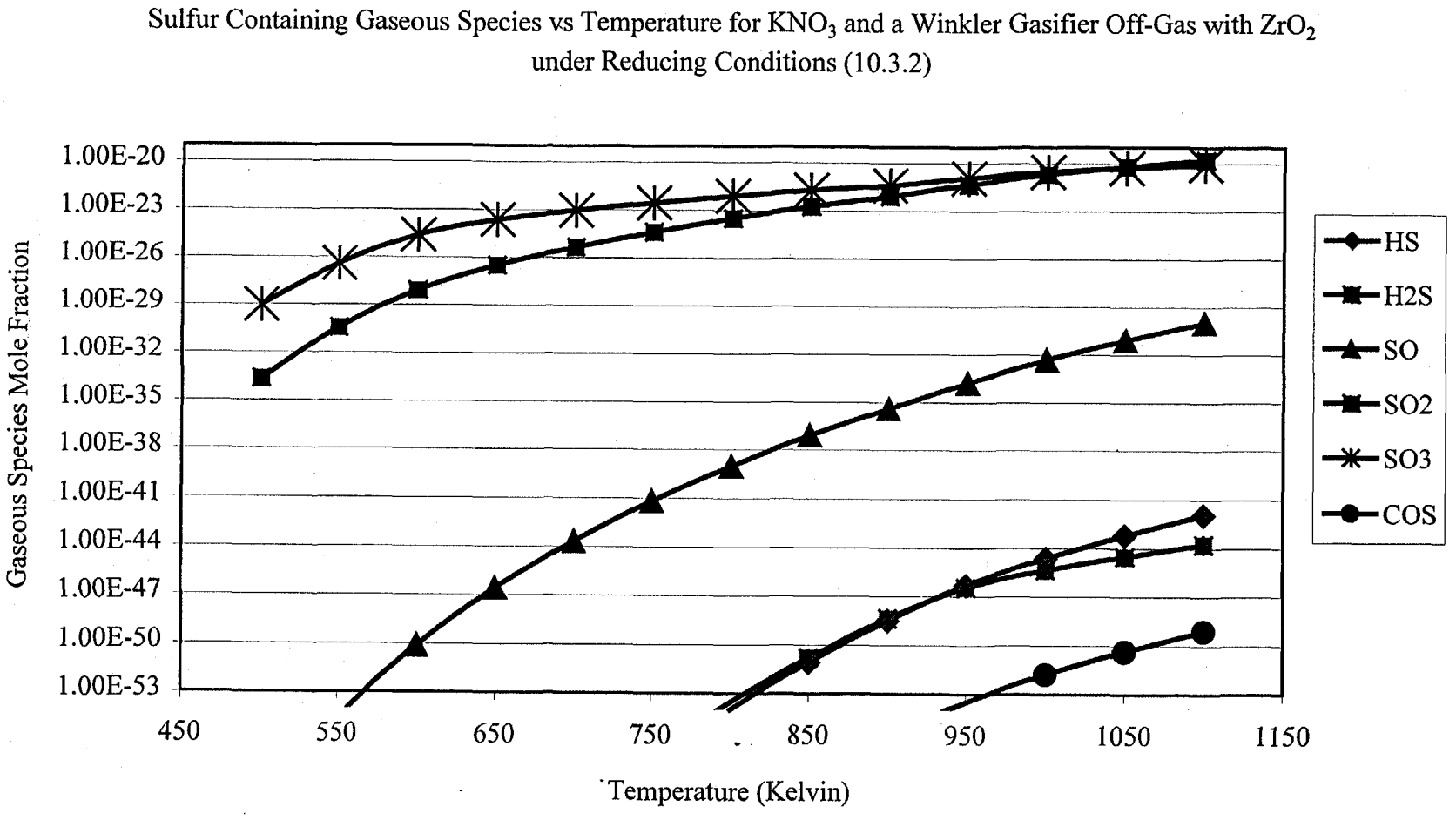

Figure A.53 Sulfur Containing Gaseous Species Mole Fraction for KNO_3 and a Winkler Off-Gas with ZrO_2 under Reducing Conditions (10.3.2).

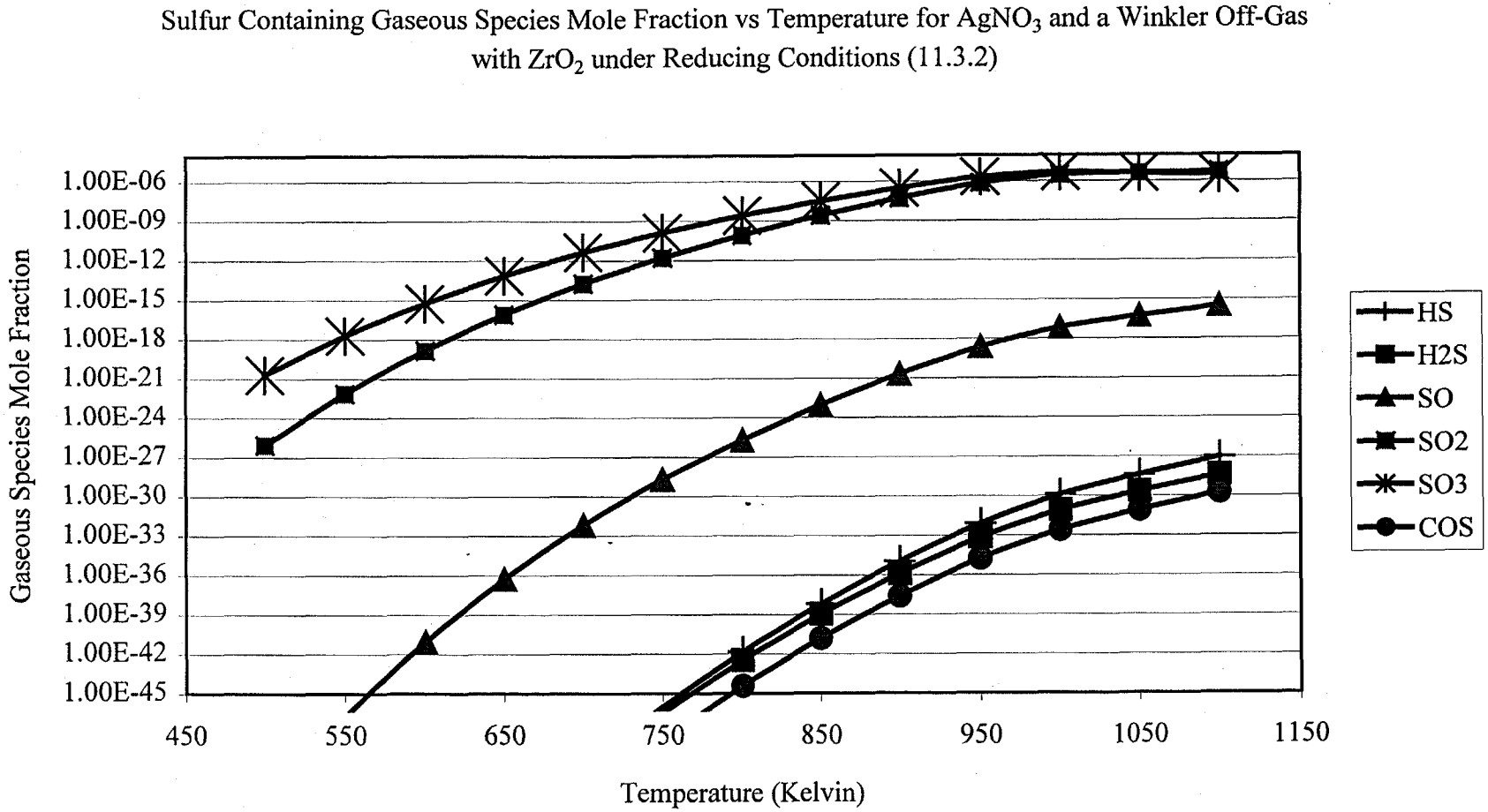

Figure A.54 Sulfur Containing Species Mole Fraction for $AgNO_3$ and a Winkler Off-Gas with ZrO_2 under Reducing Conditions (11.3.2).

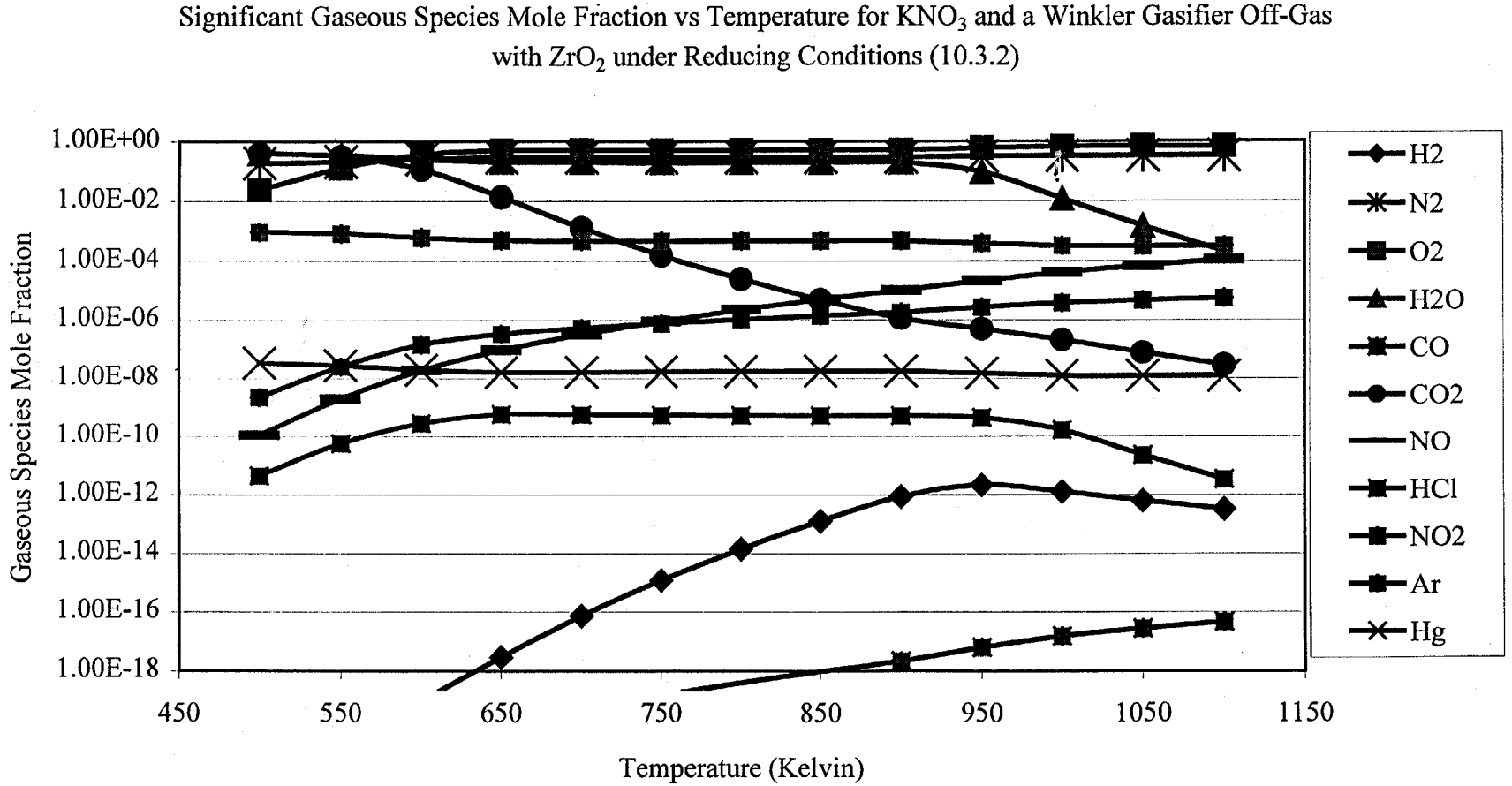

Figure A.55 Significant Gaseous Species Mole Fraction for KNO_3 and a Winkler Gasifier Off-Gas with ZrO_2 under Reducing Conditions (10.3.2).

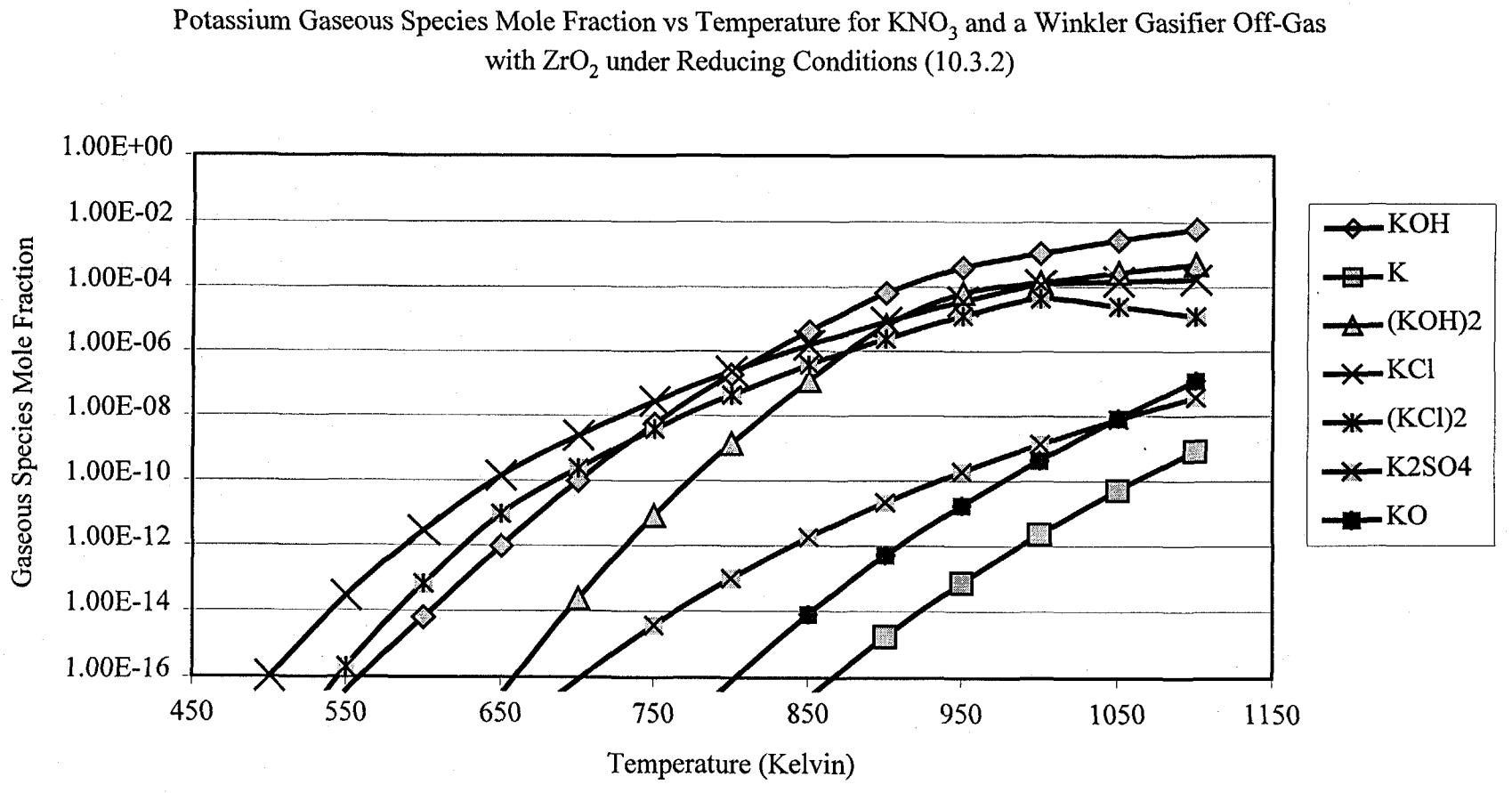

Figure A.56 Potassium Gaseous Species Mole Fraction for KNO_3 and a Winkler Gasifier Off-Gas with ZrO_2 under Reducing Conditions (10.3.2).

This section gives the results for systems tested with KNO_3 and various supports. Table A.14 lists the reactant molar ratios inputted into FACT. In this section, it turned out there were only three completely stable supports: ZrO_2, NiO, and Fe_2O_3. CaO and $Ca_3(PO_4)_2$ both reacted with the salt over a substantial portion of the temperature range forming very small amounts of $K_2Ca_2(CO_3)_3$ and K_2HPO_4, respectively. This type of behavior mirrors that of the systems in the low temperature oxidizing condition section. The amount of gas phase sulfur containing species and K_2SO_4 (s) in the partially reactive supports were still the same compared to the completely non-reactive supports. How this small reaction would affect the system's ability to be fluidized is difficult to speculate. There was no appreciable difference between the results obtained for ZrO_2 in the previous section and those found when using NiO and Fe_2O_3. This is why no graphs were provided for these systems. Both the low values of the sulfur containing gaseous species and the surprising oxidative behavior were observed with NiO and Fe_2O_3.

It is entirely possible that when kinetics are taken into account for these systems that the CO and H_2 are not oxidized. Further study using the FACT React program, literature searches, and empirical studies is needed to truly determine whether this type of system is of any practical use in conjunction with a molten carbonate fuel cell.

Table A.14 FACT entering Molar Ratios for KNO_3 and a Winkler Off-Gas with various Supports under Low Temperature Reducing Conditions.

	(10.1.2)	(10.2.2)	(10.4.2)	(10.5.2)
Support	**1.000E+00**	**1.000E+00**	**1.000E+00**	**1.000E+00**
Salt	**6.603E-02**	**1.121E-01**	**8.209E-02**	**1.755E-01**
CO	**2.593E-04**	**2.788E-04**	**2.658E-04**	**3.099E-04**
CH_4	**8.642E-06**	**9.295E-06**	**8.861E-06**	**1.033E-05**
H_2	**2.215E-04**	**2.383E-04**	**2.271E-04**	**2.648E-04**
COS	**2.881E-07**	**3.098E-07**	**2.954E-07**	**3.444E-07**
H_2S	**8.642E-07**	**9.295E-07**	**8.861E-07**	**1.033E-06**
NH_3	**0.000E+00**	**0.000E+00**	**0.000E+00**	**0.000E+00**
CO_2	**8.060E-05**	**8.669E-05**	**8.265E-05**	**9.635E-05**
N_2	**4.033E-06**	**4.338E-06**	**4.135E-06**	**4.821E-06**
O_2	**0.000E+00**	**0.000E+00**	**0.000E+00**	**0.000E+00**
Ar	**5.761E-07**	**6.196E-07**	**5.908E-07**	**6.887E-07**
Hg	**2.372E-11**	**2.551E-11**	**2.432E-11**	**2.836E-11**
HCl	**3.558E-07**	**3.827E-07**	**3.649E-07**	**4.254E-07**
	(10.6.2)	**(10.7.2)**	**(10.8.2)**	**(10.9.2)**
Support	1.000E+00	1.000E+00	1.000E+00	1.000E+00
Salt	2.153E-01	8.779E-02	6.162E-02	3.409E-01
CO	3.323E-04	2.682E-04	2.575E-04	4.230E-04
CH_4	1.108E-05	8.941E-06	8.583E-06	1.410E-05
H_2	2.839E-04	2.292E-04	2.200E-04	3.614E-04
COS	3.692E-07	2.980E-07	2.861E-07	4.700E-07
H_2S	1.108E-06	8.941E-07	8.583E-07	1.410E-06
NH_3	0.000E+00	0.000E+00	0.000E+00	0.000E+00
CO_2	1.033E-04	8.339E-05	8.005E-05	1.315E-04
N_2	5.169E-06	4.173E-06	4.006E-06	6.580E-06
O_2	0.000E+00	0.000E+00	0.000E+00	0.000E+00
Ar	7.384E-07	5.961E-07	5.722E-07	9.400E-07
Hg	3.040E-11	2.454E-11	2.356E-11	3.871E-11
HCl	4.561E-07	3.682E-07	3.534E-07	5.806E-07